Nikolay Kornilov

Fission Neutrons

Experiments, Evaluation, Modeling and Open Problems



Fission Neutrons

Nikolay Kornilov

Fission Neutrons

Experiments, Evaluation, Modeling and Open Problems



Nikolay Kornilov Department of Physics and Astronomy Ohio University Athens, Ohio USA

ISBN 978-3-319-07132-9 ISBN 978-3-319-07133-6 (eBook) DOI 10.1007/978-3-319-07133-6 Springer Cham Heidelberg New York Dordrecht London

Library of Congress Control Number: 2014945751

© Springer International Publishing Switzerland 2015

This work is subject to copyright. All rights are reserved by the Publisher, whether the whole or part of the material is concerned, specifically the rights of translation, reprinting, reuse of illustrations, recitation, broadcasting, reproduction on microfilms or in any other physical way, and transmission or information storage and retrieval, electronic adaptation, computer software, or by similar or dissimilar methodology now known or hereafter developed. Exempted from this legal reservation are brief excerpts in connection with reviews or scholarly analysis or material supplied specifically for the purpose of being entered and executed on a computer system, for exclusive use by the purchaser of the work. Duplication of this publication or parts thereof is permitted only under the provisions of the Copyright Law of the Publisher's location, in its current version, and permission for use must always be obtained from Springer. Permissions for use may be obtained through RightsLink at the Copyright Clearance Center. Violations are liable to prosecution under the respective Copyright Law.

The use of general descriptive names, registered names, trademarks, service marks, etc. in this publication does not imply, even in the absence of a specific statement, that such names are exempt from the relevant protective laws and regulations and therefore free for general use.

While the advice and information in this book are believed to be true and accurate at the date of publication, neither the authors nor the editors nor the publisher can accept any legal responsibility for any errors or omissions that may be made. The publisher makes no warranty, express or implied, with respect to the material contained herein.

Printed on acid-free paper

Springer is part of Springer Science+Business Media (www.springer.com)

Contents

1	Introduction					
2	Experiment					
	2.1					
		2.1.1	Methods of FF Counting			
		2.1.2	Neutron Spectroscopy by TOF Method			
		2.1.3	Time-Correlated Background			
		2.1.4	Time Shift in Neutron Detector			
		2.1.5	Neutron-Gamma Discrimination and its Influence on Result			
		2.1.6	Measurement of the ND Efficiency			
		2.1.7	Time Resolution and "Bin" Corrections			
		2.1.8	Additional Time Spread for "Solid Sample"			
			Experiment at Low Input Energy			
		2.1.9	Possible Distortion Factors in Second Type Experiment			
		2.1.10	The Calculation of the Detector Efficiency with			
			High Accuracy up to 20 MeV			
		2.1.11	Correction for Neutron Scattering in FF Detector			
		2.1.12	Multidetector Systems and "Cross Talk Correction"			
	2.2	Macros	scopic Experiments			
	Refe					
3	Mic	roscopic	Spectra Evaluation. Semiempirical Modeling			
	3.1	_	ellian Function and Terrell's Systematic			
	3.2	· · · · · · · · · · · · · · · · ·				
	3.3					
	3.4					
	3.5		Method			
	3.6		For Multiple Chance Fission			
	Refe	erences	1			

vi Contents

4	Phy	sical Models	77		
	4.1	Basis for Theoretical Modeling	80		
	4.2	True or Plausible Results?	82		
	4.3	Model Realized in Code FINE (FIssion Neutron Emission)	89		
		4.3.1 Estimation of the Two-Dimensional Y(A,TKE)			
		Distribution	90		
		4.3.2 Neutron Emission from Excited Fragments	92		
		4.3.3 Monte Carlo Simulation of Energy-Angular Distri-			
		bution. Verification	95		
		4.3.4 Level Density Verification	99		
	4.4	Comparison Experimental and Calculated Results	103		
	Refe	erences	110		
_		10.WO D. II	110		
5		ievements and Still Open Problems	113		
	5.1	Real Achievements	113		
	5.2	Mechanism of Neutron Emission in Fission	114		
	5.3	Left-Right and Angular Effects for Fission Neutron Emis-			
		sion at 0.5 MeV Input Energy	119		
	5.4	Contradiction Between Microscopic and Macroscopic			
		experiments (Mic–Mac Problem)	125		
	5.5 New Experimental Proposals		129		
	References				

Chapter 1 Introduction

Neutron-induced fission reaction is a unique process. First of all it produces very big energy release $\sim\!200$ MeV, and $\sim\!80\,\%$ of this energy is taken by fission fragments (FFs), which allows us to use this reaction as intensive source of energy. In addition each fission event produces $>\!2$ neutrons, stimulating the chain process for stable production of energy.

Nuclear fission of heavy elements was discovered in December 1938 by Otto Hahn and his assistant Fritz Strassmann, and explained theoretically in January 1939 by Lise Meitner and her nephew Otto Robert Frisch. It was a start point for intensive investigation of this process having in mind very important practical application and fundamental physical interest.

Fission reaction cross sections for many fissile isotopes, properties of FFs, properties of fission neutrons, and gamma-rays were investigated in broad neutron energy range from thermal energy till 200 MeV.

First experimental results for Prompt Fission Neutron Spectrum (PFNS) emitted from 235 U after thermal fission was published in 1952 [1]. The author highlighted that experimental data measured by different groups are in agreement and cover the energy range from 0.075 to 17 MeV. As a next step, B. Watt compares experimental data with developed model (N. Feather unpublished report BM-148). He reminded that "three basic assumption were (1) isotropic emission in the Center of mass (CMS), (2) neutron distribution in CMS proportional $\varepsilon^* \exp(-\varepsilon/Q)$, where Q is an energy corresponding to the 'temperature' of the fragment and ε is the neutron energy in the CMS; (3) fragment velocity at the time of neutron emission corresponding to the full kinetic energy."

The motivation for these assumptions was clearly visible in 50th. However, good physical basis (neutron emission from excited FF after total acceleration) did not help: "Attempts to find values for the two constant (Q and the product E_f^*m/M , where E_f is the kinetic energy of the fragment at the time of neutron emission and m and M are the masses of the neutron and fragment respectively) appearing in the equation assuming one average fragment were unsuccessful. The curve computed by adding the spectra of two fragments, one having the average energy and mass of the light group and the other the average energy and mass of the heavy group, is shown in Fig. 3 (Ref.1). The fit was regarded as unsatisfactory. Since, rather

2 1 Introduction

laborious calculations are necessary to determine the spectrum by Feather's formula, no attempt was made to add the spectra of a larger number of fragments."

The next paragraph from [1] is also very important.

It is interesting to note that a simple formula giving quite acceptable fit is obtained by assuming a Maxwellian distribution $(E^{1/2})*\exp(-E/Q)$ in place of assumption (2) above. (The resulting formula was named by 'Watt spectrum'.) Several early reports on the fission spectrum mentioned this formula but none give the originator. It seems likely that it was derived by several investigators and spread by private communications. Assuming only one fragment, acceptable fits are obtained...

The PFNS for ²³⁵U (and other isotopes) may be investigated with different types of the experiments. The direct information may be extracted from *microscopic* (or differential) experiment in which the spectrum shape is measured at fixed neutron incident energy. Very often these experiments were realized by time-of-flight method.

If we will place nuclei with particular threshold reactions in intensive PFNS, we may measure average cross sections. Sets of experimental data for reactions with different threshold like (n, p), (n, α) , (n, 2n), (n, 3n), and so on allow us to extract information about the PFNS shape if the cross sections of these reactions are known with reasonable high accuracy. This type of so-called *macroscopic* experiment also provides us with information about PFNS. More exactly, *macroscopic* experimental results should be applied for the verification of *microscopic* evaluated data.

A lot of experimental works were done after the first publication. Total PFNS integrated over FF properties were measured for different fissile isotopes $^{232}\mathrm{Th}, ^{233,235,238}\mathrm{U}, ^{237}\mathrm{Np}, ^{239}\mathrm{Pu}, ^{245,246,247}\mathrm{Cm},$ and $^{252}\mathrm{Cf},$ spontaneous fission and neutron-induced fission for input energies from thermal to 14 MeV (for some isotopes up to $\sim\!200~\mathrm{MeV}).$

All these data do not change the main conclusion, that total PSNF are rather close to Maxwellian distribution with average energy < E>=1.9 MeV 232 Th (at 2 MeV) to < E>=2.14 MeV 252 Cf(sf). The average energy for 235 U changes from < E>=1.97 MeV (thermal energy) to < E>=2.10 MeV ($E_0=5$ MeV). The difference between measured average energies is rather small for all investigated isotopes and input energies $\sim 6\,\%$. The average energy is only one parameter characterizing of PFNS, however it is very useful and it will be often used in this manuscript.

After long-time efforts, nuclear community collected big information about threshold reactions' cross sections, and measured average cross sections of these reaction in 252 Cf(sf) and 235 U(th). Since 1986, the 252 Cf(sf) is a standard with rather small uncertainties <1.3% in the fission neutron energy range <10 MeV. The average cross sections measured for 34 threshold reactions in 252 Cf field gave very good agreement with differential spectrum. Ration of calculated to experimental data R = C/E in the response energy range 1–15 MeV is 1.00 ± 0.02 .

However, for ²³⁵U(th) we should make another conclusion. The microscopic and macroscopic data contradict to each other (Mic–Mac problem). We should highlight that reaction cross sections were verified in ²⁵²Cf PFNS. The average energy estimated on the basis of four independent microscopic experiments (1985–2010) is 1.974±0.002 MeV (0.1%). The spectrum which may predict macroscopic data

Introduction 3

should have average energy of 2.03 MeV. The higher energy provides also better prediction for benchmark experiments.

It may seem that ~ 3 % difference is small but it is ~ 30 times higher than estimated uncertainty for average energy from microscopic experiments, it is a half of difference between all available isotopes data and a half of difference between thermal and ~ 5 MeV input neutron energies. We should add an additional excitation energy ~ 2.5 MeV to provide this changing.

What does this difference mean? As a rule it was explained due to systematical mistakes of microscopic experiments. Is it correct or not? What are the realistic uncertainties of microscopic experiments? Which corrections should be taken into account? All these problems are discussed in Chap. 2 (Experiment).

Neutron multiplicity ν_p at thermal energy is known with accuracy <0.2% for main fissile isotopes. The ν_p estimated from PFNS experiments can be useful for verification of experimental results and uncertainties, however most important is the shape of the spectrum. We will name the process of estimation of the analytical function which provides the best adjustment to experimental PFNS, data analysis, normalization of experimental data relative to this function, and the comparison of different experimental results with each other as evaluation procedure.

If after the neutron emission the excitation energy is higher fission barrier new fission reaction can happen. The neutron emitted before fission due to (n, xnf) reactions is named "pre-fission neutrons." This reaction is a good demonstration that physical clear mechanism may be predicted reasonably well.

Different approaches including pre-fission neutron emission are discussed in Chap. 3 (Evaluation).

Any theoretical model for neutron emission in fission and PFNS calculation based on three "traditional" assumptions are mentioned above. Additional mechanisms (for example neutrons emission before scission) are mentioned in many papers. However, the information about this emission is very scattered and contradictive to construct the consequent model for explanation of a lot of experimental data.

Many International Atomic Energy Agency (IAEA) Meetings and Workshops submitted in reports, TECDOC-0335 (1985), TECDOC-410 (1986), INDC(NDS)-0146 (1983), INDC(NDS)-0220 (1988), INDC(NDS)-0251 (1990), INDC(NDS)-0541 (2008) (https://www-nds.iaea.org/publications/), and numerous papers in reviewed journals discussed various models based on "traditional assumptions" with different approaches for parameters calculation. During ~50 years, the motivation of these activities was: the "traditional assumptions" are correct but we do not know many properties and parameters of FF.

The 1–3 assumptions are traditionally applied for experimental data analysis. Neutron energy distributions measured in Laboratory System (LS) are transformed to center of mass system (CMS). These data are described by equation $\varepsilon^{\lambda} \exp\left(-\frac{\varepsilon}{T}\right)$ with fitted parameters λ and T. After this, the data return back to LS with following conclusion about reliability of 3-nd assumption. It seems this procedure may provide wrong conclusion. Therefore, more realistic approach is the creation of the model and direct comparison of its prediction with experimental data in LS.

4 1 Introduction

The most sensitive parameters for successful modeling (reasonable theoretical prediction of experimental PFNS) are two simplifications: square root dependence of the spectrum shape at low <1 MeV energy and T-constant assumption for CMS spectrum. Do we have enough argument for their incorporation?

Rather brief review of existing theoretical models is given in Chap. 4. In an addition, Cascade Evaporation Model with incorporation of the detailed two-dimensional distribution of FF versus masses and kinetic energy is compared with different experimental data: PFNS for several isotopes N(E), dependence of neutron multiplicity as functions of masse and Total Kinetic Energy (TKE)–v(A), v(TKE), and neutron angular distribution relative to FF direction. This analysis allows us to conclude that "traditional assumption" cannot describe all data set.

Recently (2012) new book for "Nuclear Fission" was prepared by R. Vandenbosch [2]. The part devoted to fission neutron is very short. It is worth to give main part of this text directly:

The average neutron kinetic energy in the Laboratory System (LS) is approximately 2 MeV. Since most of the neutrons are evaporated from the moving fragments, this energy is a composite of the emission energy in the Center of Mass System (CMS) and the energy given to the neutron by virtue of the fragment's kinetic energy. The latter correspond to approximately 2/3 MeV, hence, is about 1/3 of the total neutron kinetic energy observed. The form of the emission spectrum in the CMS is expected to be approximately Maxwellian, E*exp(-E/T) (this is mistake, should be $E^{1/2}$ for Maxwellian), where T is the nuclear temperature. If we assume an emission spectrum of this form, and assume that emission occurs from fragments all having the same kinetic energy per nucleon E_{ν} , we will expect a laboratory spectrum of the Watt form....

The form of the spectrum turns out to be very little different from that of a Maxwellian. The parameters required to obtain the fit are T=0.965 MeV and Evv=0.54 MeV. The latter value is smaller than expected and may reflect the simple assumptions of a single emission spectrum of fixed T and a single fragment energy. In reality we expected the total spectrum to be a superposition of spectra of different temperature transformed with varying fragments energies. We will defer further consideration of the neutron spectrum until later, where we discuss the neutron yield as function of fragment mass and energy, in which case the CMS spectrum can be obtained by direct transformation of the experimental spectrum.

Nothing changed since 1952? The same motivations, the same arguments for PFNS description, are using as it was defined in earlier papers?

Indeed these conclusions are true. Nuclear society did not find *bright evidence* for another explanation of neutron emission in fission. However, we have got a lot of arguments that traditional explanation cannot describe the picture prepared on the basis of existing experimental data.

Now it is clear that both microscopic and macroscopic data for ²³⁵U *are correct*! What does mean this difference? Can we explain the nature of this contradiction? Indeed, some experimental functions can be described with traditional model by fitting model parameters (level density parameters, energy sharing between FF, energy distribution between excitation and deformation, and so on). However, it is not true for huge difference between v(TKE) slope predicted in traditional model (~10 MeV/n) which does not depend very much on fissile isotope and experimental data ~19 MeV/n for ²³⁵U. What does this contradiction mean? All these problems and possible direction for future investigations are discussed in Chap. 5.

References 5

References

 Watt B (1952) Energy spectrum of neutrons from thermal fission of ²³⁵U. Phys Rev 87(6):1037– 1041

2. Vandenbosch R (2012) Nuclear fission. Elsevier, 432 p. http://www.google.com/search?tbo=p&tbm=bks&q=inauthor:%22Robert+Vandenbosch%22, http://www.google.com/search?tbo=p&tbm=bks&q=subject:%22Science%22&source=gbs_ge_summary_r&cad=0, http://books.google.com/books?id=RCeaisb73M0C&sitesec=reviews> http://books.google.com/books/about/Nuclear Fission.html?id=RCeaisb73M0C. Accessed 2 Dec 2012

Chapter 2 **Experiment**

Total PFNS is formed due to contributions of different sources of neutrons. We still assume that some part of neutrons is emitted due to unknown mechanism. Another part (we still assume that this is the main part) is emitted from accelerated fission fragment (FF), and energy-angular distributions of prompt fission neutron (PFN) depend very much on the direction between FF and neutron detector (ND), and particular properties of FF like masses, total kinetic energy (TKE), and so on. Due to complicate nature of neutron emission in fission, sometimes unknown, the prompt fission neutron spectrum (PFNS) measured in particular experiment may be destroyed very much.

Fission events should be selected to avoid background counting. The best way is detecting of FF as a unique signature of fission events. This experiment may be organized in different ways.

The first type of experiment, all FF emitted from fissile material, is counting in special detector. This detector should be constructed in such a way to avoid fragment losses. Let us name this type as "total FF integrated experiment."

The experiment may be organized in such a way ("differential FF experiment") to investigate energy-angular distribution of neutrons relative to fixed FF with particular properties and direction relative to ND. This type is very important for investigation of neutron emission mechanism, but results of this may be used also to estimate the total PFNS as integral of above-mentioned experimental data. The problems connected with this procedure may destroy result and should be discussed in each particular experiment. The main criteria that the procedure is self-consistence, is the agreement of PFNS measured with this second type of experiments with total PFNS result (first experiments).

The PFNS has broad energy distribution. So any neutron spectrometer operating with input energy E_0 may be used for measurement of PFNS for energy interval $E > E_0$. Let us name this experiment as "solid sample" (third type).

All experiments have got particular advantages and disadvantages:

First experiment can be easily used at thermal point where neutron flux and fission cross section are high. At input energy > 1 MeV, a large amount of fissile material should be loaded in FF detector. This factor may give strong influence on final result

• Second experiment is unique for investigation of neutron emission mechanism, but may destroy PFNS due to numerical integration procedure.

• Third experiment is very useful for E_0 =0.5 MeV where intensive neutron source $^7\text{Li}(p,n)$ is available. An additional correction for time spread over fissile sample should be done. However, there is very big data spread for ^{235}U PFNS measured with this method. The nature of this problem is unknown. For higher input energies, experimental data cover limited energy range $E > E_0$, which complicates data analysis and evaluation.

Different techniques were used for PFNS investigations. Since the review [36] prepared in 1976, practically nothing changed. In a number of works, the method of registration of recoil protons [35], and ${}^{3}\text{He}(n,p)$ [36] and ${}^{6}\text{Li}(n,\alpha)$ [10] reactions' products were used.

Time-of-flight (TOF) method is used now practically in all experiments as the most accurate one. NDs are also the same types: on the basis of $^6\text{Li}(n,\alpha)$ reaction—lithium glasses, $^6\text{LiI}(\text{Eu})$ crystal, and $^{235}\text{U}(n,f)$ in ionization chamber (IC) for energy range <3 MeV, and hydrogen organic scintillator with neutron gamma-ray discrimination for fission neutron energy >0.5 MeV, with detail investigation of the ND efficiency.

The traditional method:—yield of mono-energetic neutrons from ${}^{7}\text{Li}(p,n)$, D(d,n), T(p,n), reactions, and (n,p) scattering were used in many experiments' ND efficiency investigation. After estimation of the ${}^{252}\text{Cf}$ PFNS like a standard in 1986 [29], the ratio measurement became the traditional method for ND calibration.

2.1 Microscopic Experiments

As was mentioned above, TOF experiments are the most accurate ones. Therefore, only this type of microscopic experiments will be discussed here.

2.1.1 Methods of FF Counting

In [25], a 252 Cf fission source of intensity $\sim 1 \times 10^4$ 1/s was prepared by electrodeposition on thin tantalum foil. The diameter of layer 252 Cf was 7 mm. The foil with layer was placed inside a vacuum chamber made of 1-mm-thick aluminum. At a distance of 1 mm from the 252 Cf a semiconductor detector was placed for counting of FF. The silicon surface-barrier detector was made of material with a specific resistance of 300 om*cm and its working diameter was 20 mm. Pulses formed by FF were separated very well from α -particles events. The specific problems were rather poor time resolution ~ 4 ns and short life time of semiconductor detector. Author changed the FF detector each time when FF count rate was reduced by ~ 1.5 %. The integral radiation dose to each counter during the experimental run was 2.7×10^8 1/cm² for FFs. The total operation time of one counter was ~ 24 h.

In the pioneering work of [13], a Cf source with an initial intensity of 6.1×10^5 f/s was mounted in a gas-scintillation detector. The 252 CF source was electrodeposited inside a 1 cm circle onto a thin foil backing. A 100-µg gold layer covered the source to reduce the migration of Cf inside the counter. The foil was mounted at one end of a thin-walled stainless-steel scintillator tube. Good high vacuum procedures the cell prior to backfilling 28 psia with high purity xenon gas. The cell was viewed by 56UVP phototube through a quartz end window.

In the following, a similar technique was applied for counting FF rate of $1 \cdot 10^6$ f/s [38]. An additional cleaning system was used to support high light output from gas scintillator.

A larger problem of the gas scintillator for FF counting is a big amount material around the neutron source, which may destroy spectrum shape very much (see discussion in following part of this section).

The IC for FF counting is the most attractive device in comparison with the one discussed above. It can provide good time resolution, long time stability, and total amount of material around fission neutron source may be reduced as much as possible.

The IC operating in fast current mode was used as FF detector in experiments [1, 7, 19]. In these experiments, ²⁵²Cf source was used for ND calibration.

In [22], Cf and U layer were placed inside the same IC. The FF count rate for U was $\sim 5 \times 10^4$ 1/s. Time resolution (IC+ND) was 1.7 ns for U section and 2.1 ns for Cf. The difference appeared due to counting of both FF for ²³⁵U.

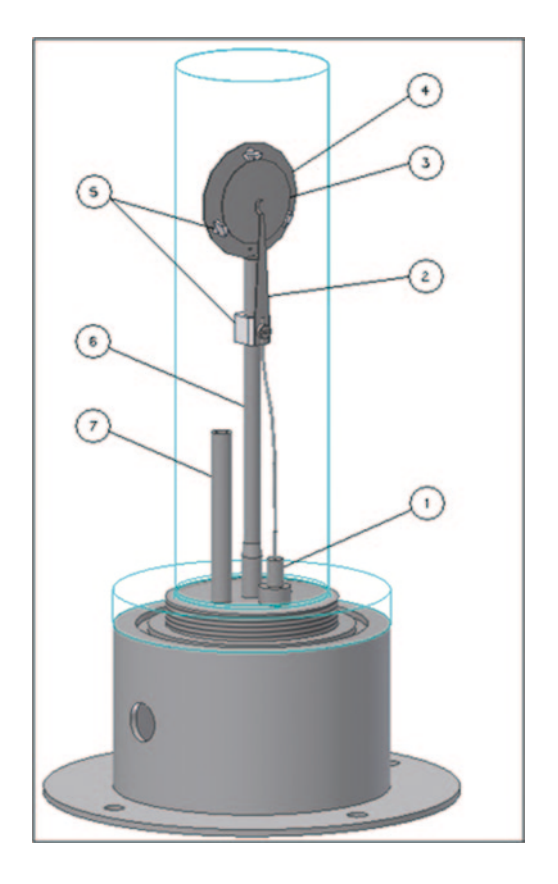
In experiments for measurement of PFNS at E>5 MeV only ICs were used by all authors [2, 17, 4, 5, 32, 27]. PFNS for the 238 U(n,f) reaction, [17] were measured relative to those of 252 Cf. Time resolutions (2–3 ns) and flight paths (\sim 2 m) in both sets of experiments were similar.

The particular feature of these experiments is a bid amount of fissile material, which should be placed in IC to provide reasonable run time. As a result layer thickness was high, and the efficiency of FF counting was rather low. Multilayer assembly was used (big input capacitor for preamplifier), which complicates timing fission events with good time resolution. For example, in the experiment of [2], the fission chamber efficiency was $\sim 70-75\%$ at $E_n \sim 14.3$ MeV and $\sim 80-85\%$ for $E_n \sim 6-9$ MeV [17]. In the experiments, [4, 5, 32, 27] the ²⁵²Cf was incorporated into one section of the fission chamber as an admixture to the uranium layer. It allowed to reduce the influence of the fragment discrimination threshold but did not remove this effect.

In the experiments by Kornilov et al. [2, 17], the problem of stable operation "fast current preamplifier" connected to multiple layers chamber was not solved. Neutrons were detected in coincidence with fission events, but there was no timing of events. The spectra were measured in a "pulsed mode" of the accelerator. Consequently, the spectrum of "background" neutrons was time dependent and the "effect/background" ratio was poor at higher neutron energies.

The IC applied for detector calibration with 252 Cf in experiments [19] was operated with count rate $\sim 5 \cdot 10^4$ 1/s. The similar detector can be operated with Cf source intensity up to $\sim 3 \times 10^5$ f/s [1].

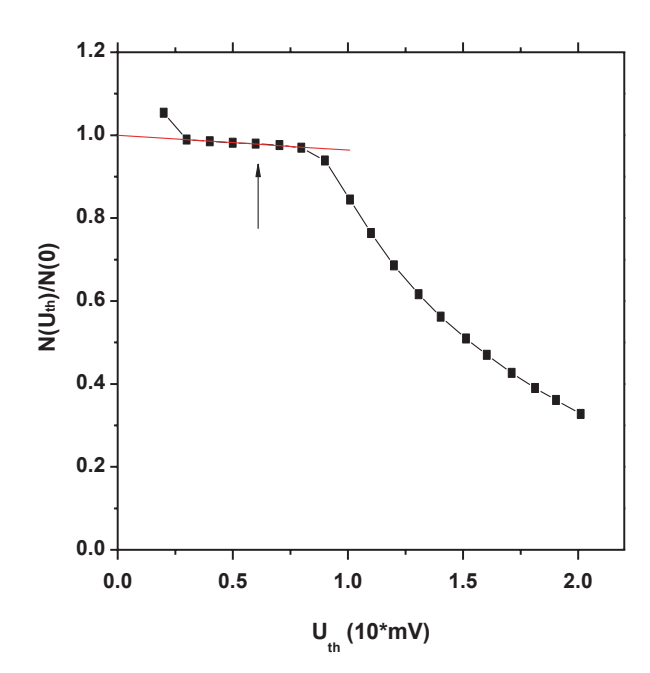
Fig. 2.1 Drawing of the ionization chamber for the ²⁵²Cf reference source. *I* high voltage, output signal, 2 contactor, 3 ²⁵²Cf layer, 4 collecting electrodes, 5 insulators, 6 holder (*thin-walled tube*), 7 gas inlet



The parallel plate IC provides the current $I = en(t) \cdot v/d$, where n(t)—total amount of electrons between the electrodes at the moment t, v—drift velocity of the electrons, d—distance between electrodes. The initial amount of electrons for FFs moving in the orthogonal direction relative to the electrodes is $n(0) = dE/dx \cdot d$. So in first approximation, the minimal current does not depend on the distance between the electrodes. A distance of d=2.5 mm provides a rather good current ratio of 10:1 between FFs (70 MeV, Mo–Ba pair) moving along the electric field and 5.5 MeV alpha-particles moving in a perpendicular direction. At U=500 V for Ar+10 %CH₂, the drift velocity is $v\sim5\times10^6$ cm/s which gives a ~50 ns pulse width.

A three-dimensional sketch of the ionization chamber is shown in Fig. 2.1. The Cf layer (\emptyset =10 mm) was placed on a polished stainless steel electrode (\emptyset =25 mm). The wall thickness of the chamber cover (stainless steel) was 0.2 mm. All massive parts were moved far away from the source. The chamber was filled with an Ar+10%CH₂ mixture up to 1.2 bar. The output signal from the chamber was fed to a fast preamplifier. Good results (stability, low noise, time resolution) were reached with the MESYTEC charge integrated preamplifier module MPR-1—single channel charge sensitive preamplifier (QPA) with two outputs [37].

Fig. 2.2 The counting efficiency of FF for fast IC. The *arrow* shows the threshold value used



The pulse height (PH) distribution of FF was measured by integrating FF events above a given threshold of a constant fraction discriminator (CFD) [21]. This dependence is shown in Fig. 2.2. The efficiency of the FF counting at the applied threshold has been determined to be 0.98 ± 0.01 . It was estimated by extrapolating the plateau region in Fig. 2.2 to zero threshold. The time resolution, estimated on the basis of the width of the prompt fission gamma-rays, measured with a small Pilot U scintillator, was ~ 1 ns at full width of half maximum (FWHM).

2.1.2 Neutron Spectroscopy by TOF Method

Since beginning of 1970s, practically all PFNS were measured by TOF method. For its realization, we should have "start" and "stop" pulses. The stop signal as a rule generated by FF or from accelerator operating in "pulse mode." The start signal is the task of ND. Several types of NDs used for spectroscopy of PFN are: 6 Li-glass scintillator, antracene (E_n <3 MeV), crystal (stilbene) or liquid organic scintillators for neutrons with energy from \sim 0.5 till 20 MeV. After subtraction of neutron background, and the transformation to energy scale taking into account relativistic formulas, the investigated spectrum S(E) is connected with experimental distribution N(E) by Eq. (2.1). If the PFNS from fissile target A is measuring relative to 252 Cf standard we have two similar equations:

$$N_{x}(E) = Y_{x} \cdot S_{x}(E) \frac{V_{x}}{4\pi} \Omega \cdot \varepsilon(E) \cdot \alpha_{1}(E) \dots \alpha_{n}(E), \tag{2.1}$$

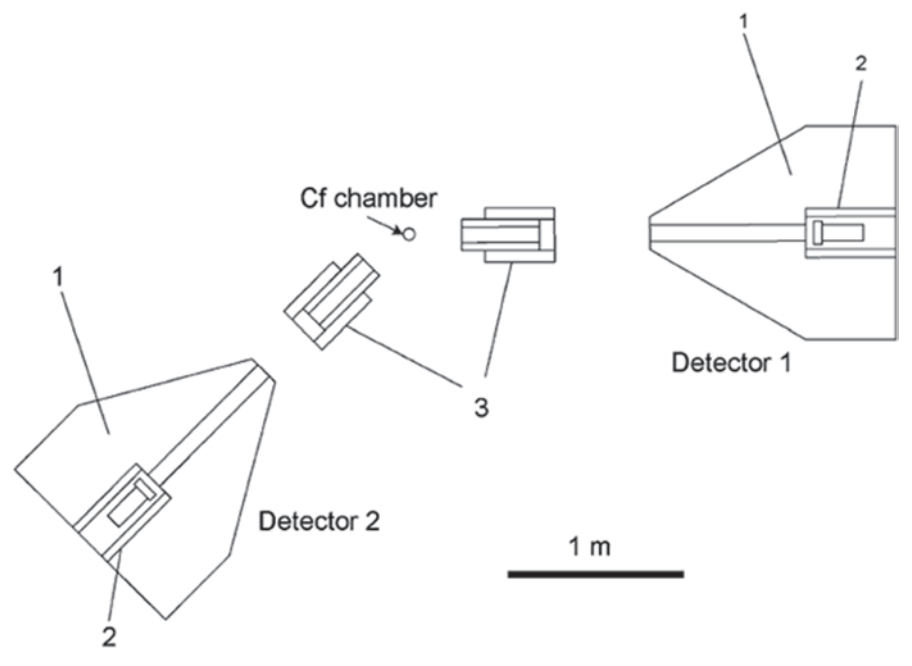


Fig. 2.3 Experimental setup for two detectors. 1 lithium carbonate; 2 lead; 3 Cu cylinders

where x=A,Cf, Y—yield of the FFs measured during the run, v—neutron multiplicity, Ω —detector solid angle, $\varepsilon(E)$ —detector efficiency, $\alpha_i(E)$ —any necessary corrections for: neutron scattering in the chamber materials, time-resolution and bin corrections, and others possible factor which may destroy PFNS.

The experimental spectra taken with $Cf-N_{Cf}(E)$ may be used for detector efficiency estimation. The comparison of this result with calculated data gives an additional verification of the experimental method. In reality, the A spectrum $S_A(E)$ may be estimated directly from the ratio $S_A(E)/S_{Cf}(E)$. So, the knowledge of the detector efficiency is not a crucial factor, more important is the correction due to multiple scattering. The FF yields, Y_x , were measured during the same experimental runs (if both layer A and Cf are placed in the same counter); therefore, in some experiments data are normalized to the neutron multiplicity. So, both values v_U and v_{Cf} are known with high accuracy, and comparison with our experimental result may be a good test, also. In case of "solid sample" experiment as a rule only relative PFNS shape is investigation (Y is unknown).

The following discussion will be based on the experimental setup which was used in JRC-IRMM [21]. In this work, the properties of several organic NE213 equivalent NDs, namely three SCIONIX LS301 (\emptyset =10 cm; h=5 cm) and the BI-CRON BC501A (\emptyset =10 cm; h=2.5 cm) were investigated. In all cases, the scintillators were coupled to XP4312 photomultiplier (PM) tubes. During the measurement the detectors were placed in massive shieldings. Up to three detectors were used simultaneously. The experimental setup for two detectors is shown in Fig. 2.3.

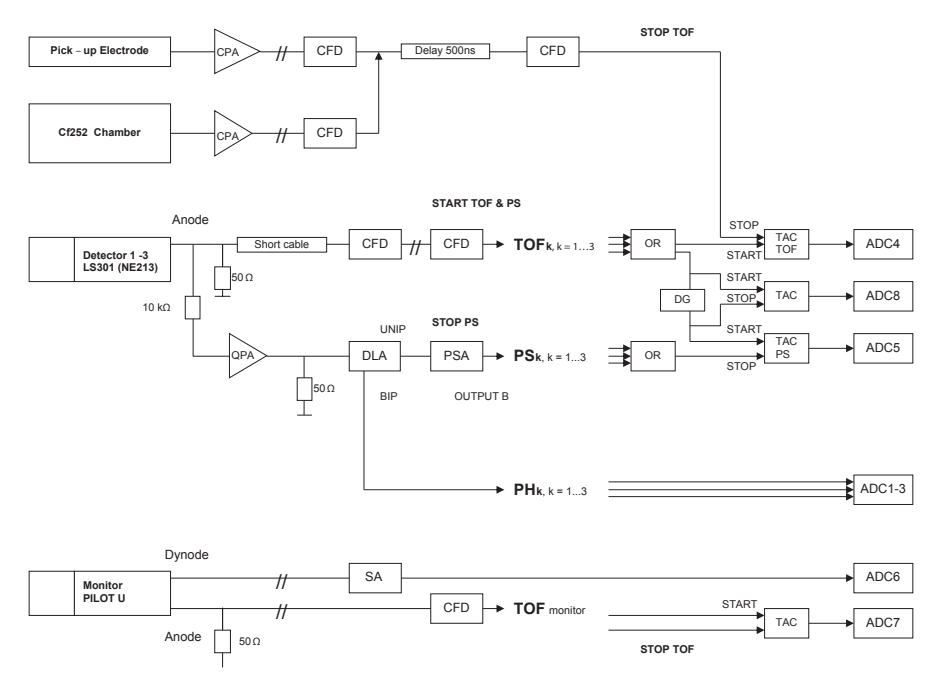


Fig. 2.4 Block-diagram of the electronic setup. *CPA* current sensitive preamplifier, *CFD* constant fraction discriminator, *QPA* charge sensitive preamplifier, *TOF* time-of-flight, *PS* pulse shape, *TAC* time-to-amplitude converter, *ADC* analog-to-digital convertor, *PSA* pulse shape analyzer, *DLA* delay line amplifier, *BIP* bipolar output, *SA* spectroscopic amplifier, *UNIP* unipolar, *PH* pulse height

The block-diagram of the electronic setup for three detectors is shown in Fig. 2.4. The anode signal of the PM tube was used for event timing and for neutron-gamma discrimination. A small part of the anode current (1/400) was transmitted to the QPA. The integrated pulse was fed over a long cable to a delay line amplifier (ORTEC 460) and its unipolar (UNIP) output signal was connected to a pulse shape analyzer (PSA, ORTEC 552). The "B outputs" of the three PSA have been linked by an OR module and via a time-to-amplitude converter (TAC PS) to the analog-todigital convertor (ADC 5) for pulse shape (PS) measurements. The bipolar output (BIP) signal was directly connected to ADCs 1, 2, 3, for PH measurements. These ADCs were used for detector identification. The main part of the anode pulse was transmitted through a rather short cable (~1–2 m) to a CFD. After the OR-unit these signals were used to provide a "start" pulse for the TOF (TAC TOF) and pulse shape measurements (TAC PS). The "B output" of the PSA is delayed by about 1 ms relative to the CFD output. Therefore, an additional delay of about 500 ns (DG—delay generator) was used to reduce the dynamic range of the PS. The real delay was measured for each event (ADC 8) and was applied in the offline analysis to remove the time drift of this device. A small Pilot U detector was used as a time resolution monitor. The dynode output was connected directly to the spectroscopic amplifier (SA) and was applied for PH analysis (ADC 6). The anode output after the CFD

was connected to the start input of the TAC and ADC 7 for the TOF measurement. The "stop" signal for the TOF measurement was generated from the Cf-IC (current sensitive preamplifier, CPA) or from the pick-up electrode of the Van de Graaff accelerator as a pulsed source of mono-energetic neutrons using the same electronic equipment. The signal was delayed with a long cable for 500 ns to detect the "parent" pulse for any ND pulse.

The data were collected in list mode with the data acquisition software. During offline analysis the data may be sorted into different combinations to provide the best way for the estimation of the detector parameters: TOF versus PH, PS versus PH, and PS versus TOF. The original data were collected utilizing 8192 channels for each ADC. The TOF channel width was 0.1173 ns.

2.1.3 Time-Correlated Background

Fission events counted with any detector have random time distribution. One may define the following possibilities correlation between FF and ND events.

Real coincidences In this case, the ND and chamber pulses belong to the same fission event.

Time-Independent Background— $S_{tib}(i)$ The natural γ-ray background or gammarays from the β-decay of FF are counted by the ND and this pulse coincides with the FF pulse. These events have an exponential time-dependence due to the random nature of the fission process. This background may be calculated with Eq. (2.2):

$$S_{tib}(i) = N_0 \cdot \exp(-i\tau A_f), \quad N_0 = \frac{\sum_{i=i_1}^{i=i_2} N_i \cdot \exp(i\tau A_f)}{i_2 - i_1 + 1},$$
 (2.2)

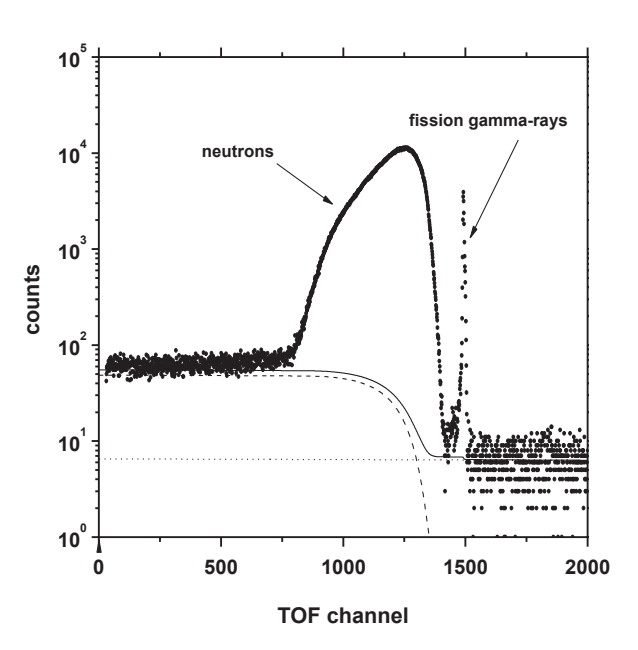
where N_i is the measured TOF distribution versus the channel number i; i_2 , i_1 are the channel numbers at the right side of the prompt gamma-ray peak used for the calculation of the time-independent background N_0 , $A_{\rm f}$ is the FF count rate, and τ is the channel width.

Random coincidences— $S_{tcb}(i)$ (time-correlated background) In this case, the ND and chamber pulses belong to a different fission event, but they conserve a time correlation due to the time dependence of the neutron and γ -rays from FFs. This background may be calculated according to:

$$S_{\text{tcb}}(i) = \tau \cdot A_{\text{f}} \cdot \exp(i\tau A_{\text{f}}) \sum_{j=i+1}^{i_{\text{max}}} N_i^{\text{cor}}, \qquad (2.3)$$

where $N_{\rm i}^{\rm cor}$ is the TOF spectrum after subtraction of $S_{\rm tib}(i)$. All background components are given in Fig. 2.5.

Fig. 2.5 TOF spectrum after $(n-\gamma)$ discrimination and background components for the ²⁵²Cf source. The channel width is 0.485 ns. *Lines* show the background components: time-independent background (*dotted*) and random coincidence (*dashed*). *The full* line is the sum of both background components



Finally, the net effect may be found according to:

$$S_{ef}(i) = \exp(i^{\tau} A_f) \cdot \left[N_i^{cor} - S_{tcb}(i) \right]. \tag{2.4}$$

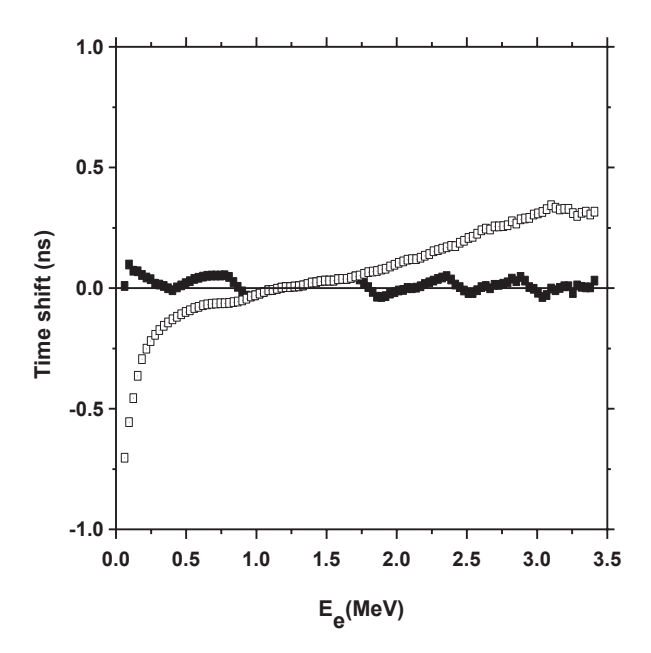
All spectra and corrections should be calculated in time scale. The time correlated background in [21] was rather small due to the low activity of the 252 Cf ($A_{\rm f}$ <4·10⁴ ff/s). So, it was smaller than 5% at an energy of about 0.5 MeV.

2.1.4 Time Shift in Neutron Detector

The time reference in the TOF spectrum is indicated by the prompt γ -peak. This time reference can also be used to observe a time shift depending on the PH. Mainly this effect is connected with nonideal operation of the CFD.

The effect has been investigated with the present setup. The data were collected in a matrix PH versus TOF of 128×2048 channels. In the first step, the centers of gravity for prompt γ -ray events have been calculated for each PH bin. This peak position information was used to compensate the time shift. Of course, we assumed that the main contribution in the time shift appeared due to the CFD operation which is common for protons and gamma-rays. In Fig. 2.6, the position of the prompt γ -ray peak is shown before and after the time shift correction. The residual difference may be explained due to the finite width of the TOF channel (0.1173 ns).

Fig. 2.6 The position of the prompt γ-rays before (*open*) and after time reference correction (*full squares*)



The specific effect may appear due to the fact that the ND pulses have a non-"standard" shape (the beginning part of the ND pulse may be distorted by multiple scattering in the scintillator). However, this effect was not investigated in details.

2.1.5 Neutron-Gamma Discrimination and its Influence on Result

The ND on the basis of NE213 liquid, and crystal scitillators like stilbene, antracene have very useful properties—PS (contribution fast and slow components) depends on particle. This fact allows us to reduce gamma rays' background very much. In the same time it may provide an additional distortion effect.

The difference between PS for protons and electrons at low proton energy, < 1 MeV, reduced very much due to small amount of emitted photons and big fluctuation. The example is shown for two amplitudes of signal ~ 0.2 MeVee and 0.4 MeVee of electron energies (Fig. 2.7). At low energies, the PS distributions are overlapping, and as a result some part of protons' events (neutrons) may be lost.

There is another factor—multiple scattering inside scintillator, which may change the PS for neutron counting. It has already been discussed in Sect. 2.1.4.

For example, the detector was exposed with 5 MeV neutron. After first scattering, it produced ~4 MeV protons and residual ~1 MeV neutron may give new pulse inside scintillator. If the scintillator has average size ~10 cm, the second pulse will be shifted relative to first one on ~7 ns. It is not clear how this PS will be treated by analyzing device. These events may be removed from counting procedure and



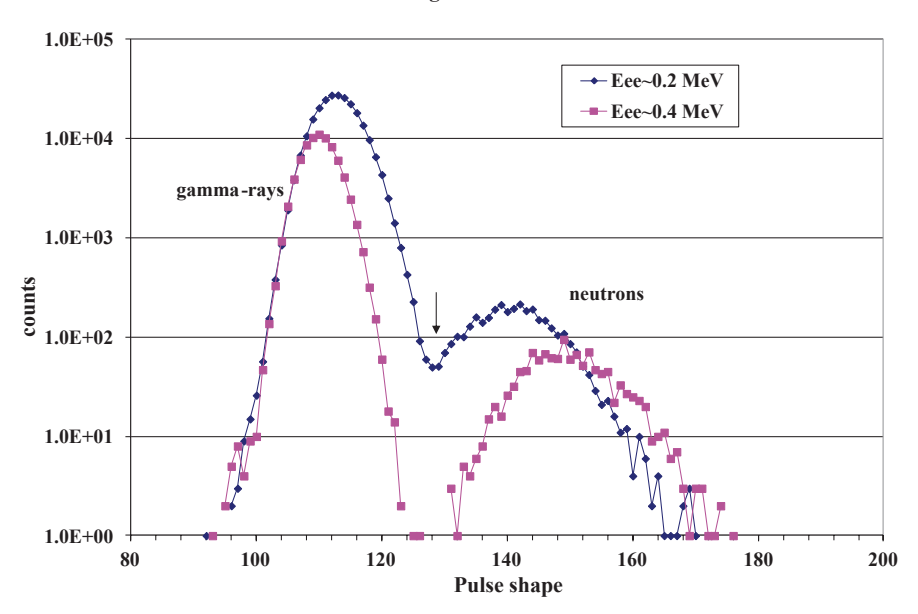


Fig. 2.7 Pulse shape distribution for selected amplitude of signals. *Arrow* shows the discrimination level for pulse-shape selection

provide an additional correction for detector efficiency. So, the very important parameter of neutron spectrometer–detector efficiency should be measured for each detector and electronics setup.

The major portion of γ -radiation in nuclear fission is emitted, as mentioned above, in less than 10^{-9} s. This radiation is generally called prompt γ -rays. The presence of isomeric γ -transitions, however, leads to the delay of some part of the γ -rays. The total amount of this type of γ -rays for 235 U (th) and 252 Cf (sf) is \sim 5–10% and emission time is 10^{-9} – 10^{-3} s. This effect may provide overlapping of delayed γ -rays and high energetic neutrons if the flight path is \sim 1 m. The contribution of high energetic portion of neutron spectrum reduces according to exponential law with $T\sim$ 1.3–1.4 MeV. Delayed γ -rays may destroy experimental result very much, so the neutron-gamma discrimination is extremely important factor for experimental investigation.

2.1.6 Measurement of the ND Efficiency

Relative ND efficiency (energy shape) can be measured if the neutron flux is known with high accuracy. There are three methods which allow us to reach accuracy of 2–3%: (1) measurements of neutron yield from "monoenergetic neutron sources" D(d,n), T(p,n), $^7Li(p,n)$ [9]; (2) measurement of angular distribution from (n,p)

scattering; and (3) 252 Cf standard [25, 21, 12]. Another so named "white neutron sources" like Be(d,n), B(d,n), Al(d,n) have very big data spread and do not allow us to reach accuracy of <20%.

Several new ideas were suggested recently. In [24], symmetric reactions $A+A \rightarrow (2A-1)+n$ were investigated. When the projectile and the target are identical, the reaction cross section is the same for a forward angle, θ , and the supplementary back angle, $180^{\circ}-\theta$, in the center-of-mass system. The neutron energies at these corresponding angles in the laboratory system are different. This allows the relative efficiency at two energies to be measured directly. A series of efficiency ratios can be measured by changing the beam-energy and angle. If more than one excited state is populated, each excited state can be used to determine efficiency ratios.

The ⁶Li(⁶Li,*n*) is a very attractive candidate to cover the energy range 1–20 MeV with an input Li ion energy of 4–12 MeV. The low energy range of the efficiency may be determined relative to the ²⁵²Cf spontaneous fission neutron spectrum standard. By using reactions with large positive *Q*-values, we may move up to 20 MeV neutrons.

However, this optimistic conclusion was not supported in experiments, the yield of high energetic neutrons (15–20 MeV) from $^6\text{Li}(^6\text{Li},n)$ and other investigated reaction is extremaly small. The D(d,n) reaction gave positive answer for deutron energy ~ 9 MeV (~ 12.5 MeV neutron energy). It is not clear that this reaction can be used for higher energy due to the competition of double break-up reactions.

The detailed discription from [25] is given here as an example of the experimental method and procedure for efficiency measurements with "monoenergetic reactions."

The detector efficiency was measured on a TOF spectrometer on the basis of the EGP-10M accelerator at the Institute of Physics and Power Engineering. The source of neutrons was the $T(p, n)^3$ He reaction, whose differential cross-section is now accurately known ($\sim 3\%$) both for the neutron emision angle and for a wide range of proton energies.

The neutron spectra from the above-mentioned reaction were measured at different angles θ , to determine the relative efficiency, so the angular distribution of the neutron yield was measured as a function of θ and of the energy of the incident protons. The neutron yield obtained for a given angle, taking into account the background, may be deirmined as:

$$S = \sigma(\theta) \cdot \varepsilon(E_n), \tag{2.5}$$

where S—area of the neutron peak, $\sigma(\theta)$ —differential cross-section of the T(p,n) reaction, $\varepsilon(E_n)$ —detector efficiency for neutrons of energy E_n .

Nine sets of independent measurements were carried out at flight length L=2 m, three of them with proton energy $E_p=3.3$ MeV, one with $E_p=3.9$ MeV, one with $E_p=5$ MeV, one with $E_p=6$ MeV, and three with $E_p=7$ MeV. Two sets of measurements with $E_p=3.3$ MeV were performed at L=2.75 m. For each proton energy, neutron spectra were measured for 11 angles between 0° and 150° with step 15° .

This detailed investigation was organized to cover the widest possible energy range in determining efficiency, to get satisfactorily overlapping efficiency points measured from diffrent proton energy, and verify reproducibility of the results.

Several monitors were used for normalization results: "long" counter, single scintillator detector, and current integrator. Finally, the experimental points covered neutron energy range 0.5–7 MeV.

Additional efforts were made to investigate background neutrons from solid targets used as neutron sources. The tritium from the targets was burnt out by evaporation in a vacuum at 400°. At proton energies, E=5-7 MeV, an important contribution of background was produced from accompanying reactions Ti(p,n) and Mo(p,n) on the base material of the target.

In work [13], ${}^{7}\text{Li}(p, n)$ reaction as a "monoenergetic" neutron source was applied for NE213 detector callibration in energy range 0.2–4 MeV. The efficiency was measured relative to a calibrated long counter. The data were corrected for second neutron group above 0.7 MeV and break-up neutrons above 2.5 MeV. Above 4 MeV, the efficiency was estimated on the basis of Monte Carlo (MC) symulation.

An associated particle method is applied with the $T(d,n)^4He$ and $D(d,n)^3He$ neutron source reactions which have high positive Q-value. The 4He and 3He particles are counted by an associated particle detector within a cone fixed by the charge particle detector entrance aperture. The neutrons corresponding to these helium ions hit the detector. The ND should cover the neutron cone corresponding to an associated particle. The detector events, the associated particle events, and the coincidence between the detectors are counted in this experiment. The efficiency can be calculated as a ratio of these numbers. The main advantage of this method can be summarized as follows [31, 15]:

- This method allows to measure the absolute efficiency with highest accuracy (1...2%);
- There is no need to determine any solid angle, an efficiency of the associated particle detector, and other geometrical factors;
- All background components of the detector are practically completely suppressed.

A limited neutron energy range (3–6 MeV and \sim 14 MeV) is the main drawback of the method.

The energy of neutrons scattered on hydrogen nuclei changes from zero to E_0 according to the scattering angle and their intensity may be estimated with high accuracy on the basis of the scattering cross section. Hence, with only a 14 MeV neutron source one may measure the detector efficiency in the energy range 1–12 MeV. The hydrogen sample is placed near the 14 MeV neutron source and the detector whose efficiency should be measured inside the shielding collimator moves around the sample. The hydrogen scintillator as a scattering sample coupled with PM tube and TOF technique is used to reduce the background and to eliminate the scattering on carbon nuclei.

The description of method one may find in [16 and references in it]. The scattering sample was stilbene scintillator H=3 cm and R=0.5 cm, coupled with phototube

FEU-13. The "stop" signal was taken from anode of scatter-detector. "Start" signal was produced from detector whose efficiency should be measured. The investigated detector was placed in moveble shielding and may be placed at scattering angles 30–66°. The distance from 14-MeV target to scatter l=15 cm, the flight path L=2 m.

Let us incorporate following parameters and functions which are important for correct estimation of the efficiency. We should define the $N(\theta)$ —number of neutrons counted by detector placed at angle θ . The energy of these neutrons is connected with incident neutron energy E_0 and scattering angle θ by equation $E_1 = E_0 \times \cos^2(\theta)$.

$$N(\theta) = N_1(\theta) \cdot \left(1 + \frac{N_2}{N_1}\right) \cdot \eta(E_1) \cdot \xi(E_1) \cdot \varepsilon(E_1) \cdot \Omega, \tag{2.6}$$

where $N_1(\theta)$ —neutron flux outside the scatter-detector at angle θ in direction of the main detector, N_2/N_1 —contribution of neutrons with energy E_1 after multiple scattering which may reach detector, $(1-\eta)$ —share of proton recoils which was lost due to edge effect, $(1-\xi)$ —share of protons which was lost due to resolution in scatter, ε —efficiency of the detector under investigation, and Ω —solid angle.

After simplification of integrals, which determine $N_1(\theta)$, function one may estimate with the following relation:

$$N_{1}(\theta) = F \cdot N_{H} \cdot \sigma(\theta) \cdot \left(1 - \frac{8\Sigma(E_{0})R}{3\pi}\right) \cdot \exp(-\Sigma(E_{1}) \cdot l_{1})$$
 (2.7)

$$l_0 = \left(\frac{8}{3}R - \pi R^2 \Sigma(E_0)\right) / \left(\pi - \frac{8}{3}R \cdot \Sigma(E_1)\right),$$

where l_0 , l_1 —average path of input and output neutrons inside the sample and $\Sigma = N_{HC} \cdot R$ —macroscopic cross sections for carbon and hydrogen.

The uncertainties of Eqs. (2.6) and (2.7) is less then $(\Sigma \cdot R)^2$. In our case, $(\Sigma \cdot R) \sim 0.3\%$.

In case of small sample, the distribution of the input neutron flux inside sample is constant, and $l_0 = l_1 = \frac{8R}{3\pi}$, and does not depend (l_1) very much on emission angle. The small dependence one may estimate with simple relation:

$$l_1 = \frac{8R}{3\pi} + |\Delta l| \cos(\theta), \tag{2.8}$$

where
$$\Delta l = -\frac{\sum (E_0)R^2}{4\left(1 - \frac{8\sum (E_0)R}{3\pi}\right)}$$

In case of R = 0.5 cm $\Delta l/l \sim 1.7$ %.

Table 2.1 Energy dependences of functions for (n,p) scattering method

E ₁ (MeV)	$l_1(\theta)$ (cm)	$\exp(-\Sigma(E_1)\cdot l_1)$	η
2	0.427	0.908	0.972
4	0.428	0.920	0.973
6	0.429	0.948	0.982
8	0.429	0.948	0.986
10	0.430	0.955	0.990

The edge effect correction can be calculated with equation [16]:

$$\eta = \frac{2}{\pi} \left(\arcsin(1 - x^2)^{0.5} - x(1 - x^2)^{0.5} \right), \tag{2.9}$$

where $x = \frac{r}{2R}$, r—the proton range where energy higher than discriminator bias will be produced $r = 1.63 \cdot E^{1.8} \cdot 10^{-3}$ cm, E-proton energy in MeV.

In paper [16], it was shown that $N_2/N_1 < 2 \cdot 10^{-2}$ %, and $(1-\xi) < 0.3$ %. So the main function which is important for efficiency estimation is self-absorption of output neutrons with energy E_1 and edge effect. These functions are collected in Table 2.1. Correction for edge effect was calculated for fixed threshold energy 0.9 MeV.

In work [16] the main problem limited of experimental uncertaities $\sim 10\%$ at high neutron energy (small proton energy) was rather high level of noncorrelated background. At small neutron energies 2–4 MeV uncertaities were $\sim 4\%$ (mainly statistical component).

2.1.7 Time Resolution and "Bin" Corrections

The PFNS in time scale has very sharp shape at high energy. This fact provides big sensitivity of TOF and energy distribution which is mesured in particular experiment to time resolution of the spectrometer. An additional distortion effect is connected with time channel width of spectrometer. With increasing the energy, time interval defined by channel width is transformed to bigger energy interval. The PFN spectrum shape is changing very much inside this interval (at high neutron energy), and average energy corresponding to this collected amount of event is sensitive to shape of investigated distribution.

There are several methods for estimation of these correction. I shall discribe the method applied in [21]. In this approach, the experimental distribution was simulated by the MC method.

The experimental TOF events as integer value N_t estimated with channel width δt are collected in list mode file. During the off-line analysis, these "integer" time events are transformed to "real" velue applying "random generator" for example rand(NN).

$$t = N_t + \delta t \cdot (0.5 - rand(NN)). \tag{2.10}$$

Real time value *t* is trasformed into energy *E* taking into account relativistic relation. Each energy event is distributing into energy array. This array is extrapolating to the "fixed-step" energy scale for simplification of the future analysis.

The simulation procedure is repeating all these steps. At first step, we selected energy from interval $E_1 - E_2$ according to equation:

$$E = E_1 + (E_2 - E_1) \cdot rand(NN).$$

The "weight" of this event is calculated according to shape of PFNS, for example Maxwellian M(E). The TOF t can be estimated with this energy and known flight path L, and may be treated as an experimental value after an additional smoothing due to time resolution.

Let us assume that our time resolution may be described by law $\varphi(t-t_0)$. The "real" time is estimated with Eq. (2.11):

$$rand(NN) = \int_{0}^{t} \varphi(x - t_0) dx.$$
 (2.11)

If $\varphi(t-t_0)$ is normal distribution, one may use the analytical function. In this case parameter t will have normal distribution with average value t_0 and variance σ :

$$t = t_0 + \sigma \cdot sqrt(-2\ln(rand(NN)) \cdot \sin(2\pi \cdot rand(NN))). \tag{2.12}$$

The parameter t is transformed to integer value N_t with channel width δt . The simulated event is treated as experimental event with weight M(E). All TOF events return to energy scale starting with Eq. (2.10) to prepare the simulated array $M_s(E)$. The time resolution and bin correction may be found with Eq. (2.13):

$$\alpha(E) = \frac{M_s(E)}{M(E)}. (2.13)$$

Both corrections may be estimated independently to check the influence of both components. "Time resolution correction" may be found if we will use reduced channel width in simulation procedure. "Bin correction" may be found for reduced time resolution. Both components and total correction are shown in Fig. 2.8. Original parameters δt and σ were reduced in factor 100 for separate components estimation.

2.1.8 Additional Time Spread for "Solid Sample" Experiment at Low Input Energy

The "solid sample" experiments are realized with a neutron source operating in pulse mode. $^{7}\text{Li}(p, n)$ neutron-produced reaction is very popular because of high yield of neutrons with energy ~ 0.5 MeV, and simple construction of Li-target. The

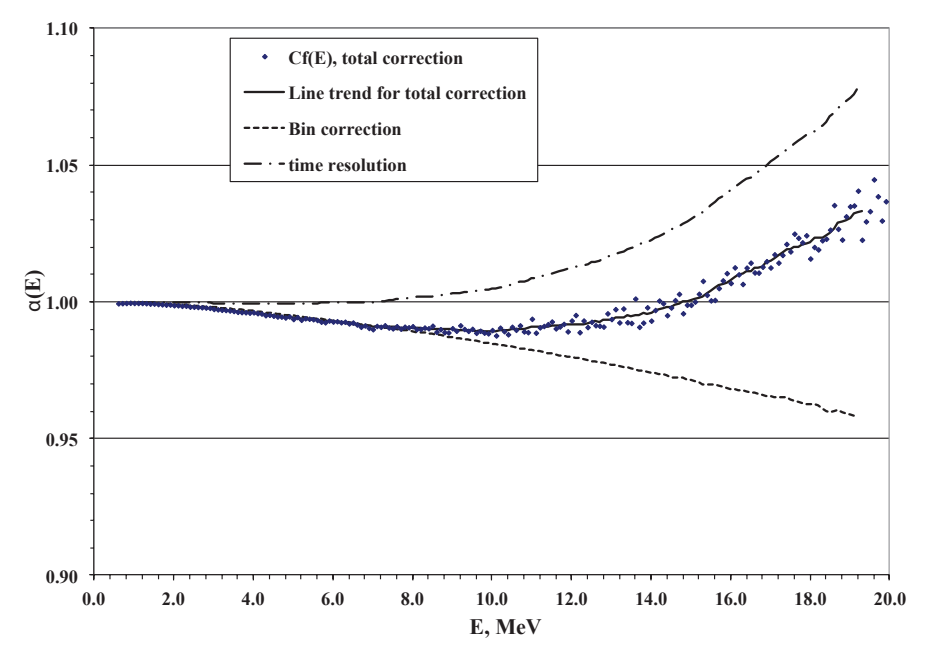


Fig. 2.8 Time resolution and "bin" corrections. Total (*solid line* and *dots*), resolution (*dashed-dotted*) and "bin" correction (*dotted*). *Solid line* shows smoothed dependence calculated on the basis of MC estimated points

realization of this experiment is also rather simple: one should have pulsed Van-de-Graaff accelerator with energy ~ 2.2 MeV. As a rule, LiF layer is applied as rather stable material.

The time resolution of the neutron TOF spectrometer applied for PFNS measurements with this type experiment consists of the following components: detector resolution, shape of the pulse beam from the accelerator, and neutron distribution inside the sample.

The cylindrical metal U-sample with outside diameter 3.0 cm, inside diameter 2.12 cm, and height 2.41 cm was used in experiment [20]. This sample was placed at 5.0 cm from the neutron produced target at 0° angle.

The circular disk sample (diameter 7.68 cm, thickness 0.5 cm) was applied in [33].

Time distributions in both samples simulated by MC method are shown in Fig. 2.9. The pulse mode of VdG accelerator provided time resolution ~ 1 ns in experiment [20] and ~ 0.6 ns in experiment [33]. However, in reality, neutron distribution inside the sample and experimental time resolution was much worth. It is interesting, that cylindrical sample provide double bump distribution.

An additional convolution of "sample time resolution," pulse mode of accelerator and detector resolution was simulated by MC method to verify the procedure.

The experimental prompt gamma-rays' peaks, produced inside neutron target (Li(p, p') and F(p, $\alpha\gamma$) reactions), and time distribution of fission gamma-ray (real

Fig. 2.9 Comparison between the TOF distribution of the input neutrons inside samples for different experiments [20] (full symbols) and [33] (open symbols). TOF time-of-flight

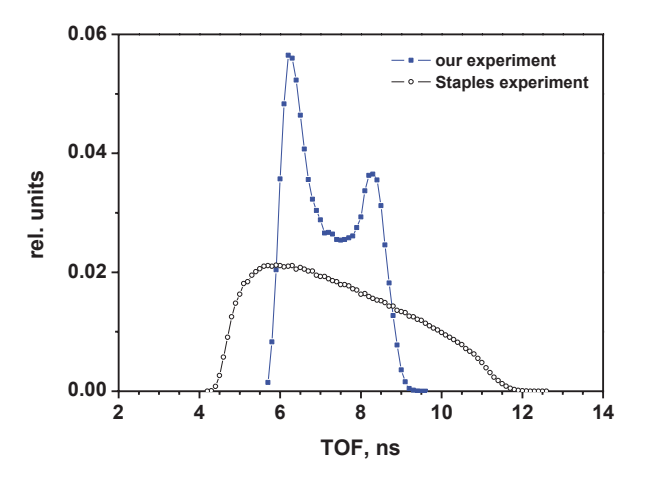
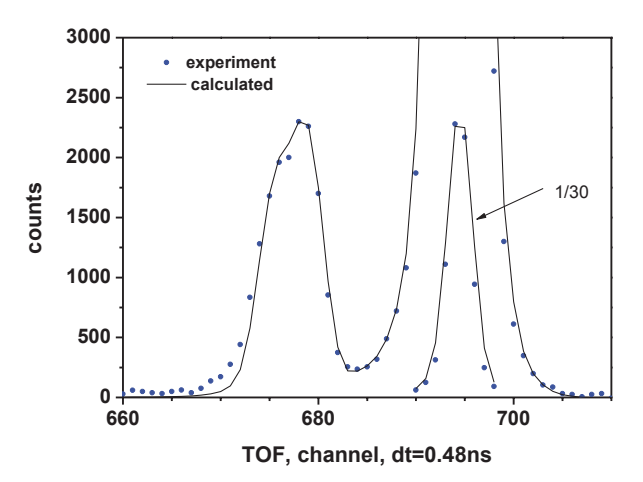


Fig. 2.10 Prompt-gamma rays peaks measured with threshold ~1.2 MeVee in [20] points. The channel width is 0.47 ns. The convoluted result is shown by *line*. The target gamma-rays (*right*) peak gives the detector resolution and proton pulse width. The prompt fission gamma-rays gives total time resolution including neutron spread inside the sample (Fig. 2.9). *TOF* time-of-flight



time distribution for fission neutron experiment) are shown in Fig. 2.10. Experimental and simulated results are in reasonable agreement.

2.1.9 Possible Distortion Factors in Second Type Experiment

The total integration FF experiment (first type) is very important for practical application and understanding of neutron emission mechanism. However, the possibility for understanding of the neutron emission nature is very limited. Much more important information for fission physics may be extracted from second type experiment, in which neutron spectra and multiplicity are investigated relative to selected FF, and properties of emitted neutrons are estimated relative to FF direction, masses, and TKE.

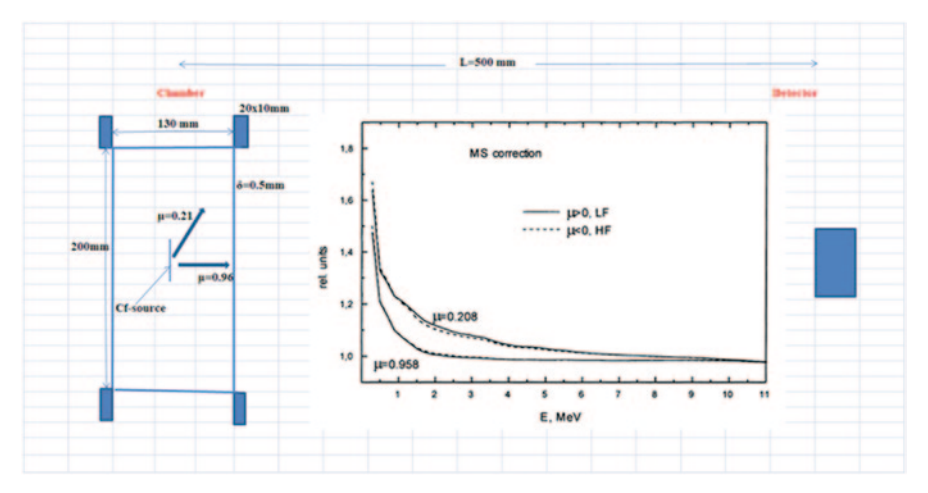


Fig. 2.11 Corrections [18] for neutron spectra measured at different direction of FF in ²⁵²Cf experiment [6]

The main problem for the second type of experiment is rather low count rate, and as consequence, authors are obliged to reduce flight path. The smaller distance between fission source and ND does not allow us to use good shielding. ND looks on all environment material around fission neutron source, and detected neutron spectrum is overloading with big contribution of background due to multiple scattering on environment. Two experiments realized in IRMM 1986 [6] and in PNPI 2009 [34] will be discussed in this section.

In experiment [6], FF detector was made using the gridded IC. This equipment allows them to measure FF angle, kinetic energy, and masses for ²⁵²Cf(sf). For timing of FF events, the common cathode was used giving the resolution <0.7 ns FWHM together with ND. The fragment angle information is determined as a cosine of angle between the normal of the electrodes and the path of FF. The ND 4"×1" NE213 scintillator, is located on the axis of the IC. The distance between the ²⁵²Cf(sf) source and the ND was 0.51 m. Drawing of the experimental setup is shown in Fig. 2.11.

Another type of the FF detector was used in [34] for investigation of neutron emission from 235 U(th) fission. In this experiment, the TOF was measured for paired FF. The "time zero" was generated by the signal from multiwire proportional detector (MWPD) located within 7 mm from fissile target, and parallel to the target plane. The MWPDs were also used for the simultaneous detection of FF, the determination of its direction, and time arriving to "stop" detector. The 16 rectangular MWPD were placed on 14 cm from FF source. The size of each was $H \times d = 7.2 \times 3.8$ cm.

PFNs were detected by two neutron counters (stilbene $D \times h = 5$ cm $\times 5$ cm and 4 cm $\times 6$ cm coupled with Hamamatsu PMT R6091) placed at 90° between them at 50 cm flight path. Detectors were shielded with lead (3 cm thickness cylinder) and polyethylene (4 cm thickness cylinder).

Factor	IRMM, 2010	PNPI, 2009
Flight path (m)	3	0.5
Neutron detector (Ø*h) (cm)	100×5	$5\times5, 4\times6$
FWHM (ns/m)	0.6	~3
Shielding n-detector	Yes	Yes, but thickness is small
Scattering on chamber	Small, MC simulation	Big? It was not estimated
Possible distortion effect	It is not known	Due to angle integration
Comparison with previous results	Agreement inside uncertainties	Contradiction

Table 2.2 Comparison of recent PFNS experiments

MC Monte Carlo

Main parameters of experiments' first type IRMM [22] and second type PNPI [34] for measurement of PFNS at thermal fission ²³⁵U are collected in Table 2.2.

In both experiments, ²³⁵U PFNS was measured with scintillation ND calibrated relative to ²⁵²Cf standard. In both cases, authors used neutron-gamma discrimination. The most important advantages for IRMM experiment are: much better time resolution, shielding around ND reduced very much scattering on detector environment, an additional scattering on the source materials was simulated by MC, FFs were integrated during experiment (efficiency of fragment's counting ~98%). These advantages are typical for first type experiments.

The authors of second type of experiment should understand obvious disadvantages, which they should pay for realization of these experiments. The development of the proper corrections which may remove possible distortion effect is very important part of these experiments.

Let us demonstrate the influence of several factors which are important for second type experiments.

Authors [6] tried to reduce amount of material near FF source. The wall thickness of the IC was 0.5 mm. However, the flanges have rather big thickness.

Neutron emission relative to FF direction is the function of energy and emission angle. The multiple scattering correction, taking into account neutrons energy-angular dependence relative to FF direction was investigated in [18].

This effect will be discussed also in following sections. As a rule the effect of multiple scattering is estimated on the basis of angular integrated PFNS and isotropic angular distribution. However, this is rather simple assumption.

Let us check two FF directions, marked in Fig. 2.11 as $\mu \sim 1$ and $\mu \sim 0.2$. According to Fig. 2.12a, b, the total amount of neutrons emitted at $abs(\mu) \sim 1$ to 7 times higher than for emission at $\mu \sim 0$, and average neutron energy is much higher also.

So, in both cases neutron after the scattering on flanges may be counted by ND. However, when FF is moving in detector direction, the intensity of neutron and their energy is higher in comparison with the neutrons which are moving into flanges direction, and after the scattering may be counted in the detector, but with smaller energy. When FF is moving on flange direction the scattered neutrons will have higher energy and intensity in comparison with direct counting in the ND.

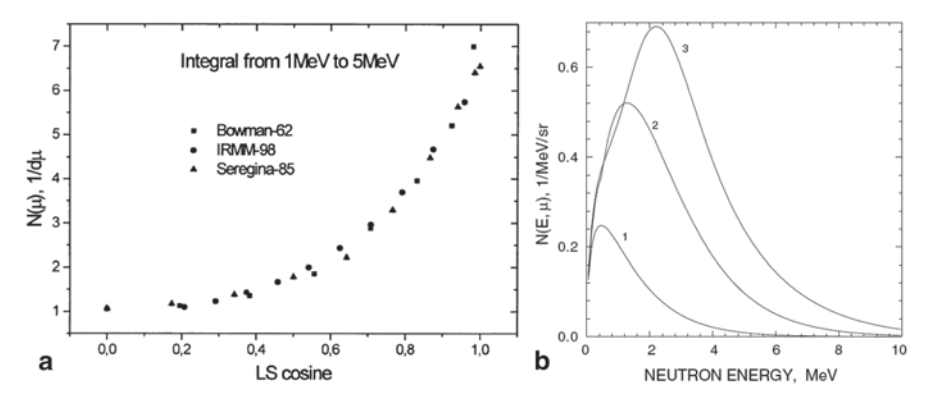


Fig. 2.12 a Angular distribution of PFN for 252 Cf for both fragments. The experimental data were integrated in energy range 1–5 MeV [18]. **b** PFNS for 235 U in Laboratory System (LS) relative to FF direction. *I* spectrum for μ =0, 2μ =-1 (mainly from heavy fragments), 3μ =1 (mainly from light fragments). The figure was taken from [30]

The MC code developed for simulation of this effect [18] confirms this qualitative argument. The correction for multiple scattering in fission source environment depends very much on FF emission angle and particular structure of the FF detector (insert in Fig. 2.11).

So, the conclusion is: the scattering on the fission chamber material may change shape of PFNS very much. The distortion effect is very sensitive to peculiarity of the construction and should be estimated for each experimental setup.

The azimuth angle in [34] was fixed by the "belt" of FF counters. This factor was also simulated by MC method.

It was assumed that fission neutrons are emitted from fixed FF with CMS energy $E_{\rm v}$. The Maxwellian spectrum with parameter T was assumed for CMS. So if we did all integration correctly we should have Watt distribution for LS. The ratio of simulated spectra with angle selection to expected Watt function is given in Fig. 2.13. This simple calculation demonstrates the scale of effect. The real correction factor requires special efforts and investigations.

Limited number of angles between FF and neutron direction and as a consequence big step for $\Delta\mu$ for second type experiment is an additional problem for investigation. Eight pairs of FF detectors, covered angles for $-1 < \mu < 1$ were used in experiment [34]. Analytic relations describing experimental data [34] were constructed as function of energy and cosine of neutron emission in LS. The angular integrated spectrum was estimated by numerical integration of angular dependence with different steps $d\mu = 0.1$, 0.01, 0.001. Result as a ratio to known function is shown in Fig. 2.14.

So, we should conclude that there are several factors which may destroy result of "differential FF experiment" very much. Therefore, these experimental data cannot be used for evaluation of "standard" spectra.

After proper corrections this result should be compared with "total FF integrated experiment" for verification of the experimental procedure.

Fig. 2.13 Distortion effect due to non-complete azimuth integration

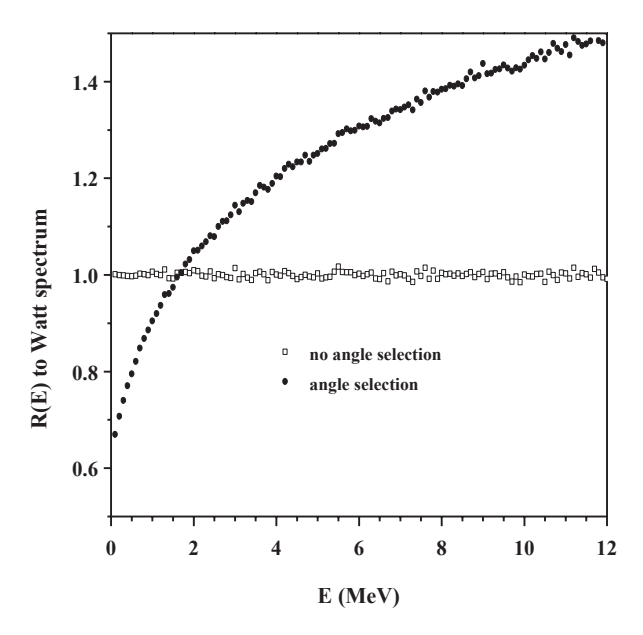
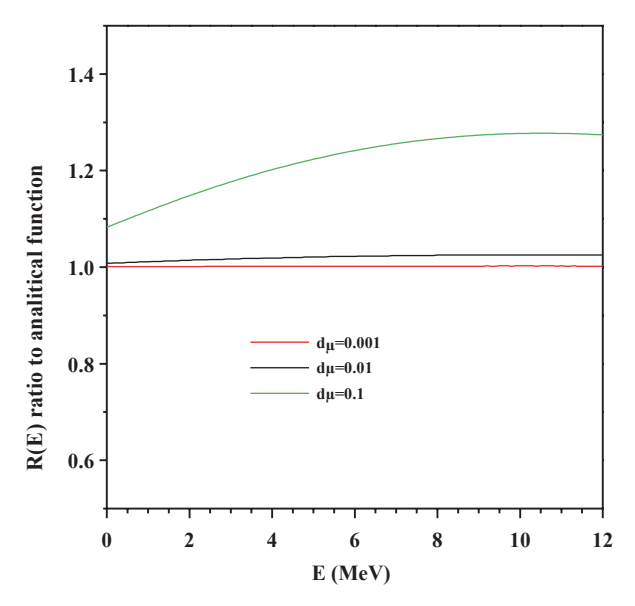


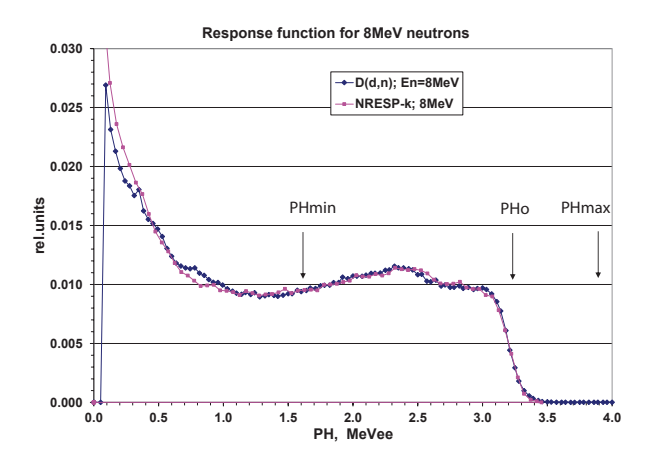
Fig. 2.14 Influence of the step for cosine integration



2.1.10 The Calculation of the Detector Efficiency with High Accuracy up to 20 MeV

²⁵²Cf as a standard neutron source for calibration of ND was discussed before. It is very useful for practical applications. The only problem is "high energy limit." Neutrons with energy > 10 MeV have very low intensity, and this energy range is practically unavailable for experimental research.

Fig. 2.15 RFs for NE213 neutron detector. *Blue points* experimental data measured with D(d,n) reaction, *Red* Monte Carlosimulation. *PH* pulse height



Reaction of (n, p) scattering, which is the main process in hydrogen ND, is the standard. This fact stimulated the MC simulation of neutron interaction with detector and estimation of its efficiency. However, there are some obstacles for realization of these calculations with high accuracy. The contribution of (n, α) (Q=-5.7 MeV) reaction at neutron energy >10 MeV relative to (n, p) scattering is ~10%. Alphaparticle produces small PH just near the detector threshold or less. The light output for alpha particle is unknown. The second problem is the scattering on the detector environment. The estimation of the intensity of this process and neutron angular-energy distribution is rather difficult task. So the extrapolation of the MC calculation to neutron energy ~20 MeV can be done with accuracy not less than ~10%, or even higher.

Different experimental methods for measurement of ND efficiency mentioned above have got the similar problem, it is very difficult (or even impossible) to reach high energy limit ~ 20 MeV.

Can we suggest new idea; realize new method to increase accuracy for calculating procedure? The question was answered in [23] with incorporation of "dynamic threshold" for an additional data selection.

The detector used in [23] consists of an NE213 scintillator with a diameter of 12.7 cm and a depth of 5.08 cm. The scintillator is coupled to an RCA 4522 PM tube with a 12.7 cm diameter photocathode. Modern techniques allow us to collect all detected event in list mode. So each event is available for off line analysis.

For realization of this method we should have following information for each event: TOF, PH, and PS. After traditional neutron-gamma selection we may analyze only neutron events.

The response function (RF) for 8 MeV neutrons produced with D(d,n) reaction is shown in Fig. 2.15. The calculation was made with code developed in **Physikalisch-Technische Bundesanstalt** (PTB) (NRESP) [8] and modified in [21]. An additional selection requires the following information: PH_0 , PH_{\min} , and PH_{\max} (see Fig. 2.15)

 PH_0 is highest proton energy (without energy resolution) for selected neutron energy. $PH_0 = L(E)$ —where L(E) is light output for proton energy E (Fig. 2.16). Hence,

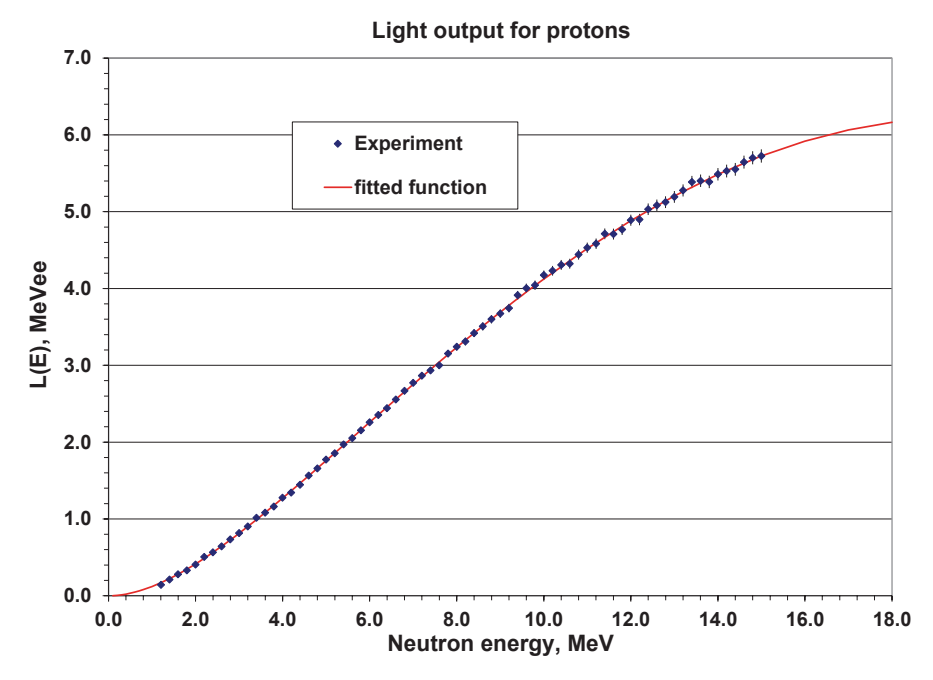


Fig. 2.16 Experimental and calculated light output L(E) dependence

the edge of the RF may be found from TOF information. The highest proton energy (average) is equal energy of input neutrons. One may also incorporate $E_1 = E\cos(\theta)^2$, $PH_{\min} = L(E_1)$, and $PH_{\max} = PH_0 + 3*\sigma(PH_0)$. The angle θ may be selected in such way to remove all unwonted events. In analysis of [23] $\theta = 45^\circ$ was used.

The selection of events for each neutron energy was made with simple equation:

$$PH_{\min} < L < PH_{\max}. \tag{2.14}$$

Functions L(E) and $\sigma(L)$ are very important and should be measured for each detector. Both dependences were measured with "white" neutron spectrum from reaction B(d, n) in thick target, $E_{\rm d}$ =7.44 MeV, angle of neutron emission 60° and are shown in Figs 2.16, 2.17. It is important to highlight that we do not need information about spectrum shape. The high neutron yield at high energy is the only request for reaction selection.

The light output data were fitted with Eq. (2.15) [21]:

$$L(E) = (a_0 + a_1 \cdot E) \frac{E^2}{E + E_0},$$
(2.15)

where a_0 , a_1 , E_0 are fitted parameters. The a_1 parameter is connected with nonlinearity of electron pulses (saturation in PM tube).

PH resolution function was measured in the same experiment, and was describe by Eq. (2.16):

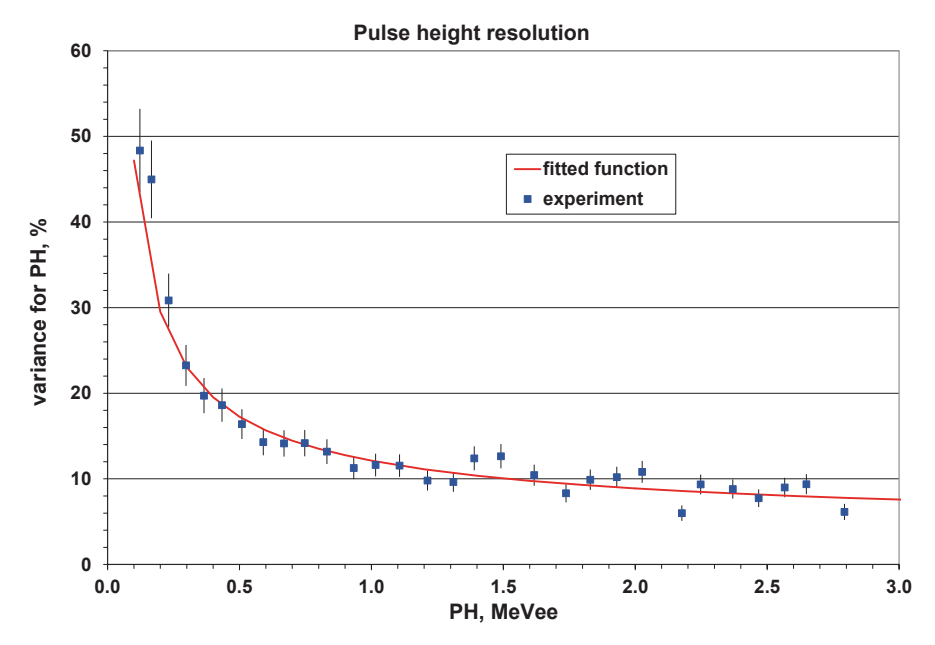


Fig. 2.17 Experimental and calculated resolution function. PH pulse height

$$\sigma = L \left(\alpha^2 + \frac{\beta^2}{L} + \left(\frac{\gamma}{L}\right)^2\right)^{0.5}$$

$$\alpha = 0.04, \beta = 0.11, \gamma = 0.10.$$
(2.16)

Experimental and calculated resolution functions are given in Fig. 2.17.

The absolute efficiency NE213 detector was measured with 252 Cf neutron source as was discussed above. FF count rate was 2.28×10^4 1/s, total time resolution 2.4 ns, flight path 4.108 m. Time channel width was 0.209 ns (4096 channels). Run time was ~100 h. Count rate for net effect ~1 1/s and total background ~120 1/s.

The MC simulation was realized with code NEFF7-DYTH modified from NEFF7 [8]. It is interesting to demonstrate how new selection changes traditional TOF distributions.

The TOF spectra with neutron-gamma selection are given in Fig. 2.18. These spectra were collected with following conditions: $\cos(\theta) = 0.1$, $PH_{\text{max}} = 20$ MeVee. So, the spectrum was measured with "traditional" condition and has "traditional" shape.

The selection condition $\cos(\theta) = 0.1$ and $PH_{\text{max}} = PH_0 + 3 \times \sigma(PH_0)$ changes results very much. Time-independent background as in Fig. 2.18 for gamma-rays distribution was transformed to time-dependent function (Fig. 2.19) at low energy range.

The working selection $\cos(\theta) = 0.707$ and $PH_{\text{max}} = PH_0 + 3 \times \sigma(PH_0)$ changed very much and high energetic part of TOF distribution (Fig. 2.20). Background was reduced (practically concealed) in comparison with data in Fig. 2.18.

32 2 Experiment

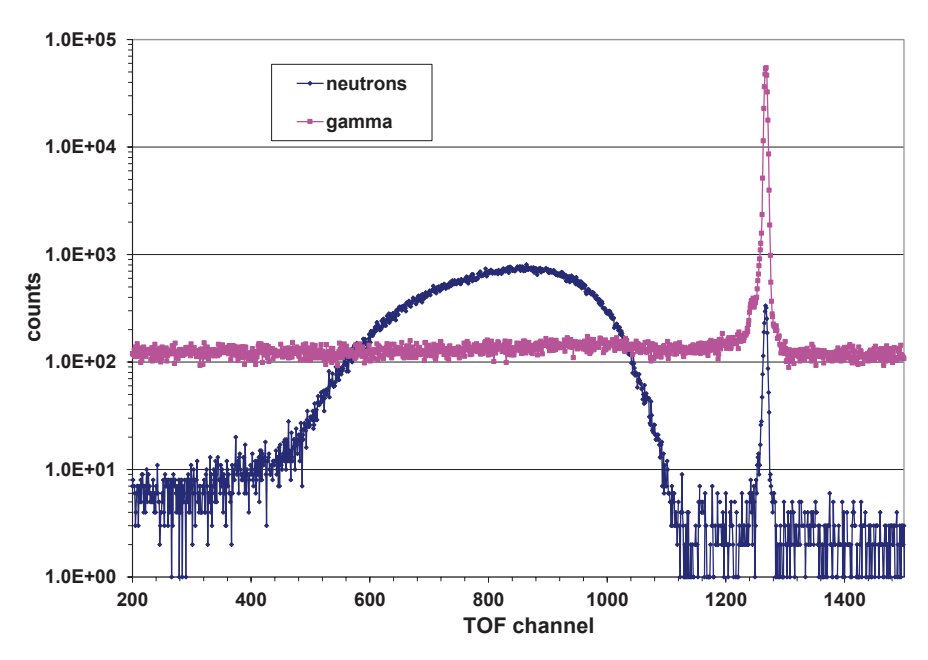


Fig. 2.18 TOF distribution without an additional selection. TOF time-of-flight

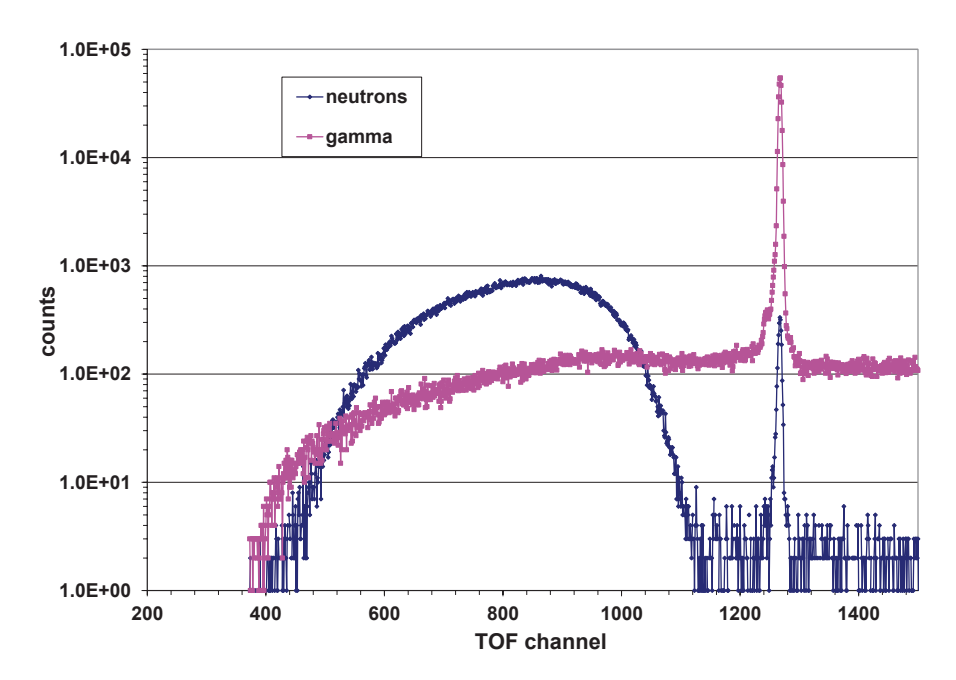


Fig. 2.19 Selection for high energy limit $(\cos(\theta) = 0.1, PH_{max} = PH_0 + 3\sigma)$. TOF time-of-flight

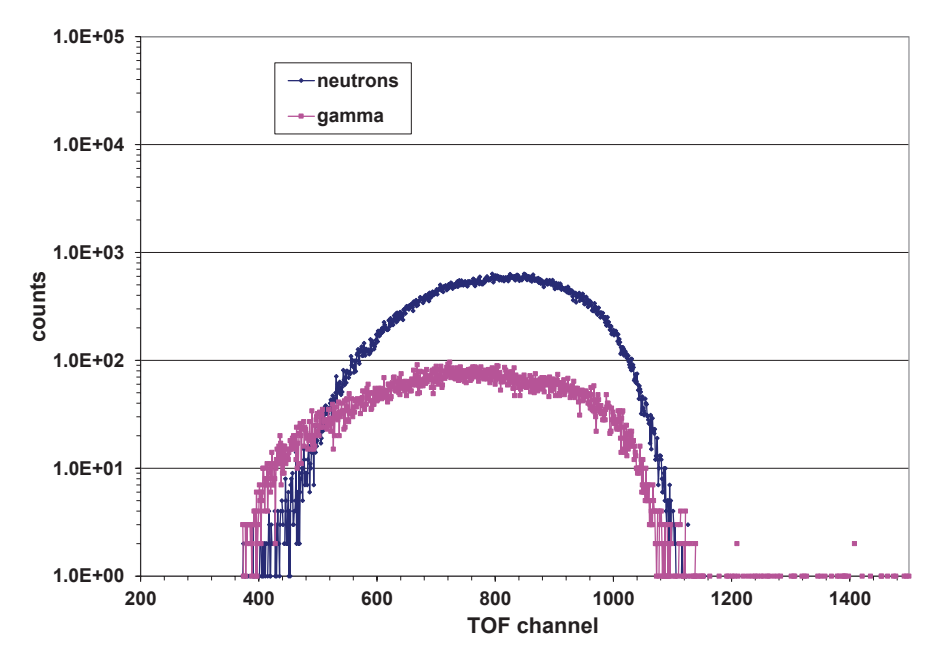


Fig. 2.20 TOF for working selection $(\cos(\theta) = 0.707, PH_{\text{max}} = PH_0 + 3\sigma)$. TOF time-of-flight

Experimental and calculated efficiency are shown in Fig. 2.21. The average ratio $R=E/C=1.012\pm0.004$ for energy range 1.3–6 MeV. So, MC simulation reproduces the energy dependence and absolute value with high accuracy. The resolution function is very important parameter for MC simulation in energy range E_n <2 MeV. Calculated results are very sensitive to absolute value and energy dependence $\sigma(L)$.

In whole energy range \leq 20 MeV only one reaction (n, p)-scattering is responsible for formation of the detector efficiency after application of the dynamic threshold. It seems that the contribution of multiple scattering inside detector, interaction with detector environment may be reduced very much.

In the energy range <8 MeV, the agreement between experimental and calculated results is perfect. Hence, we may expect that extrapolation to energy range 10–20 MeV may be done with high accuracy also. However, the first application of this method was realized recently [23]. Therefore, the detailed investigation of uncertainties in whole energy range is very important.

2.1.11 Correction for Neutron Scattering in FF Detector

In experiment [22], the PFNS ²³⁵U(th) was measured relative to ²⁵²Cf. Both neutron sources were placed inside the same detector—IC with greed for ²³⁵U and simple fast two electrodes camber for ²⁵²Cf (see Fig. 2.22). The Cf source was shifted

34 2 Experiment

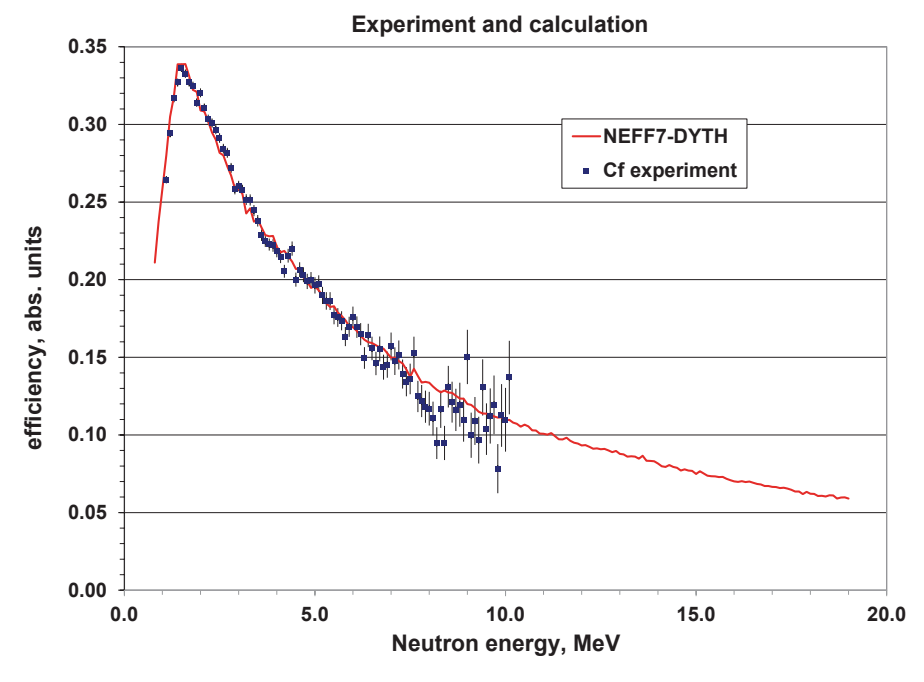
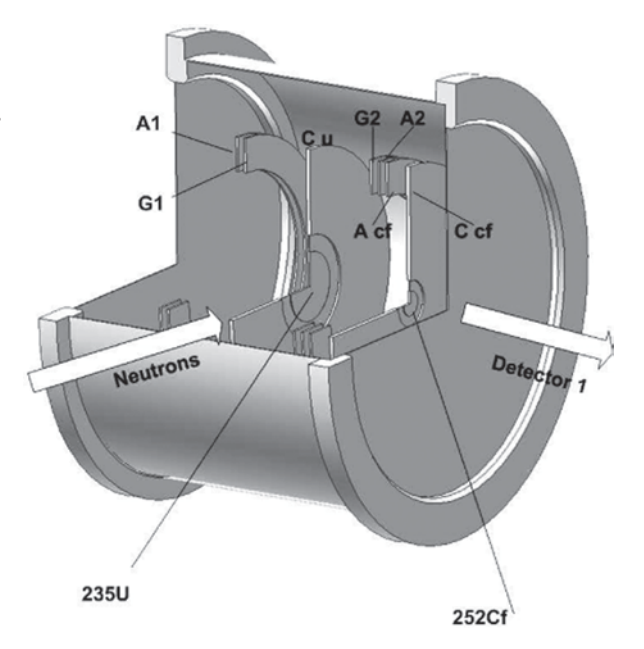


Fig. 2.21 Experimental and calculated efficiency with "dynamic threshold." MC simulation was multiplied with factor 1.012

Fig. 2.22 Drawing of the fission ionization chamber. C_u , C_{cf} cathodes with U and C_f neutron sources, A_1 , A_2 , G_1 , G_2 anodes and grids for U section of ionization chamber, A_{cf} anode for C_f section





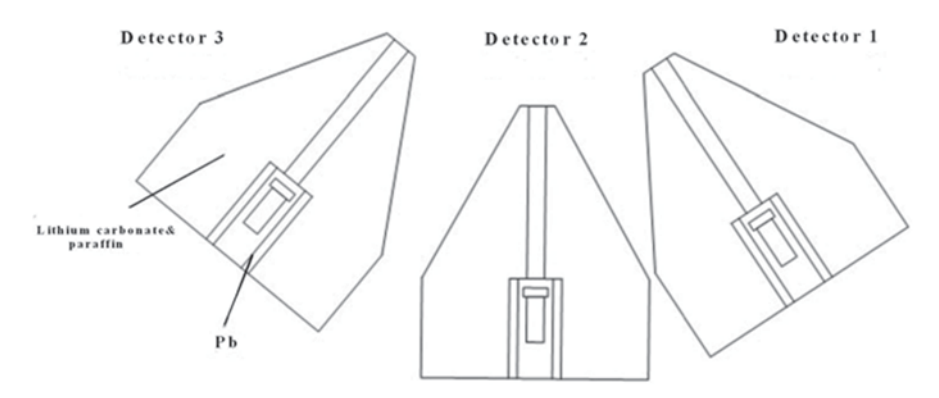


Fig. 2.23 Experimental setup in [22]

relative to U source by 5 cm. The total height of the chamber was 13.5 cm and diameter 18.0 cm. The chamber walls were 0.5 mm. Flanges are the most heavy part of the chamber. The orientation of the chamber relative to NDs is shown in Fig. 2.23.

The geometry of the experiment was selected to reduce amount of material around U and Cf layers. Both sources were placed in the same counter, which should provide the similar scattering effect, which should be reduced due to relative nature of experiment. The correctness of this assumption was verified with MCNP simulation.

The correction factors for multiple scattering and attenuation were calculated with the MCNP code as a ratio of a neutron spectrum emitted from the source surrounded by the real chamber to a spectrum calculated without chamber materials. The neutron spectra were calculated separately for the U- and Cf-sources. The ratio of the correction factors of Cf to U is shown in Fig. 2.24 for the three detectors. The experimental data were multiplied by these functions to cancel the contribution of the scattered neutrons on the fission chamber materials.

The difference $\sim 5\%$ was found for different detector's position. The corrected experimental data are the same inside error bars for three detectors (Fig. 2.25).

This fact may be used as a good argument for correctness of the procedure. Of course, one should assume that neutron emission is isotropic relative to the neutron beam direction.

2 Experiment

Fig. 2.24 Ratio of multiple scattering corrections for Cf-and U-sources

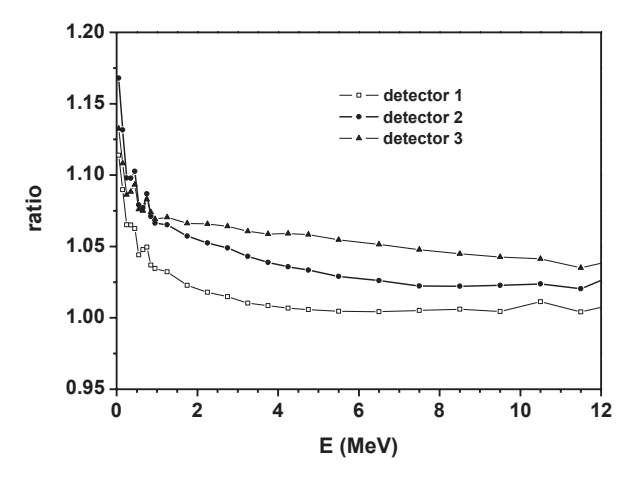
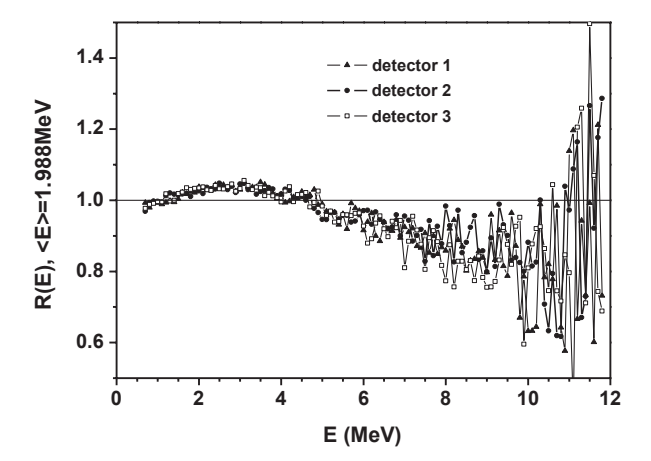


Fig. 2.25 The PFNS measured by three detectors as a ratio to Maxwellian with average energy $\langle E \rangle$ = 1.988 MeV



2.1.12 Multidetector Systems and "Cross Talk Correction"

Several experimental setups were developed recently "Spider" (LANL), "Chi-nu" (LANL), and "Crystal ball" (Michigan Un). The description of these experiments can be found in Proceeding of ND2013 (New York, in press), or in internal reports. The particular features of these experimental equipments are large amount of neutrons detectors without any shielding between them.

The PFNS experiments have got rather low count rate, in particular if we would like to measure differential characteristics, depending on masses, TKE, emission angle and so on. Therefore, the best solution according to authors' opinion is multi-detector systems which will reduce experimental time.

However, authors will be faced with two rather dangerous problems in this type of experiments:

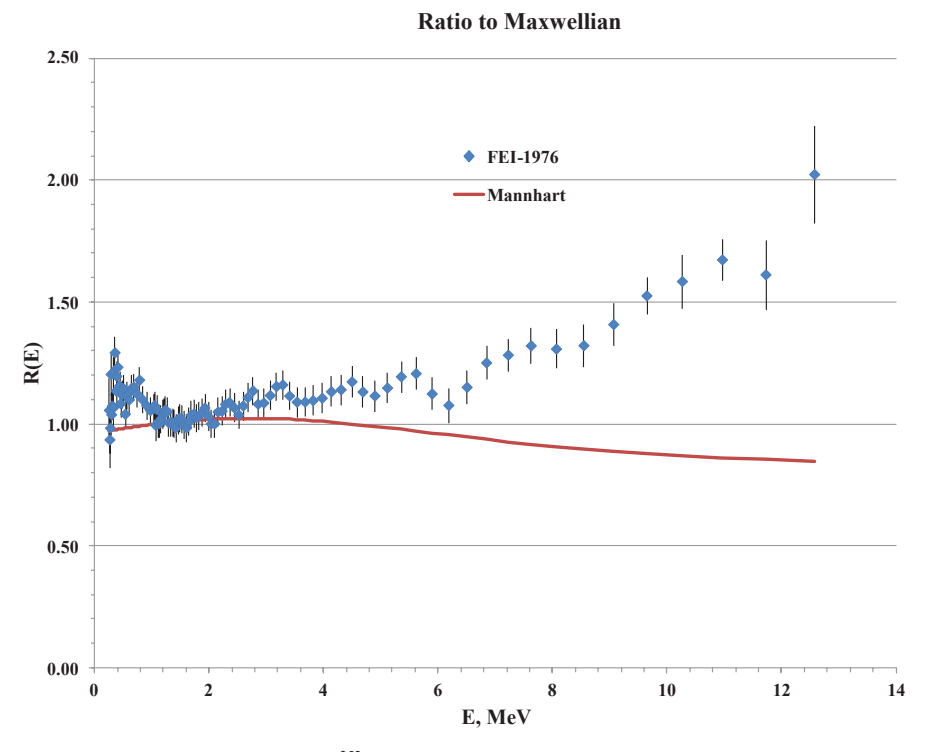


Fig. 2.26 Ratio to Maxwellian for ²⁵²Cf, according to experimental data from [25] and Mannhart evaluation [29]

- 1. huge amount of scattering materials around each non-shielding detector;
- 2. "cross talk" interaction inside the multidetectors system.

I would like to remind the result of [25], authors understand very well the task of the experiment—measurement ²⁵²Cf with high accuracy as a standard. They took into account practically all factors which may destroy results. They explained in details how the necessary corrections were estimated. Nevertheless, the measured spectrum [25] contradicts very much all another experiments and was not taken into account during the evaluation procedure.

The experimental and evaluated results are given in Fig. 2.26. There are two problems: an additional amount of neutrons $\sim 20\%$ measured at low energy < 2 MeV, very strong overestimation of evaluated function $\sim 70\%$ at ~ 10 MeV neutron energy.

It seems that low energy surplus is connected with an additional scattering on the detectors (FF and neutron) environment. Authors tried to remove his background contribution, but final result demonstrates that they did not estimate the correction in proper way. ND without shielding is a particular detail of this experiment.

An additional factor which destroys high energy part may be connected with rather poor time resolution. And again, the authors understand the importance of 38 2 Experiment

this correction. They applied new method (see Ref. [25]) for its estimation. However, the result was negative.

The similar peculiarity—extra amount of materials (PMT, high voltage divider, glasses, scintillation container, and so on for neighbourhood detectors) which are visible by single scintillator—is a particular feature of multidetectors systems, and this may provide the effect similar to the one discussed above.

It is important not only energy reduction due to neutron scattering on the environment materials but time delay due to an additional flight path. High energetic neutron due to this factor will be detected as low energy event, increasing contribution of low energy part of PFNS.

It seems that this effect destroyed the experimental spectrum in [13]. In this experiment "gas scitillator" was applied as an FF counter. The FF and NDs were placed in different experimental halls, and they were visible through the collimator in wall. The problem is that ND may see not only fission source but also PMT and divider. The experimental spectrum [13] was overloaded with low energy neutrons.

Main part of neutrons will be counted several times due to re-scattering in multidetector system. However, the contribution of this background may be reduced with so named "cross talk" correction. Only one neutron event may be counted inside selected TOF interval.

The problem is that several neutrons are emitted in fission process. The neutron multiplicity and average energy depend very much on angle between FF direction and ND (see Fig. 2.12). Hence, the "cross talk" correction may provide an additional selection of neutrons and will disturb measured PFNS. The proper simulation of all these processes is not simple task—many parameters and functions are unknown. Therefore, all corrections should be verified if possible.

2.2 Macroscopic Experiments

Several remarks should be done before discussion about macroscopic experiments. An important method of fast neutron dosimetry is the use of radiometric monitors for measuring neutron fluence and fluence rate. By selecting a set of reactions each of which is sensitive to a different neutron energy range, information on both the shape and the magnitude of neutron spectrum is obtained. This is not only the important method but also the only way to measure the neutron energy distribution inside different nuclear reactors.

Application of this approach to PFN (assuming that their spectra are known) gives a possibility to verify different dosimetry reactions, and confirms uncertainties of these cross sections. After long time efforts, nuclear society collected independent information about dosimetry reactions' cross sections. Hence, this gave a possibility to apply this method for verification of the PFNS shape evaluation.

The information about neutron spectrum may be obtained from comparison of a measured reaction cross section σ_{exp} with calculated one σ_{cal} corresponding to energy <E>:

$$\sigma_{\text{cal}} = \frac{\int S(E)\sigma(E)dE}{\int S(E)dE}; \langle E \rangle = \frac{\int ES(E)\sigma(E)dE}{\int S(E)\sigma(E)dE}.$$
 (2.17)

This is a more complicated procedure (not only calculated but experimental also) than which was discussed above. It is necessary to highlight, that in case of agreement of microscopic evaluation and macroscopic results, one may proclaim that PFNS *are correct*. One should understand that the application of macroscopic data for direct evaluation of PFNS may stimulate wrong conclusion. Only microscopic experimental data should be applied for PFNS evaluation. Macroscopic data should be applied for their verification (demonstration of weak points).

Practically only ²⁵²Cf(sf) and ²³⁵U(th) PFNS were investigated in macroscopic experiments. The experimental setups are rather different for both reactions. One feature is common: both contains fissile material and activated sample.

The NBS ²⁵²Cf(sf) [26] facility consists of a californium source made up of CfO₂ bead in an aluminum pellet singly encapsulated in a aluminum pellet singly encapsulated in this-walled stainless steel cylinder. The source is raised into the irradiation position between nearly identical foils to be irradiated. In this compensated beam geometry, the first-order distance error is associated only with the separation of detectors; the uncertainties in source deposit to foil distance become second order. The samples are high purity, natural metal foils having 12.7 mm diameter and range in thickness 0.13–0.25 mm.

In experiment [28], the 252 Cf source was encapsulated in double zircaloy cylinder with outer dimensions of 10 mm in diameter and 10 mm in height. The wall thickness of cylinder was 1.5 mm. Spectrum perturbation due to the encapsulation were of the order of 1%, somewhat dependent on the neutron energy. The beginning activity of different sources was $\sim 10^8 - 10^9$ 1/s. The similar construction of 252 Cf source was used in experiment [3].

The ²³⁵U experimental setup is more complicate. The draw of NBS source is shown in Fig. 2.27. This device operates at the center of a 30 cm diameter spherical cavity located in the center of graphite thermal column. The fission neutron source consists of two coaxial disks of ²³⁵U (16 mm diameter, 0.13 mm thick) placed outside of cadmium box. The fluence rate gradient of PFN in between sources' disk was measured by simultaneous irradiation of 13 nickel foils each 0.076 mm thick.

The similar ($\sim 4\pi$ construction) has been used in CEN/SCK Laboratories [11]. The size of MARK sources are shown in Fig. 2.28. In the configuration called MARK-II, there was no aluminum cladding around the 235 U foil. In MARK-IIA and MARK-III, the aluminum clad thickness was 0.7 mm inside the uranium and 0.75 mm outside. The most important correction—so-called "wall return" was investigated in detail. The corrections due to scattering on Cd-tube and Al-clad were also applied.

In experiment [14], a big fission plate 31.2 cm in diameter and 1.1 cm thick was used to produce neutrons from thermal induced fission of 235 U. The fission plate was made of 90% 235 U enriched uranium oxide aluminum (UO₂–Al). This disk

40 2 Experiment

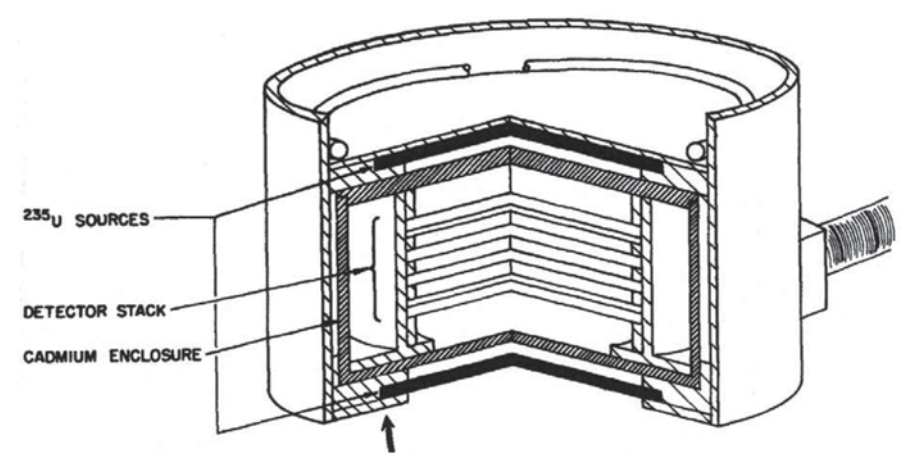


Fig. 2.27 The NBS facility used for irradiation in ²³⁵U(th) PFNS

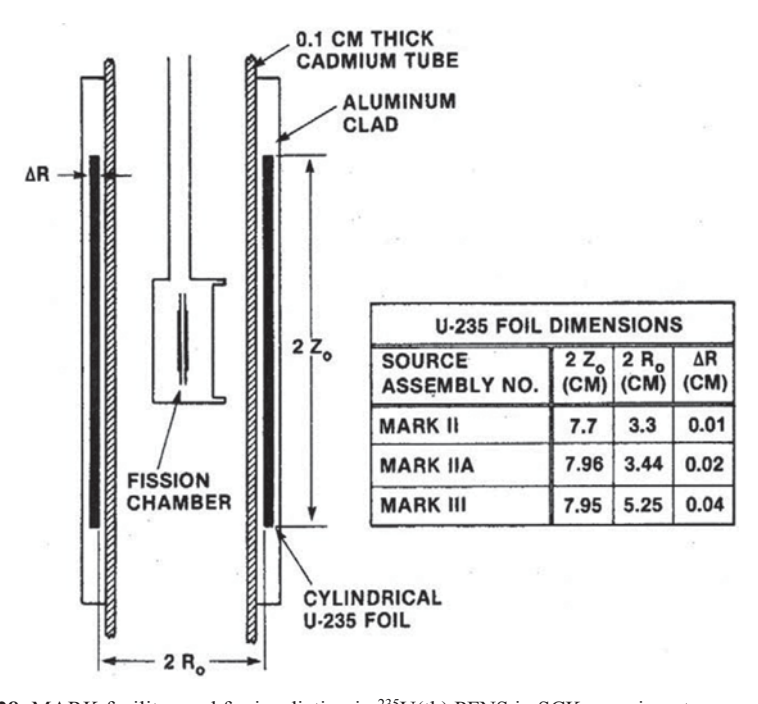


Fig. 2.28 MARK facility used for irradiation in ²³⁵U(th) PFNS in SCK experiments

was placed in Al clad. The total amount of uranium was 1.1 kg. The advantage of this setup is very high flux of PFN $(1.8 \cdot 10^9 \text{ 1/cm}^2/\text{s})$. The disadvantage is big possible distortion effect due to multiple scattering in this source. However, authors

References 41

average energies of response Eq. (2.17)					
Reaction	$\langle E \rangle$ (MeV) (252Cf)	²⁵² Cf	²³⁵ U		
	(E) (Me) (C)	$\sigma \pm \delta \sigma$, mb	$\sigma \pm \delta \sigma$, mb		
19 F(<i>n</i> ,2 <i>n</i>)	14.37	0.0161 ± 0.0005	0.0072 ± 0.0010		
27 Al (n,p)	6.32	4.88 ± 0.11	4.133 ± 0.074		
$^{46}\mathrm{Ti}(n,p)$	6.37	14.07 ± 0.25	11.5 ± 0.2		
$^{48}\text{Ti}(n,p)$	8.76	0.425 ± 0.008	0.31 ± 0.02		
$^{51}\mathrm{V}(n,\alpha)$	10.38	0.0390 ± 0.0009	0.0243 ± 0.0006		

 1.4650 ± 0.026

 0.2218 ± 0.0042

 0.6887 ± 0.0135

 0.2210 ± 0.0064

 117.5 ± 1.5

 147.5 ± 2.5

 197.4 ± 2.7

 20.9 ± 1.2

 325.7 ± 5.3

 0.749 ± 0.038

 1210.0 ± 14.5

 1361.0 ± 21.6

 1.13 ± 0.07

 108.2 ± 1.4

 147.6 ± 7.0

 188.2 ± 2.3

 18.9 ± 2.0

 312.0 ± 7.2

 0.458 ± 0.023

 1200.0 ± 22.8

 1359.0 ± 28.5

 0.530 ± 0.026

 0.1563 ± 0.0035

 0.0860 ± 0.0065

Table 2.3 Experimental average cross sections for ²⁵²Cf and ²³⁵U according to evaluation [39] and average energies of response Eq. (2.17)

concluded after the simulation by MC method, that the neutron spectrum with the fission plate is close to PFNS of ²³⁵U, and that the effect of neutron scattering by the wall, floor, and window of reactor are negligibly small above 1 MeV.

The experimental efforts during last 30 years collected big data set (35 average reaction cross sections) for ²⁵²Cf and ²³⁵U (Table 2.3).

References

 $^{56}\text{Fe}(n,p)$

 59 Co(n, α)

 58 Ni(*n*,*p*)

 63 Cu(n,α)

 90 Zr(n,2n)

93Nb(n,n')

 93 Nb(n,2n)

 $^{115}In(n,n')$

 204 Pb(n, n')

 235 U(*n*,*f*)

 238 U(*n*,*f*)

 $^{237}Np(n,f)$

7.99

8.70

4.52

7.61

14.7

3.01

3.05

5.42

2.13

3.32

2.51

11.69

- Baryba VYa, Kornilov NV, Semenova NN (1977) Neutron source on the basis of ²⁵²Cf VANT. Vopr at Nauki i Tech 5:45 (in Russian)
- Baryba VYa, Kornilov NV, Sal'nikov OA (1979) Fission prompt neutron spectrum of ²³⁸U for energy 14.3 MeV. Preprint FEI–947
- Benabdallah H, Paic G, Csikai J (1982) Measurement of some average cross sections in ²⁵²Cf neutrons. Report for nuclear data for science and tech., 6–10 Sept 1982, Antwerp, p 421
- Boykov GS, Dmitriev VD, Kudyaev GA et al (1991) PFNS from ²³²Th, ²³⁸U, ²³⁵U at neutron energy 2.9 and 14.7 MeV (low and upper the threshold for emission fission). Yad Fyz 53:628. EXFOR 41110, 41094
- 5. Boykov GS, Dmitriev VD, Svirin MI et al (1994) Measurement and evaluation of spectrum and average energy for neutrons from reaction $^{235}U(n, f)$. Phys At Nucl 57:2047
- Budtz-Jorgensen C, Knitter H-H (1988) Simultaneous investigation of fission fragments and neutrons in ²⁵²Cf(sf). Nucl Phys A 490:307
- 7. Cub J, Finckh E et al (1989) NIM A274. 217
- 8. Dietze G, Klein H (1982) Gamma-calibration of NE213 scintillation counter. Nucl Instrum Methods Phys Res 193:549. (G. Dietze and H. Klein, PTB-ND-22 Physikalisch-Technische Bundesanstalf)

42 2 Experiment

 Drosg M (2000) DROSG-2000: neutron source reactions. https://www-nds.iaea.org/ drosg2000.html (IAEA-NDS-87, Rev.) Accessed 6 Jan 2000

- Dyachenko PP et al (1977) Fission neutron spectrum ²³⁵U at thermal energy. Atomnaya Energiya 42:25 (Russian)
- 11. Fabry A, Minsart G et al (1982) The mol cavity fission spectrum standard neutron field and ite application. Fourth Symposium on Reactor Dosimetry, Washington, DC, March 1982
- 12. Trotter DEG, Maneses FS, Tornow W et al (2009) Neutron detection efficiency determinations for the TUNL neutron–neutron and neutron–proton scattering-length measurements. Nucl Instrum Methods Phys Res Sect A 599:234
- Green L, Mitchell JA, Steen NM (1973) The Californiun-252 fission neutron spectrum from 0.5 to 13 MeV. Nucl Sci Eng 50:257
- 14. Kobayashi K, Kobayashi T (1990) Measurement of ²³⁵U fission spectrum-averaged cross sections for some threshold reactions. Report NEANDC(J)-155/U, IDNC(JPN)-142/L
- 15. Kornilov NV (1999) Neutron detectors. Landolt-Bornstein, I/16A
- 16. Kornilov NV, Pljaskin V (1974) Measurement of the detector efficiency relative to scattering on hydrogen scintillator. Preprint FEI-496, Obninsk, (Russian)
- 17. Kornilov NV, Zhuravlev BV, Salnikov OA et al (1980) PFNS for ²³⁸U at neutron energies 6-9MeV. In: Proceedings of the 5th conference on neutron physics, Kiev, 15–19 Sept, Vol. 2 (TsNIIAtominform, Moscow, 1980), pp. 44–49
- 18. Kornilov NV, Kagalenko AB, Poupko SV et al (2001) New evidence of an intense scission neutron source in the ²⁵²Cf spontaneous fission. Nucl Phys A 686:187–203
- 19. Kornilov NV, Fabry I, Hambsch F-J et al (2006) High intense, standard neutron source for time of flight experiments. Scientific report 2005, EUR 22239 EN, p 45
- Kornilov NV, Hambsch F-J, Fabry I et al (2007) New experimental and theoretical results for the ²³⁵U fission neutron spectrum. In: Proceedings of the International Conference for Nucl. Data for Sci. and Tech., ND2007, Nice, France, April 2007
- Kornilov NV, Fabry I, Oberstedt S et al (2009) Total characterization of neutron detectors with a ²⁵²Cf source and a new light output determination. Nucl Instrum Methods Phys Res Sect A 599:226–233
- 22. Kornilov NV, Hambosh F-J, Fabry I et al (2010) The ²³⁵U(*n*, f) prompt fission neutron spectrum at 100 K input neutron energy. Nucl Sci Eng 165:117–127
- 23. Kornilov NV, Grimes S, Mossey T (2013a) Scintillation neutron detector with dinamic threshold. Report for NEMEA-7/CIELO workshop, 5–8 Nov 2013
- Kornilov N, Mossey T, Grimes S et al (2013b) Development of a new method for measurementof neutron detector efficiency up to 20 MeV. Report for nuclear data conference 2013, New York
- 25. Kotelnikova GV, Kuzminov BD, Lovchikova GN et al (1976) The energy spectrum of neutrons from spontaneous fission of ²⁵²Cf in the energy range 0.5–7 MeV. INDC (CCP)-81/U
- Lamaze GP, McCarry ED, Schima FJ (1982) Integral reaction rate measurements in ²⁵²Cf and ²³⁵U fission spectra. Report for nuclear data for science and tech., 6–10 Sept 1982, Antwerp, p 425
- Lovchikova GN, Trufanov AM, Svirin MI et al (2000) Energy spectra of neutrons accompanying the emission fission of ²³⁸U. In: Proceedings of the XIV international workshop on nuclear fission physics. Obninsk, 12–15 Oct 2000 (State Scientific Center of Russian Federation—Institute for Physics & Power Engineering, (SSC RF IPPE), Obninsk, Russia, 2000) pp 72–82
- 28. Mannhart W (1982) Measurements and evaluation of integral data in the Cf-252 neutron field. Report for nuclear data for science and tech., 6–10 Sept 1982, Antwerp, p 429
- Mannhart W (1987) Evaluation of the Cf-252 fission neutron spectrum between 0 MeV and 20 MeV. IAEA-TECDOC-410, p 158
- 30. Maslov VM, Poprodzinskij YV, Baba M et al (2003) Prompt fission neutron of ²³⁸U(*n*, f) above emission fission threshold. Eur Phys J A 18:93
- Shpakov VI, Kuzminov VN (1988) Development of the time correlated associated particle method for absolute measurements of reaction cross-sections. IAEA-TECDOC-469, p 89

References 43

 Smirenkin GN, Lovchikova GN, Trufanov AM et al (1996) Energy spectra of neutrons accompanying the emission fission of ²³⁸U. Phys At Nucl 59:1934

- 33. Staples P, Egan JJ, Kegel GHR, Mittler A, Woodring ML (1995) Prompt fission neutron energy spectra induced by fast neutrons. Nucl Phys A 591:41
- Vorobyev AS, Sherbakov OA, Pleva YS et al (2009) Measurements of angular and energy distributions of prompt neutrons from thermal neutron-induced fission. Nucl Instrum Methods Phys Res Sect A 598:795–801
- 35. Watt B (1952) Energy spectrum of neutrons from thermal fission of ²³⁵U. Phys Rev 87(6)
- 36. Werle H, Bluhm H (1972) Prompt fission neutron spectra (Proc. Cons. Meeting, Vienna 1971), IAEA, Vienna 65
- Catalogue nuclear physics (02/2010) mesytec GmbH&Co. KG. www.mesytec.com, detector electronics and readout system
- 38. Zhuravlev B, Kornilov N et al (1974) Neutron source on the basis of ²⁵²Cf and gas scintillator. Prib I Tech Exp 2
- Zolotarev KI (2003) Evaluated cross section data from russian reactor dosimetry file. INDC(NDC)-448, 25

Chapter 3 Microscopic Spectra Evaluation. Semiempirical Modeling

A lot of experimental results were published in physical journal (not only the internal reports) after first Watt's paper. The prompt fission neutron spectrum (PFNS) was measured for main isotopes, and input neutron energies from thermal till ~ 14 MeV (even up to $\sim \! 200$ MeV). Problems connected with experimental procedure were discussed in Sect. 3.2. There are a lot of factors destroying results. How to select correct experimental data, how to find the possible systematic uncertainties, or mistakes?

The PFNS experiments give information about spectrum shape and total neutron multiplicity. As a rule the total multiplicity, measured in these experiments has rather low accuracy, and may be used as secondary factor for verification of data normalization and extrapolation to zero energy. So the traditional case is: from the experiment, we have the PFNS shape with numerical (artificial) normalization.

Rather realistic theoretical model was in hand of researcher since 1950th, sonamed "traditional assumptions" (see introduction), however the spectrum shape calculated on the basis of this assumption contradict to experimental data, and this "physical" approach cannot help with main request—to provide any useful function for data analysis.

The PFNS shape in Laboratory System (LS) has two peculiarities, visible in first experiments (40–50 years): 1—exponential slope \sim exp(-E/T) at high energy and 2—square root dependence at low energy \sim E^{1/2}. As it was discussed in introduction, models based on traditional assumption may reproduce first peculiarity, but \sim E^{1/2} was a big "puzzle" from the beginning. So-named Watt distribution, which is in agreement with experiment, requires \sim E^{1/2} dependence in center of mass system (CMS) (Maxwellian distribution) which cannot be supported by any theoretical idea.

Hence, one may formulate some definition, what does evaluation for PFNS analysis mean: one should construct semiempirical function, which may have no strong physical basis, but it may describe existing experimental result, and allow us to extrapolate into energy range, and isotopes where experimental data are absent. This function with adjusted parameters may be also used for data library calculation.

3.1 Maxwellian Function and Terrell's Systematic

Maxwellian function is defined by Eq. (3.1):

$$M(E,T) = \frac{2\sqrt{E}}{T\sqrt{\pi T}} \exp\left(-\frac{E}{T}\right)$$
 (3.1)

where T is "temperature" parameter connected with average energy of emitted particles $\langle E \rangle = 1.5 \, T$. This function may describe the PFNS reasonably well, so, the deviation in $^{252}\mathrm{Cf}$ case is <6% in the energy 0–7 MeV, and reaches \sim 20% at \sim 15 MeV neutron energy. This approach was reasonably good for 1950th but cannot be used now. For example, the deviation of $^{252}\mathrm{Cf}$ standard spectrum from Eq. (3.1), \sim 3 time higher estimated uncertainties.

Terrell [45] investigated this problem on the basis of experimental data collected before 1960th. "It is found that all experimental energy distributions for fission neutrons are indistinguishable from Maxwellian distributions; it has been shown that distributions of essentially this form are predicted by Weisskopf's evaporation theory" (motivation for constant *T*).

The average energy of PFNS was estimated with Watt spectrum only for one fission fragment (FF). In reality (the "big" set of FF, the relation of excitation energy with number of neutrons ν), the average energy may be found with the semiempirical equation:

$$\langle E \rangle = a + b \times (\nu + 1)^{1/2} \tag{3.2}$$

Terrell estimated parameters a and b on the basis of theoretical analysis with small correction to 235 U(th). At his time, eight experimental results were available for 233 U(th), 235 U(th), 239 Pu(th), and 252 Cf(sf). The average energies estimated for these isotopes were reproduced with simple Eq. (3.2) inside error bars.

Zamyatnin et al. [53] analyzed new data set which included thermal data ²²⁹Th, ²³⁵U, ²³⁸Pu, ^{242m}Am, ²⁴⁵Cm, ²⁴⁹Cf; spontaneous data ²⁴⁴Cm, ²⁵²Cf; and ~14 MeV data ²³²Th, ²³⁸U, ²³³U. New parameters in comparison with Terrell ones were found.

In addition, they demonstrated very interesting splitting of T-dependences as function of Z^2/A for thermal, spontaneous, and ~ 14 MeV data.

New data set was investigated in [12]. The authors also used the prompt neutron multiplicity instead of total multiplicity in Eq. (3.2).

In [17] it was shown, that prefission component may change the slope for PFNS, so only data <6 MeV for induced fission were applied for a and b parameters' estimation.

Parameters a and b are given in Table 3.1. The following facts must be high-lighted. The average energy estimated with different fitted parameters is practically the same for any systematic. The uncertainties of parameters (if they were found as in [12, 17]) are very high. These error bars were estimated from data spread of individual experimental results. Hence, they may be connected with experimental

References	а	b	235 U(th) $\langle E \rangle$ (MeV)	δE (MeV)
[41]	0.78	0.62	1.93	0.00
[53]	0.25 ± 0.16	0.90 ± 0.08	1.91	0.22
[12]	0.53	0.77	1.94	0.00
[17]	0.62 ± 0.23	0.71 ± 0.12	1.92	0.32

Table 3.1 Parameters for average energy estimation. Average energy for 235 U(th) and its uncertainties, $v_a = 2.42$

Table 3.2 Experiments which were taken into account for evaluation

References	E_1-E_2 (MeV)	N points	FF eff. (%)	Neutron detector	L (m)
Lajtai et al. [29]	0.025-1.22	70	99.0	Li-glass	0.30 ± 0.01
Böttger et al. [8]	2.00-14.0	60	95.4, 99.5	NE-213	12.0 ± 0.02
Poenitz and Tamura [41]	0.25–9.25	51	71	Black detector	2.58, 3.47
Blinov et al. [4]	0.042 - 11.36	73	99	$^{235}U(n, f)$	0.50 ± 0.02
Boldeman et al. [7]-I	0.124-2.66	28	97	Li-glass	0.40
Boldemann et al. [6]-II	1.05-14.25	59	97	NE-102	3.02
Märten et al. [36]	9–20	16	86	NE-213	4.5

mistakes or systematical uncertainties. In this case, this systematic does not have any reasonable sense.

However, this spread may be connected with unknown physics. In work [53], the big difference for the same Z^2/A value for 14 MeV, thermal, and spontaneous fissions was demonstrated. The increasing of T parameter for ~14 MeV fission is connected with prefission neutron emission (see latter). The origin of difference between spontaneous and neutron-induced fission is not clear. In any case, this peculiarity was never discussed before, as a physical effect.

3.2 ²⁵²Cf Spectrum Evaluation

In 1896, Mannhart [33] submitted the evaluation of ²⁵²CF PFNS, which was adopted as standard spectrum soon. Taking into account the importance of this result, more experimental details and evaluation procedures are discussed here (Table 3.2).

The data used for this evaluation comprise most of post-1979 experiments. All of the experiments were based on time-of-flight techniques. The experiments were described in details, including method, corrections, and possible uncertainties.

Efficiency of thick Li-glass detector in [29] (NE-912) was measured relative to thin NE-908. The efficiency of thin detector was calculated by Monte Carlo method.

Several runs were realized in (PTB) The Physikalisch-Technische Bundesanstalt [8]. Three or four NE-213 detectors were used for spectrum measurements. The efficiency of the neutron detectors were determined by Monte Carlo calculations. Between 3 and 12 MeV, the results were confirmed within±3% by *n-p* scattering

experiments. Altogether, between 2 and 14 MeV, a total of 1018 data points at slightly different neutron energies due to different thresholds and time scale calibration of the individual detectors was produced. Including all necessary corrections these data were available for the evaluation. Finally, all these data were transformed to 70 points included in Mannhart's evaluation.

Authors of [41] used two "black detectors" of different sizes. Data for 0.2–4 MeV were obtained with smaller detector and a flight path of 2.58 m. In energy range 0.7–10 MeV, the flight path was 3.47 m, and the large detector was used. The efficiency of smaller detector changed between 98% (\sim 0.2 MeV) and 83% (\sim 4 MeV), for larger detector from 96% (\sim 1 MeV) and 77% (\sim 10 MeV). Authors estimated that uncertainties of the efficiency are very small 1–2%.

Blinov et al. [4] used nontraditional detector for neutron counting—²³⁵U fission ionization chamber. The mass of the detector was very small. After proper correction the efficiency was calculated on the basis of well-known fission cross sections.

In low energy part [7], the efficiency of neutron detector was measured relative to a "long counter" between 124 keV and 1.35 MeV, and above, the efficiency was based on calculations. The data from Li-glass detector was normalized to NE 102 data in the energy range 1–1.65 MeV.

In experiment [6], NE-102 neutron detector efficiency for energy range 2–11 MeV was measured with associated particle method. The uncertainty is about 2%. Between 1 and 2 MeV the efficiency was measured relative to a "long counter," and above 11 MeV Monte Carlo simulation tested in 2–11 MeV was used. Seven different experiments were carried out. The data were combined by authors and submitted for evaluation.

After collection of all experimental data an additional analysis has been done. For all experiments, the calculation of the time resolution correction and the bin width correction has been repeated. Comparison of the present results with those expressly stated by the authors shows full agreement with the exception of the experiment of Boldeman et al., where the quoted time resolution correction factors were larger. This discrepancy may originate from an asymmetry in the time resolution function mentioned by the authors.

For each experimental data set, an uncertainty covariance matrix was generated, based on the documented uncertainty information and on additional information directly obtained from the authors. The dominating systematic uncertainty component of all experiments was due to the efficiency calibration of the neutron detectors. Another systematic contribution, which was not expressly taken into account in most of the experiments, is the uncertainty of the energy scale definition.

To obtain a common basis for the evaluation, a fixed energy grid was established. The selection of the grid point energies was governed by the density of the available data points as well as by the necessity to represent the structure of the spectrum adequately. Altogether, 70 grid point energies were chosen. Each of the original data points was transformed to the neighboring energy grid point. Before doing this, the approximate slope of the data was determined. This was done by fitting a Maxwellian to the original data of each experiment. The specific Maxwellian of each experiment was applied in the transformation of a data point from its original energy to the grid energy. Based on the common energy grid, the data sets were

E_1 (MeV)	E_2 (MeV)	dS/S (%)	E1 (MeV)	E_2 (MeV)	dS/S (%)
0.015	0.035	10.4	10.05	10.55	2.7
0.035	0.095	4.8	10.55	11.05	2.9
0.095	0.135	3.4	11.05	11.55	2.9
0.135	0.225	2.7	11.55	12.05	3.4
0.225	1.05	1.8	12.05	12.55	3.6
1.05	4.45	1.2	12.55	13.05	5.0
4.45	7.05	1.5	13.05	13.55	4.5
7.05	7.55	1.8	13.55	14.05	6.3
7.55	8.05	1.9	14.05	14.6	9.6
8.05	8.55	2.1	14.6	15.9	12.2
8.55	9.05	2.2	15.9	16.9	14.5
9.05	9.55	2.2	16.9	17.9	19.0
9.55	10.05	2.5	17.9	19.1	31.8

Table 3.3 Uncertainties for ²⁵²Cf fission neutron spectrum

combined by generalized least-squares techniques with regard to their uncertainties. The uncertainties were also estimated (see Table 3.3).

The author of evaluation tried to find theoretical model to calculate the smooth dependences. He was obliged to conclude that, at present, neither theory is adequate to describe within the uncertainties the evaluated data over the whole energy range. To obtain a smooth curve for the evaluated neutron spectrum a spline-interpolation procedure was applied. This procedure used the variances of the evaluated neutron spectrum data at discrete energies as weights and generated a continuous curve through the data points.

This evaluated spectrum and uncertainties were proclaimed as the standard spectrum and were applied in different data library.

In the following [18], this spectrum was described by following formula for simplification of the calculation:

$$\begin{split} S^{\text{Cf}}(E) &= M(E)(a_0 + a_1E + a_2E^2 + a_3E^3 + a_4E^4 + a_5E^5 + a_6E^6 + a_7E^7) \\ M(E) &= \frac{2\sqrt{E}}{T\sqrt{\pi T}} \exp\left(-\frac{E}{T}\right), \quad T = 1.42 \; MeV \\ a_0 &= 9.62240 \text{E-}01, a_1 = 3.99740 \text{E-}02, a_2 = -1.44500 \text{E-}03, \ a_3 = -3.18750 \text{E-}03 \\ a_4 &= 6.17640 \text{E-}04, \ a_5 = -4.86040 \text{E-}05, a_6 = 1.77680 \text{E-}06, a_7 = -2.49540 \text{E-}08 \end{split}$$

The Eq. (3.3) describes the Mannhart's evaluation with accuracy <0.2% up to 20 MeV.

The k-momentum $\langle E^k \rangle$ of this function may be found with Eq. (3.4).

$$\langle E^{k} \rangle = \int_{0}^{\infty} E^{k} S^{Cf}(E) dE = \frac{2}{\sqrt{\pi}} \sum_{i=0}^{7} a_{i} T^{k+i} \int_{0}^{\infty} x^{k+i+0.5} e^{-x} dx$$

$$= \frac{2}{\sqrt{\pi}} \sum_{i=0}^{7} a_{i} T^{k+i} \Gamma(n+0.5), \quad n = k+i+1$$
(3.4)

where $\Gamma(n+0.5)$ is Gamma function.

The first order momentum k=1 may be calculated with Eq. (3.5):

$$\langle E \rangle = 2 \sum_{i=0}^{7} a_i T^{i+1} \frac{(2(i+2))!}{4^{i+2}(i+2)!} = 2.12113 MeV$$
 (3.5)

The average energy after numerical integration of Eq. (3.3) is $\langle E^{\text{Cf}} \rangle = 2.1214 \text{ MeV}$.

3.3 Two Watt Spectra (TWS) Approach

In [50], formula was given (so-named Watt formula) for PFNS calculation:

$$W(E,T,E_{\nu}) = M(E,T) \times \exp\left(-\frac{E_{\nu}}{T}\right) \frac{\sinh\sqrt{b \times E}}{\sqrt{b \times E}}, \quad b = \frac{4E_{\nu}}{T^{2}}$$
(3.6)

where E is neutron energy in LS, T is "temperature" parameter in CMS, and $E_{\rm v}$ is the energy of neutron moving with velocity of CMS.

This formula may be easily calculated if we assume that: (1) all neutrons are emitted from moving fragment and (2) neutron spectrum in CMS may be described by Maxwellian Eq. (3.1).

The first assumption is rather reasonable one, and is used practically in any models of neutron emission in fission. However, the second assumption—Maxwellian shape in the CMS—cannot be predicted in frame of traditional model. Having in mind this difficulty, one may treat this relation as semiempirical, including parameters which appeared in Eq. (3.6). We should have in mind this compromise. From one side we are using semiempirical relation which does not have physical support. From another side we are using real physical values like, excitation energy, temperature, CMS velocity, light and heavy fragment, and so on. But this strange situation is typical for fission neutron emission treatment.

The following assumptions were used for representation of the experimental data and PFNS calculation on the basis of TWS approach [22]:

1. The PFNS may be described as a sum of two Watt distributions for light and heavy fragments with equal contribution:

$$S(E, E_0) = 0.5 \sum_{j=1}^{2} W_j (E, E_0, T_j^x(E_0), \alpha)$$
(3.7)

where T_j^x is the temperature parameter for nucleus x and light and heavy fragments (j=1, 2), E_0 is the incident neutron energy, α is the ratio of the total kinetic energy (TKE) at the moment of the neutron emission to full acceleration value.

Fissile nucleus	E_0 (MeV)	$r = T_{\rm l}/T_{\rm h}$	References
²⁵² Cf	SF (Spontaneous Fission)	1.275 ± 0.042	[35]
^{238}U	2.9	1.231 ± 0.104	[9]
^{235}U	0.53	1.222 ± 0.022	[13]
	2.9	1.011 ± 0.260	[9]
²³² Th	2	1.481 ± 0.076	[2]
	7.3	1.283 ± 0.143	[34]

Table 3.4 Ratio of temperature parameters

2. Temperature parameters for any fissile system were calculated with ²⁵²Cf data according to the following formula:

$$T_{l,h}^{x} = T_{l,h}^{Cf} \sqrt{\frac{U_{x}A^{Cf}}{U_{Cf}A^{x}}}$$
 (3.8)

where $U = E_{\rm r} + B_{\rm n} + E_0$ – TKE, $E_{\rm r}$ —energy release, $B_{\rm n}$ —binding neutron energy, E_0 —incident neutron energy, and A—mass number of fissile nucleus.

- 3. There is only one free parameter α fitted to the experimental data for incident neutron energy <6 MeV. The Eq. (3.8) was obtained under the following assumption:
 - Level density may be described with Fermi gas model;
 - Level density parameter a is proportional mass number;
 - Parameter T is temperature parameter $T = (U/a)^{1/2}$.
- 4. The energy of neutron with CMS velocity was calculated for light $E_{\rm vl}$ and heavy $E_{\rm vh}$ fragments with equation:

$$E_{vl} = \frac{A_h}{A_l A} \alpha TKE; \quad E_{vh} = \frac{A_l}{A_h A} \alpha TKE; \quad A = A_l + A_h$$
 (3.9)

The "temperature" parameters were estimated from several experimental spectra. In this case, T_1 , T_h were free parameter together with α (Table 3.4).

The average ratio is $\langle r \rangle = T_1 / T_h = 1.248 \pm 0.031$. We assumed that this value does not depend on fissile nucleus and incident energy.

The experimental data for ²³²Th, ²³³U, ²³⁵U, ²³⁸U, ²³⁷Np, and ²³⁹Pu (26 spectra) have been described in the framework of this model inside the experimental errors. The results of the fitting procedure are collected in Table 3.5

The comparisons of experimental and calculated spectra for some fissile target are shown in Figs. 3.1, 3.2, 3.3, 3.4, 3.5, and 3.6. The PFNS are given as a ratio of experimental N(E) to calculated function $S(E, E_0)$ Eq. (3.7), R(E) = N/S. The $S(E, E_0)$ functions were calculated with fitted parameters from Table 3.5.

Target	E_0 (MeV)	χ^2/N	$\alpha \pm \delta \alpha$	$\langle \alpha \rangle$	References
²³² Th	2.0	0.63	0.940 ± 0.021	0.947 ± 0.010	[2]
	2.9	0.49	0.954 ± 0.010		[9]
	7.3	0.38	0.910 ± 0.060		[34]
^{233}U	0.025 eV	0.61	0.958 ± 0.004	0.920 ± 0.040	[42]
	0.025 eV	1.72	0.881 ± 0.015		[30]
^{235}U	0.025 eV	1.11	0.945 ± 0.010	0.936 ± 0.027	[42]
	0.025 eV	1.3	0.926 ± 0.013		[30]
	0.025 eV	2.08	0.957 ± 0.010		[52]
	0.03	0.72	0.950 ± 0.010		[1]
	0.53	0.21	0.985 ± 0.010		[13]
	0.5	0.58	0.919 ± 0.018		[47]
	2.9	1.11	0.900 ± 0.010		[9]
	5	0.49	0.906 ± 0.016		[47]
^{238}U	2	1.67	0.850 ± 0.011	0.880 ± 0.030	[3]
	2	2.17	0.877 ± 0.011		[3]
	2.9	0.38	0.927 ± 0.012		[9]
	6	1.63	0.866 ± 0.023		[28, 18]
²³⁷ Np	0.52	0.46	0.799 ± 0.015	0.808 ± 0.010	[23]
	2.9	1.95	0.817 ± 0.010		[5]
	5	1.24	1.038 ± 0.023		[46]
²³⁹ Pu	0.025 eV	0.36	0.858 ± 0.015	0.873 ± 0.051	[42]
	0.025 eV	1.73	0.927 ± 0.019		[30]
	0.03	0.82	0.798 ± 0.010		[1]
	0.22	0.93	0.934 ± 0.010		[15]
	1.5	0.51	0.847 ± 0.014		[46]
²⁵² Cf	SF	0.15	0.809 ± 0.003	0.809 ± 0.003	[33]

Table 3.5 Results of data analysis with TWS approacha

3.4 Maxwellian Together with Power Expansion for ²³⁵U(th)

At the middle of 1990th there were four experiments that investigated the neutron spectra for ²³⁵U for incident neutron energy <30 keV results of which are available through EXFOR library [42, 30, 52, 1]. The detailed analysis of the PFNS measured in these experiments was done in [21].

The original data have a different normalization, therefore, these data were renormalized applying the TWS approach. The total data set after the normalization is shown in Fig. 3.7. As one can see, the data of different experiments does not contradict to each other and may be used as a single data set for estimating the average neutron energy and spectrum shape in the energy range from ~30 keV to 14 MeV. Two percent error was added to the original values of work [52]. All 294 points were suggested as independent ones.

 $^{^{\}rm a}$ $T_{\rm h}$ = 0.8868 MeV for ^{252}Cf was used for all calculations. Total kinetic energy (TKE) was taken from [32] and binding energy from [49] TWS two Watt spectra

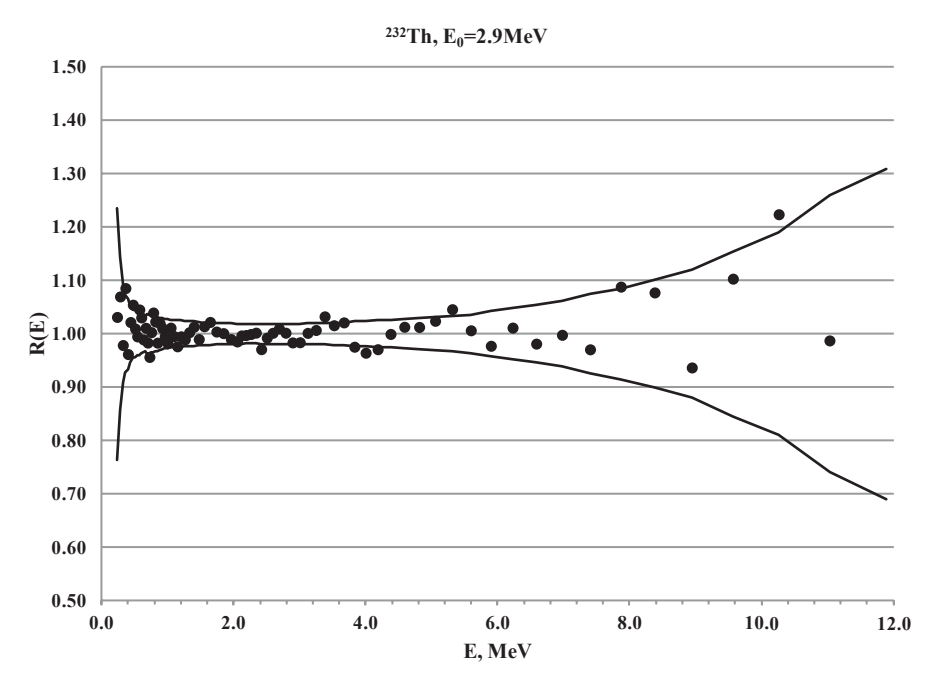


Fig. 3.1 R(E) [9] solid symbols and error bars (lines)

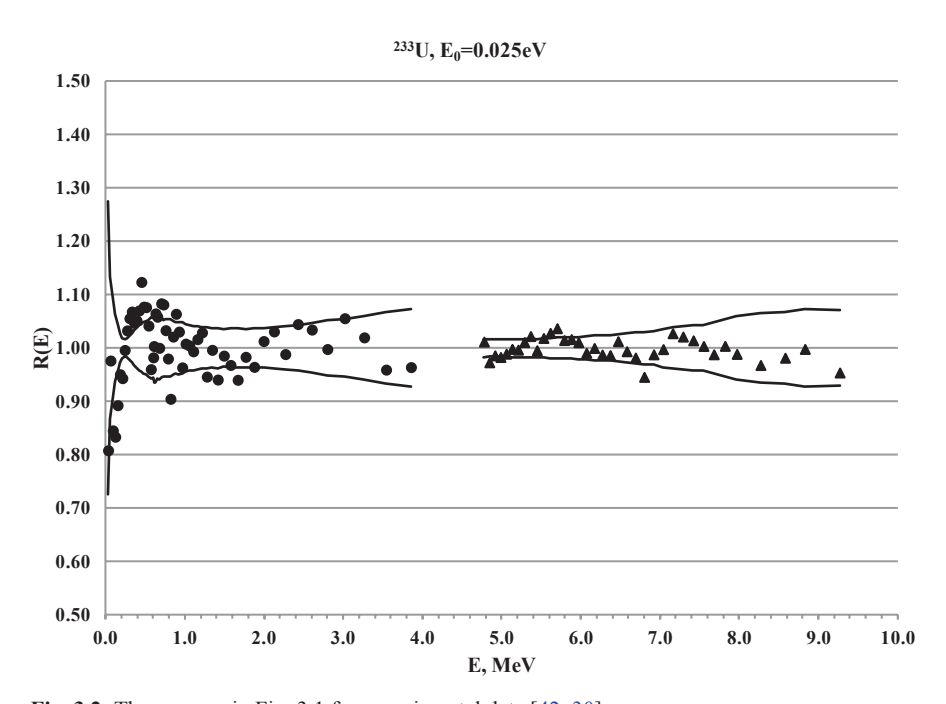


Fig. 3.2 The same as in Fig. 3.1 for experimental data [42, 30]

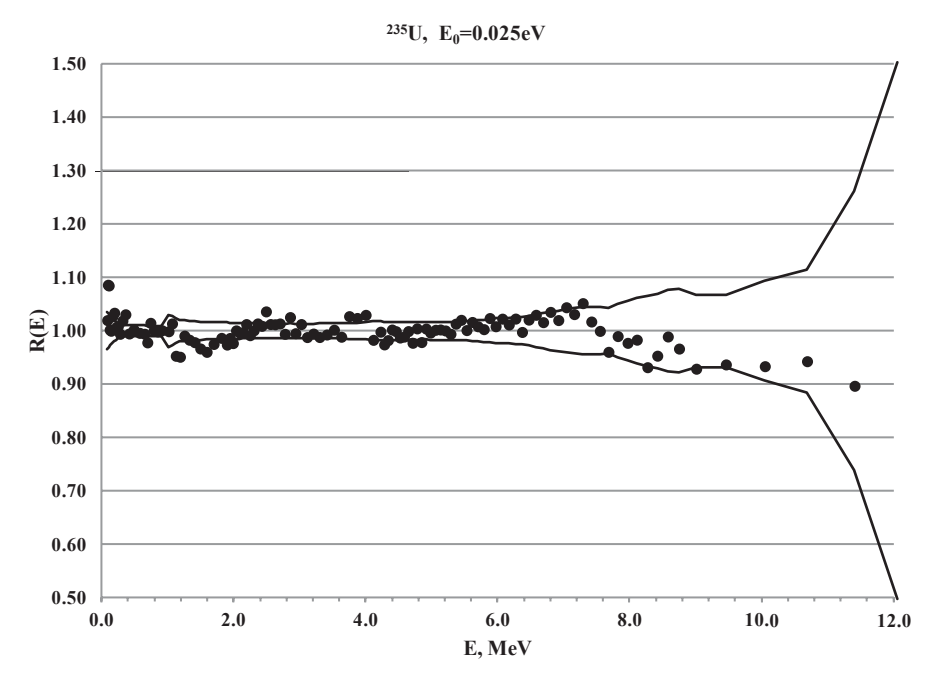


Fig. 3.3 The same as in Fig. 3.1 for experimental data [42]

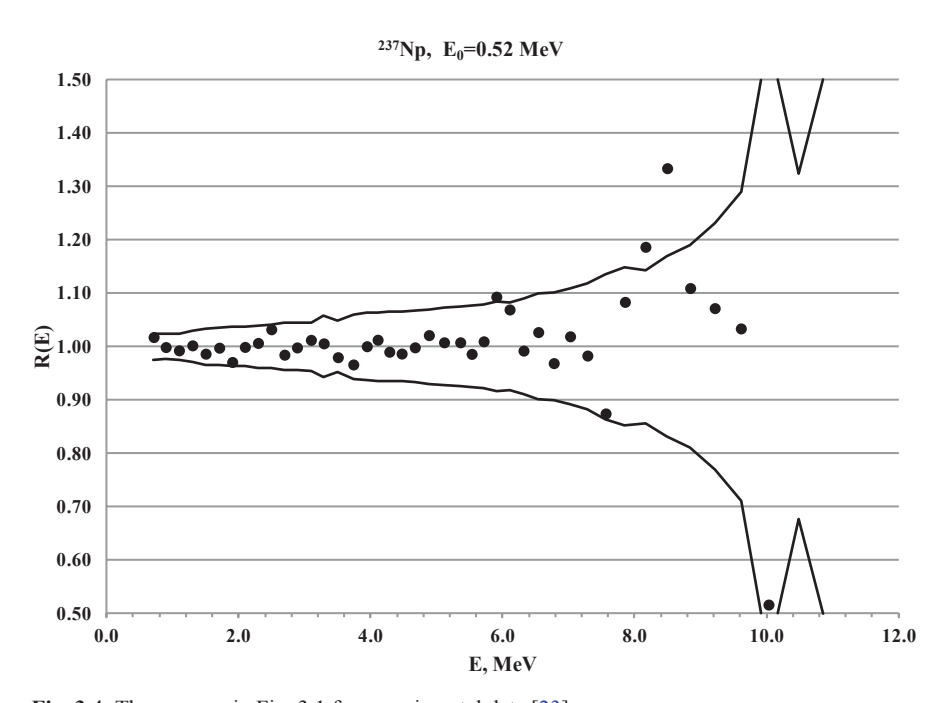


Fig. 3.4 The same as in Fig. 3.1 for experimental data [23]

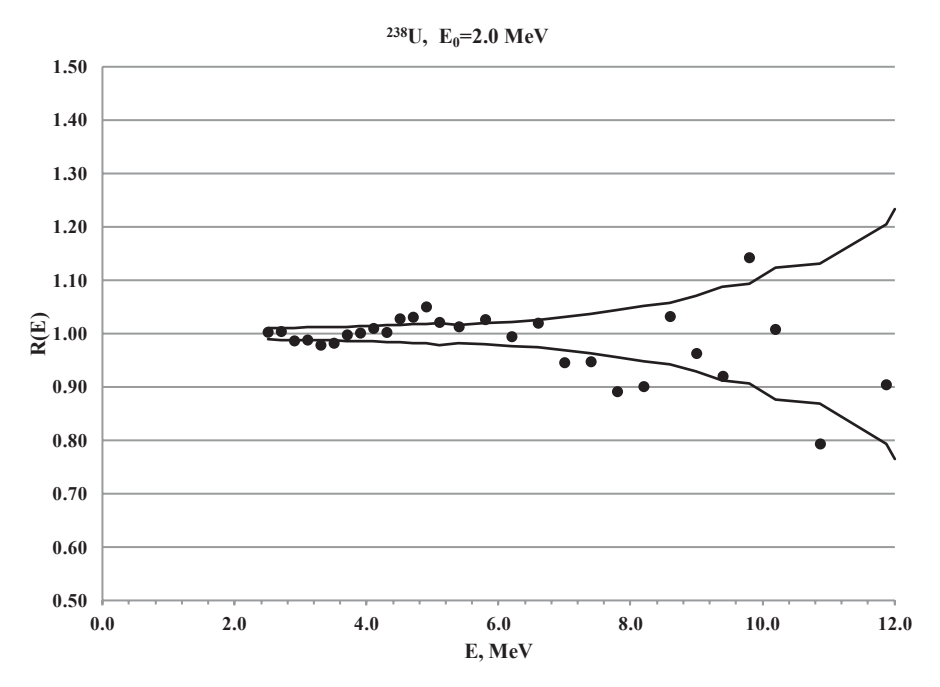


Fig. 3.5 The same as in Fig. 3.1 for experimental data [3]

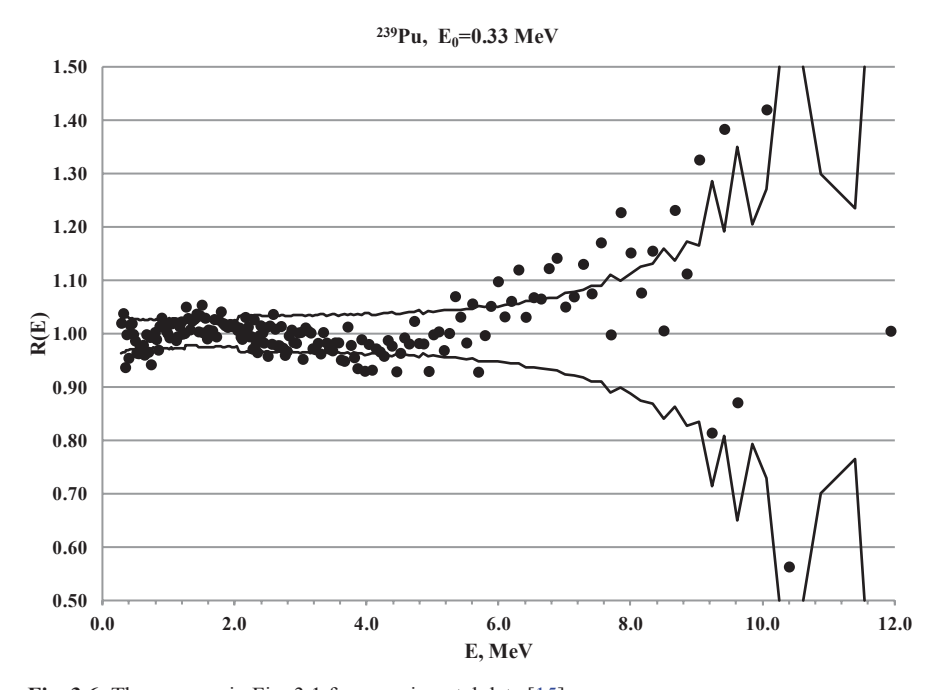


Fig. 3.6 The same as in Fig. 3.1 for experimental data [15]

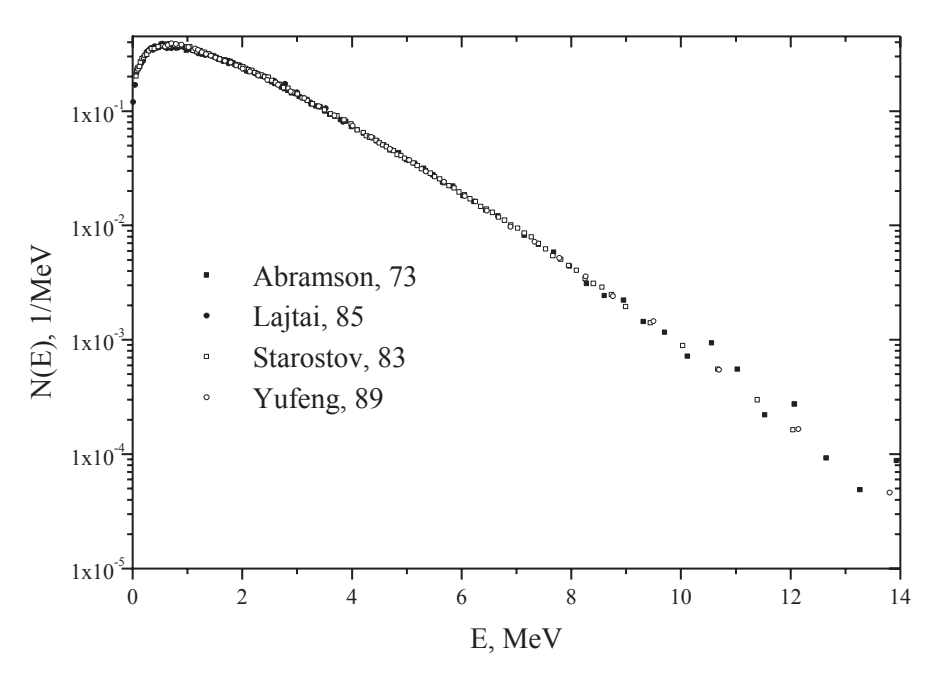


Fig. 3.7 The normalized experimental data from works [42, 30, 52, 1]

First of all these data were fitted with Eq. (3.7) ($\chi^2 = 1.1$). It was found that $\alpha = 0.945 \pm 0.002$ and $\langle E \rangle = 1.971 \pm 0.002$ MeV.

To avoid the uncertainties due to large data spread at low and high limits, we used the following procedure for average energy calculation. Average energies and ratios r_{E_1,E_2} were calculated for various low E_1 and high E_2 limits:

$$r_{E_{1},E_{2}} = \frac{\langle E \rangle_{E_{1},E_{2}}^{exp}}{\langle E \rangle_{E_{1},E_{2}}^{cal}}, \quad \langle E \rangle_{E_{1},E_{2}} = \frac{\int_{E_{1}}^{E_{2}} ES(E)dE}{\int_{E_{1}}^{E_{2}} S(E)dE}$$
(3.10)

The S(E) denotes the experimental or calculated spectra with fitted parameter α =0.945. The average $\langle r \rangle$ =1.0029±0.0019 was used to calculate the experimental average neutron energy $\langle E \rangle_{0,\infty}^{exp} = \langle r \rangle \langle E \rangle_{0,\infty}^{cal}$. It was found that $\langle E \rangle_{\rm exp} = 1.977 \pm 0.008$ MeV . So, the experimental average energy is in agreement with semiempirical modeling with accuracy ~0.2%.

As a next step, the ratio of the experimental data to Maxwellian distribution M(E, T) (T=1.314 MeV=1.971/1.5 MeV) was calculated. The deviation of the experimental points from the Maxwellian was described by power expansion (χ^2 =0.87):

$$N(E) = (0.95342 + 0.4909 \times 10^{-1} E - 0.92331 \times 10^{-2} E^{2} + 0.24973 \times 10^{-3} E^{3}) M(E, 1.314)$$
(3.11)

3.5 Scale Method 57

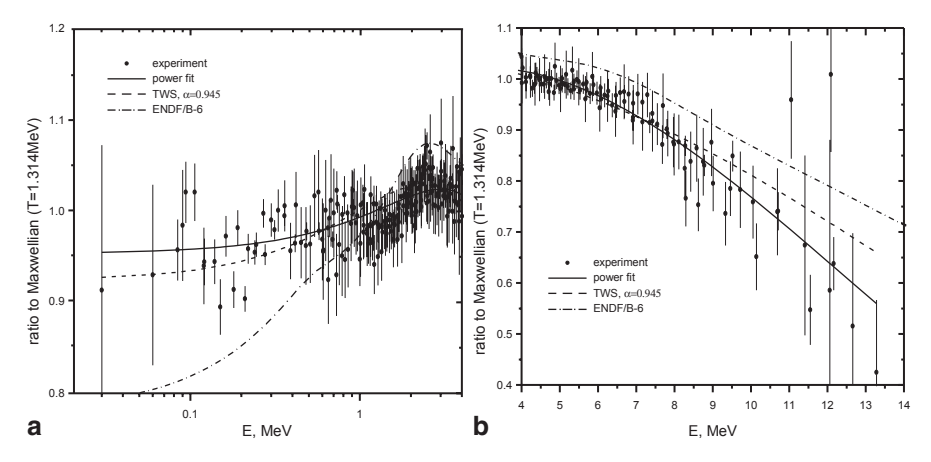


Fig. 3.8 Experimental data and evaluated spectra as a ratio to Maxwellian a low energy range, b high energy range. TWS two Watt spectra

Table 3.6 Average neutron energy for ²³⁵U

No-	$\langle E \rangle$, (MeV)	Comments
1	2.033	ENDF/B-VI
2	1.977 ± 0.008	Experiment
3	1.971 ± 0.002	$\alpha = 0.945 \pm 0.002$
4	1.971	Power fit

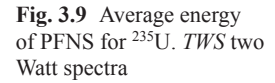
The deviations of the experimental and calculated spectra from Maxwellian distribution are shown in Fig. 3.8. As one can see the ENDF/B-VI evaluation is going out of the experimental error limits.

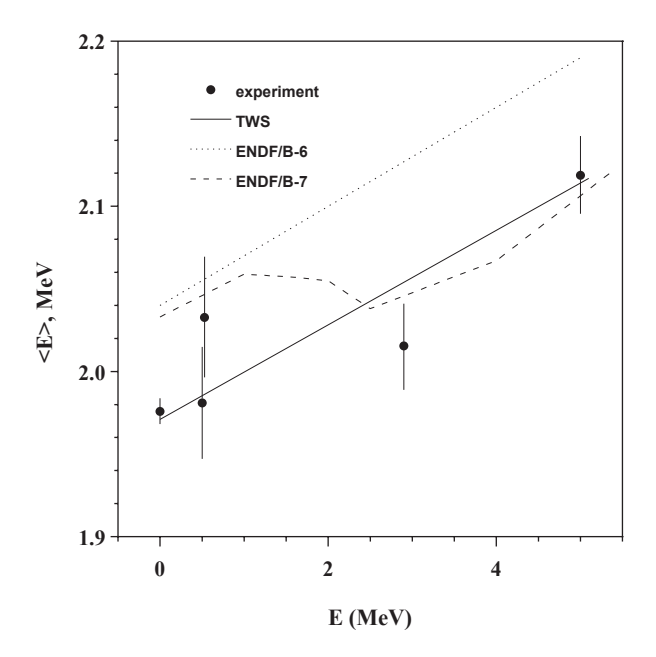
The average energies for the ²³⁵U fission neutron spectrum at thermal energy estimated with various approaches are collected in the Table 3.6. The systematic error for the $\langle r \rangle$ calculation (3.6 keV) and the uncertainty for calculation of $\langle E \rangle_{E_1,E_2}$ (6.6 keV) give the total error for the experimental average energy (Table 3.6).

The contradiction between data libraries (for example ENDF/B-VI) applied for benchmarks and practical calculations and evaluation based on the microscopic data clearly visible on Fig. 3.8 and in Table 3.6. Authors of [21] were the first who proclaimed that this contradiction cannot be explained due to systematical uncertainties (or mistakes) of microscopic data.

3.5 Scale Method

Authors of [22] (*solid line* in Fig. 3.9) demonstrated that PFNS ²³⁵U from ENDF/B-VI which is reasonably good for macroscopic experimental results and benchmark experiments, contradict to microscopic spectra.





Authors of new data library—ENDF/B-VII, took into account the remark of [22], but in a very strange way. They reduced average energy for $E_0>2$ MeV, but did not change low energy part. This action has no physical sense, but kept the possibility for reasonable benchmark prediction, and answer on the remarks [22]. At the end of 1990th the Nuclear Energy Agency (NEA)-Organisation for Economic Co-operation and Development (OECD) activity connected with fission neutrons for 235 U was stimulated. Finally the conclusion has been done [51]: "...no calculated thermal spectrum has been found that simultaneously reproduces either of the two modern thermal differential measurement and the set of measured integral cross-sections to within an acceptable level." And finally "... a new and highly accurate measurement of the prompt fission neutron spectrum for the reaction $n(\text{thermal})+^{235}$ U should be undertaken as soon as possible. This measurement is the best—and perhaps only—way to resolve existing discrepancy in the thermal spectrum." So, the systematic errors of *microscopic* experiments are responsible for this contradiction.

New experiment was realized, and new "scale" method was applied for evaluation of available data set. The experimental data of [1] was removed from data analysis because low input energy ~30 keV may provide rather bid time spread due to the size of the sample (see Sect. 2.1.8) and rather poor description of this experiment. So data from [27, 42, 33, 52] was included in the new evaluation.

The "scale method" investigated in paper [18] is based on the assumption that the PFNS for different isotopes has "similar" shape and the spectra difference is connected with scale factor only. There are not any strict proofs which support the method. However, direct comparison with existing experimental data gives evidence that this semiempirical method is working with an accuracy $1-2\,\%$, in any case for $^{235}\text{U}(n_{\text{th}}\,f)$.

3.5 Scale Method 59

Reference	aling factor after the final a_i , first step	a_s , first step (MeV)	χ^2 , first step	$a_{\rm i}$, second step
[27]	1.007 ± 0.002	1.975 ± 0.003	0.52	1.007 ± 0.002
[42]	0.631 ± 0.001	1.973 ± 0.002	1.10	0.631 ± 0.001
[30]	1.001 ± 0.008	1.987 ± 0.015	1.17	0.993 ± 0.005
[52]	1 200 ± 0 005	1.067 ± 0.003	2.06	1 294 ± 0 005

Table 3.7 Fitted parameters, their uncertainties, and χ^2 estimated after the first and second steps of data evaluation. The experimental spectra should be divided with a_i parameters. In the third column, the scaling factor after the first step is given

It was assumed that PFNS for 235 U and 252 Cf in nondimensional scale have the same shape. The 252 Cf spectrum is a standard and was described with Eq. (3.4). The 235 U PFNS $S^{U}(E)$ at energy E was calculated with equations:

$$X = E / a_{s}$$

$$E^{Cf} = X \times \langle E^{Cf} \rangle$$

$$S^{U}(E) = a_{i} \frac{S^{Cf}(E^{Cf}) \times \langle E^{Cf} \rangle}{a_{s}}$$
(3.12)

where a_s is a scaling factor and a_i is a normalization parameter for *i*-th experiment. These parameters were found by a nonlinear least square method.

The evaluation procedure consists of three steps. At first step, the main assumption was verified. The experimental data were fitted separately with free parameters a_s and a_i . Fitted parameters and residual χ^2 per point after this step are given in Table 3.7. The experimental data for [27] are shown in exponential scale (Fig. 3.10a) and as a ratio R(E) of experimental data to fitted values (Fig. 3.10b). Another experimental data are shown as a ratio only. (Figs. 3.11, 3.12, 3.13 and 3.14).

It is a very impressive fact that all experimental data were described inside error bars with one free shape parameter only. The small <2% regular deviation from calculated spectrum like a "positive" curvature are visible for experimental data of [27, 52]. However, the data of [42] does not demonstrate this type of deviation.

All experiments were realized by time-of-flight method. The channel width was ~ 0.1 ns in [27] and ~ 1.4 ns in [42]. So, the strong deviation in the energy range > 8 MeV visible in Fig. 3.11 may be connected with "bin width" effect. The channel width in [52] is unknown. But according to the energy step, the time channel width was also rather big ~ 1 ns.

There is an unexpected deviation of [52] data in the energy range <2 MeV, which may be connected with wrong estimation of a neutron detector efficiency (see Sects. 2.1.5 and 2.1.6). The similar explanation may be connected with high energy part of the [30] data. These data points were removed from second step of evaluation.

The following data points were used for next evaluation: 0.7–11 MeV [27], 0.08–8.58 MeV [42], 0.03–2.27 MeV [30], and 1.21–9.52 MeV [52].

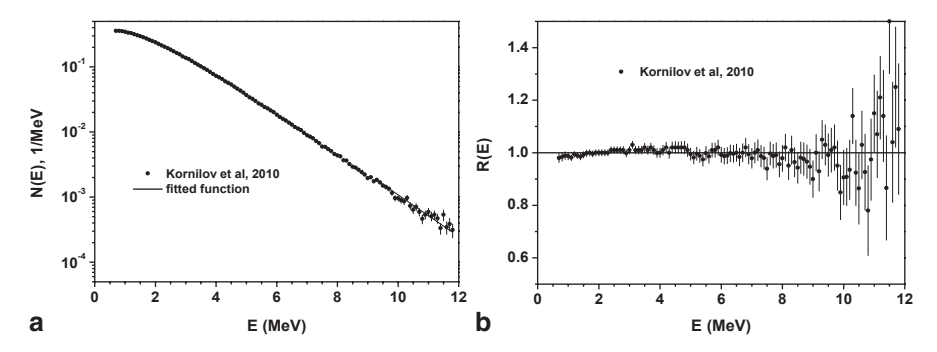


Fig 3.10 a Experimental data and evaluated spectra, b Ratio experimental to fitted spectrum

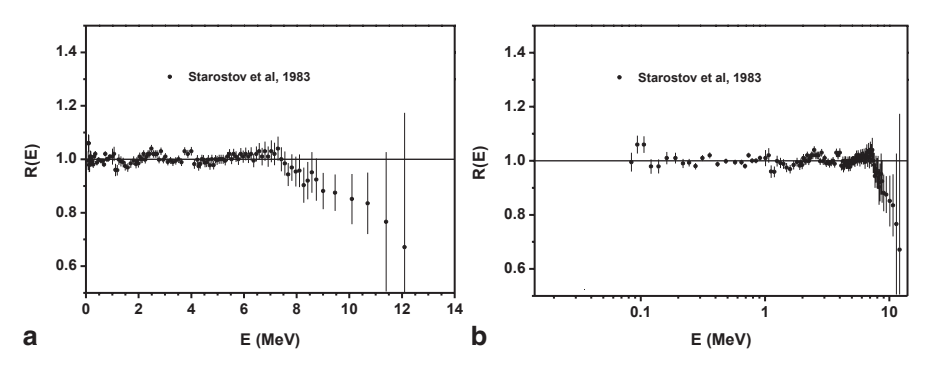


Fig. 3.11 a R(E) in linear scale [42] b The same as in a in logarithmic scale

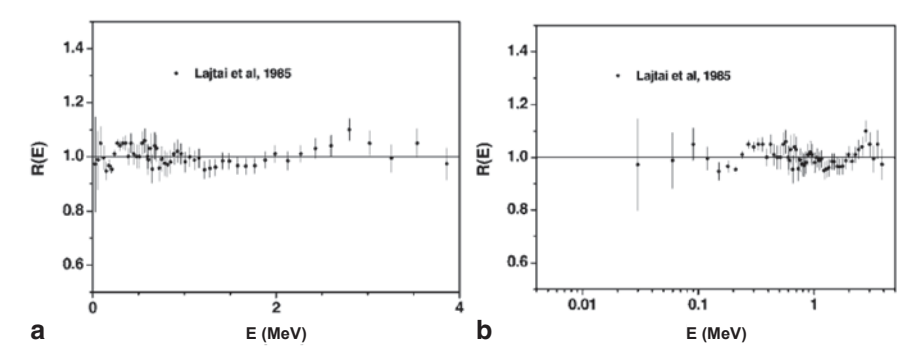


Fig. 3.12 a R(E) in linear scale [30] b The same as in a in logarithmic scale

3.5 Scale Method 61

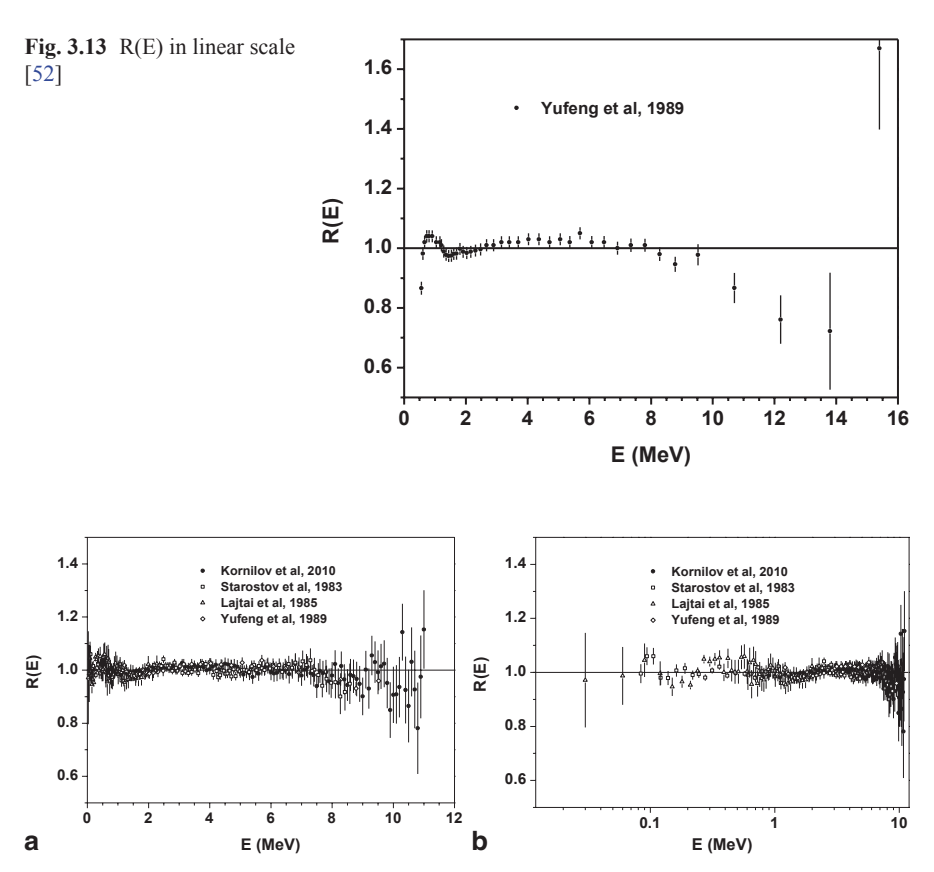


Fig. 3.14 a All experimental data after normalization as a ratio to fitted function. b R(E) as in a in logarithmic scale

At this stage all 292 data points were treated as a single data array which was fitted with five parameters: a_s —scale factor which is common for all experiments and different normalization parameters a_1 – a_4 .

The residual deviation is χ^2 =0.84. The normalization parameters and their uncertainties are collected in Table 3.7.

The final stage of the evaluation was realized after data normalization. At this stage, the average energy of the fitted spectrum was calculated by the direct integration. The final parameters are: $a_{\rm s}=1.9742\pm0.0015$ MeV and $a_{\rm l}=1.000\pm0.001$ and the average energy from integration of the fitted spectrum is $\langle E \rangle=1.9740$ MeV.

The normalized experimental data as a ratio to fitted spectrum are shown in Fig. 3.14. The average ratios and their standard deviation for different experiments and energy intervals are collected in Table. 3.8. The summary of the uncertainty estimation is given in Table 3.9. The deviation between experimental data and evaluated function is 1-2% in the energy range <10 MeV. The 64% of the total amount 292 points are in the range 0.98 < R(E) < 1.02.

$\overline{E_1 - E_2}$	Ref. 12		Ref. 57		Ref. 58		Ref. 59	
(MeV)	$\langle R \rangle$	δR						
< 0.3			1.006	0.029	0.996	0.038		
0.3 - 0.5			0.999	0.016	1.031	0.027		
0.5 - 0.7			0.998	0.014	1.021	0.039		
0.7 - 1.0	0.984	0.003	1.000	0.021	0.995	0.024		
1.0 - 2.0	0.993	0.007	0.986	0.009	0.987	0.020	0.991	0.013
2.0 - 3.0	1.006	0.005	1.012	0.012			0.998	0.009
3.0-4.0	1.013	0.007	1.002	0.015			1.023	0.001
4.0 - 5.0	1.015	0.007	0.992	0.014			1.023	0.004
5.0 - 6.0	0.996	0.013	1.006	0.009			1.024	0.011
6.0 - 7.0	0.997	0.011	1.014	0.010			0.998	0.007
7.0 - 8.0	0.983	0.021	0.991	0.037			0.985	0.018
8.0 - 9.0	0.967	0.035	0.930	0.026			0.952	0.019
9.0 - 10	0.976	0.064						
10.0-11	0.940	0.097						

Table 3.8 Average ratio of experimental data to fitted values and its standard deviations for different experiments and energy intervals

In the previous analysis, three data sets and all calculated spectra are using the same Cf-standard. So, the obvious correlation may exist in this approach. In case of the absolute ratio, the Cf-standard is applying for calculated spectra only. It is interesting to use and verify this method for evaluation of ratio data.

The absolute ratio of ²⁵²Cf to ²³⁵U spectra was measured in [42, 19]. The ratio of two PFNS can be found with Eq. (3.13):

$$R(E) = a_i \frac{v^{Cf}}{v^U} \frac{S^{Cf}(E)}{S^U(E)}$$
(3.13)

where $v^{\rm U} = 2.421~{\rm ENDF/B-7}, v^{\rm Cf} = 3.759~{\rm ENDF/B-7}$ are prompt neutron multiplicities, a_i —normalization parameter for *i*-th experiment, $S^{\rm Cf}(E)$ and $S^{\rm U}(E)$ are spectra $^{252}{\rm Cf}$ Eq. (3.4) and $^{235}{\rm U}$ Eq. (3.12).

The scale parameter was fixed (see previous section) and a_i parameters were fitted. It was found that both data sets require small normalization. The experimental data of [19] have been multiplied with 1.0195 ± 0.0008 and data of [42] with 0.9808 ± 0.0016 . The error bars of the normalization factors are uncertainties of the fitting procedure with assumption that all points are noncorrelated. The uncertainties of data are less than used before because they do not include errors due to Cf standard. The residual $\chi^2=1.31$ (211 points for two experimental ratio data) was calculated with "scale method" after the normalization.

The experimental data of spectra ratio after normalization was also fitted with simple power expansion:

$$R(E) = r_0 + r_1 E + r_2 E^2 (3.14)$$

3.5 Scale Method 63

E_1 – E_2 (MeV)	$\langle R \rangle$	δR	N points	
< 0.3	0.999	0.034	19	
0.3-0.5	1.020	0.025	11	
0.5-0.7	1.011	0.033	11	
0.7-1.0	0.997	0.021	16	
1.0-1.5	0.987	0.017	27	
1.5-2.0	0.990	0.013	21	
2.0-2.5	1.006	0.013	20	
2.5-3.0	1.010	0.009	12	
3.0-4.0	1.009	0.012	23	
4.0-5.0	1.003	0.017	28	
5.0-6.0	1.004	0.014	25	
6.0-7.0	1.006	0.013	21	
7.0-8.0	0.988	0.027	20	
8.0-9.0	0.960	0.032	16	
9.0-10	0.974	0.062	11	
10-11	0.959	0.112	11	

Table 3.9 Average ratio of experimental data to fitted values, its standard deviations, and number of points for each energy interval

Fitted parameters are:

$$r_0 = 1.4168 \ (0.23\%),$$
 $r_1 = 4.949 \times 10^{-2} \ (5.5\%),$ $r_2 = 5.904 \times 10^{-3} \ (7.4\%),$ and $\gamma^2 = 0.95.$

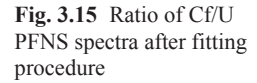
Both dependences together with normalized experimental data are shown in Fig. 3.15.

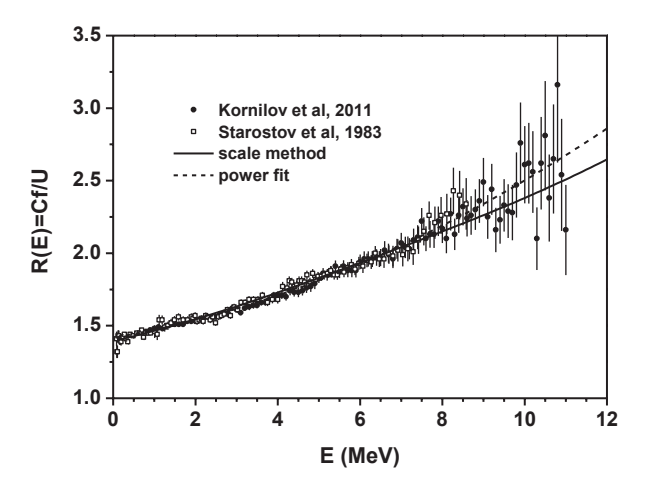
In the energy range 0.1-8 MeV the difference between these two functions Eqs. (3.13) and (3.14) < 2% and it increases up to 10% at 15 MeV.

The different evaluations for ²³⁵U(th) (1998–2011) are compared on Fig. 3.16. The conclusion is the same as in [21]. The difference between ENDF/B-VII data library and another evaluations based only on microscopic data is outside of the estimated uncertainties. The expected request for PFNS, that this data should predict macroscopic and benchmark experiments, provides obvious conflict with microscopic data. Average energy of ENDF/B-VII ²³⁵U PFNS at thermal energy is 2.031 MeV. The ENDF/B-VII underestimate low energy part ~0.1 MeV (up to 20%), and overestimate high energy part (~5% at 4 MeV).

There is a big temptation to explain the difference at <1 MeV energy range by neutron multiple scattering. So, it is experimental problem, and ENDF/B-VII data based on the "most physical" model is correct. Therefore, it is interesting to estimate average energy for all available experimental data from thermal to 5 MeV, so to use not only thermal PFNS where low energy part may be overloaded with extra neutrons but experiments which were realized for fission neutron energy $E > E_0$ (where $E_0 \sim 0.5-3$ MeV). The scale "method" was applied for realization of this goal. The references, average energies, and their uncertainties are collected in Table 3.10.

Data from [43] have been corrected due to "sample size effect" (see Sect. 2.1.8). Data from [13] was recalculated with new angular distribution neutron production





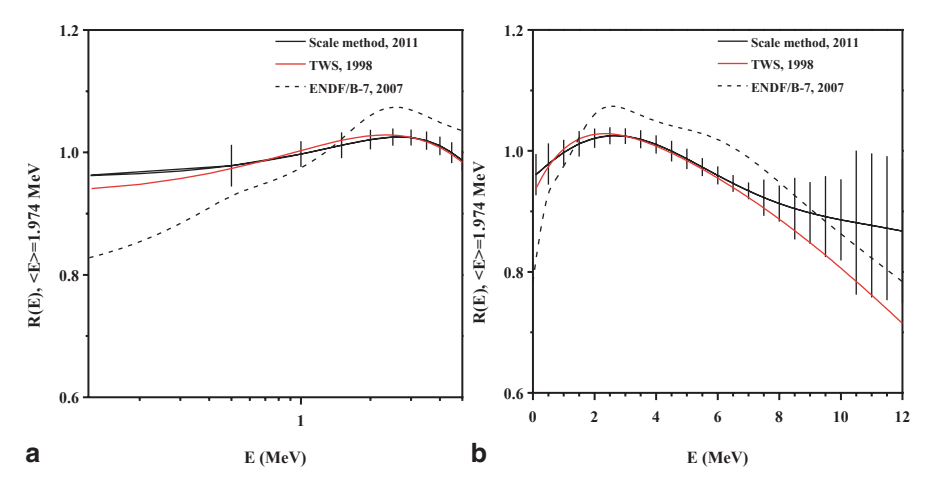


Fig. 3.16 Ratio of evaluated spectra to Maxwellian distribution $\bf a$ low energy part, $\bf b$ full energy scale. $\it TWS$ two Watt spectra

reactions [10] applied for efficiency measurement, and for "sample size effect." Average energies are plotted on Fig. 3.17. The data were fitted with two functions. The simple linear dependence:

$$\langle E \rangle = a_1 + a_2 E_0 \tag{3.15}$$

And more complicate function assuming dependence similar with Terrell's systematic:

$$\langle E \rangle = a_1 \sqrt{(a_2 + E_0)} + a_3 \tag{3.16}$$

References	E_0 (MeV)	$\langle E \rangle$ (MeV)	$\delta E (\text{MeV})$
Kornilov [27]	0	1.975	0.003
Starostov [42]	0	1.973	0.002
Lajtai [30]	0	1.987	0.014
Yufeng [52]	0	1.966	0.003
Johansson [13]	0.5	2.008	0.007
Trufanov [47]	0.5	1.972	0.014
Staples [43]	0.5	1.987	0.008
Staples [43]	1.5	1.990	0.010
Staples [43]	2.5	2.030	0.014
Boykov [26]	2.9	2.030	0.005
Staples [43]	3.5	2.059	0.018
Trufanov [47]	5	2.096	0.012

Table 3.10 Average neutron energy for ²³⁵U for energy range 0–5 MeV

The extrapolation to zero energy gave the same results inside uncertainties: $\langle E \rangle = 1.973 \pm 0.002$ Eq. (3.15) and $\langle E \rangle = 1.974 \pm 0.002$ Eq. (3.16). These values agree very well with average energy estimated for thermal point only.

3.6 PFNS for Multiple Chance Fission

At incident neutron energy E_0 higher then fission barrier $B_{\rm f}$ several processes give contribution in fission, and neutrons emitted in these processes should be included to PFNS calculation.

Let us investigate this process for reaction ${}^{A}X(n, f)$. After the absorption of the input neutron with input energy E_0 the fission of nucleus ${}^{A+1}X$ is the only contribution in this reaction. For this case, one may apply approaches discussed in upper sections without an additional complication.

If the input neutron energy is rather high and after neutron emission the compound nucleus has excitation energy higher than fission barrier, new fissile system 4 X will participate in fission reaction [(n, nf) process]. We may use the previous method but in this case we should re-estimate properties of fissile system. In addition, one should add the prefission neutron contribution in the total neutron multiplicity and the PFNS.

If the input energy is high enough to provide fission after the emission of two neutron, this (n,2nf) process also should be included, and so on.

Parameters of the model for each fission chance depend on masses of new nuclei involved in fission and their excitation energy. We will demonstrate the application of TWS approach for this difficult task.

The equations used before should be re-defined for each chance taking into account *i*-th nuclei with mass number (A+1-i) involved in fission process:

$$S_i(E, U_i) = 0.5 \sum_{i=1}^{2} W_i(E, E_0, T_{ij}(U_i), \alpha)$$
(3.17)

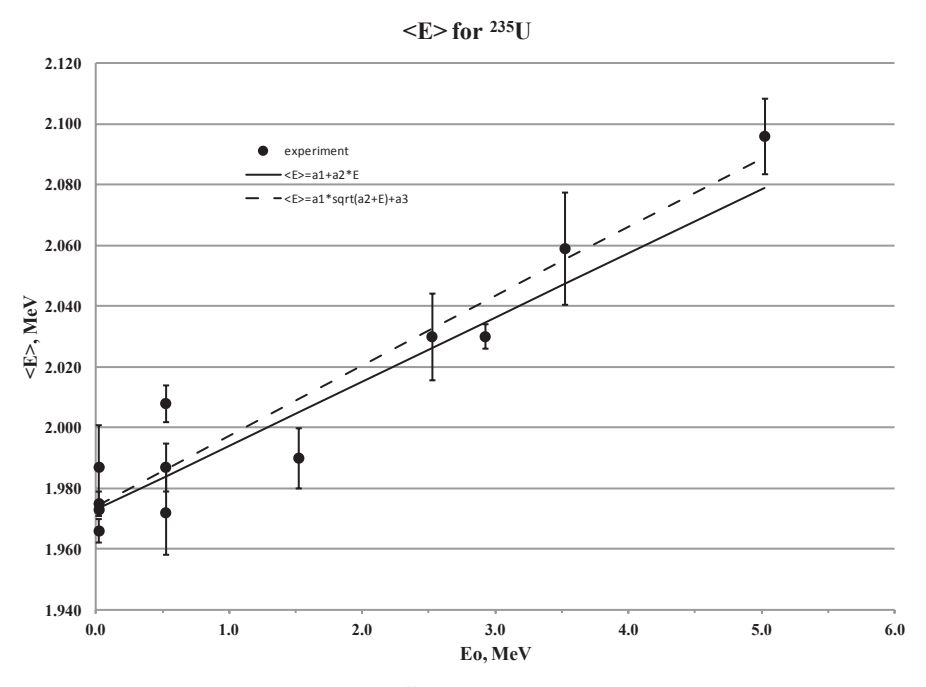


Fig. 3.17 Average energy of PFNS for $^{235}\mathrm{U}$ for energy range 0–5 MeV estimated by "scale method"

$$W_{ij}(E, T_{ij}, E_{vij}) = M(E, T) \times \exp\left(-\frac{E_{vij}}{T_{ij}}\right) \frac{\sinh\sqrt{b_{ij} \times E}}{\sqrt{b_{ij} \times E}}, \quad b_{ij} = \frac{4E_{vij}}{T_{ij}^2} \quad (3.18)$$

$$T_{ij} = T_{j}^{cf} \sqrt{\frac{(E_r - TKE_i + U_i)A^{cf}}{U_{cf}A_i}} = k_{ij} \sqrt{E_r - TKE_i + U_i}$$
(3.19)

$$U_{i} = E_{0} + B_{n} - \sum_{k < i} (\langle E_{ik} \rangle + B_{k})$$
(3.20)

where T_{ij} are the temperature parameters for light (j=1) and heavy (j=2) fragments of the i-th nucleus after emission of i=0,1,2,... prefission neutrons, E_0 is the incident neutron energy, α is the ratio of the total kinetic energy (TKE $_i$) at the moment of the neutron emission to the appropriate TKE $_i$ value for the i-th fissioning nucleus. In Watt's equation Eqs. (3.18)–(3.20) the CMS energy per nucleon is reduced as $E_{vij} = \alpha \times E_{vij}$, i.e., $E_{v1i} = A_{2i} / (A_{1i} \times A_i) \times \alpha \times \text{TKE}_i$, $E_{v2i} = A_{1i} / (A_{2i} \times A_i) \times \alpha \times \text{TKE}_i$.

Experimental PFNS data were fitted as was described above, assuming that α is a free parameter. The ratio of "temperatures" for light and heavy fragments $T_{i1}/T_{i2}=1.248$ is the second semiempirical fitting parameter, which was assumed to be independent of the nucleon composition, and fission chance.

Above the emissive fission threshold, i.e., in the incident neutron energy range $E_0 > 6$ MeV, PFNS are described as a superposition of prefission (n, xnf) reaction neutrons and prompt fission neutrons, emitted from $^{A+1-i}X$ (i=0,1,2) nuclides due to fission process itself, and an additional contribution due to the emission of i prefission neutrons:

$$v(E_{0})\tilde{S}(E, E_{0}) = \tilde{S}_{A+1}(E, E_{0}) + \tilde{S}_{A}(E, U_{1}) + \tilde{S}_{A-1}(E, U_{2}) + \tilde{S}_{A-2}(E, U_{3}) + \dots$$

$$\tilde{S}_{A+1}(E, E_{0}) = v_{0}(E_{0})\beta_{0}(E_{0})S_{A+1}(E, E_{0})$$

$$\tilde{S}_{A}(E, U_{1}) = \beta_{1}(E_{0})[v_{1}(U_{1})S_{A}(E, U_{1}) + P_{11}(E, E_{0})]$$

$$\tilde{S}_{A-1}(E, U_{2}) = \beta_{2}(E_{0})[v_{2}(U_{2})S_{A-1}(E, U_{2}) + P_{21}(E, E_{0}) + P_{22}(E, E_{0})]$$
(3.21)

The total number of prompt fission neutrons may be estimated as:

$$\nu(E_0) = \sum_{i=0} [\nu_i + i] \beta_i(E_0)$$
(3.22)

So we have got several fissile nuclei for i=0,1... for example 236 U, 235 U, 234 U, and 233 U and so on in case of 235 U(n,f) reaction. Functions $P_{ik}(E,E_0)$ (i>1, k <= i) is the spectrum of k^{th} neutron emitted before fission of A+1-i nucleus. These functions are normalized by definition on unit.

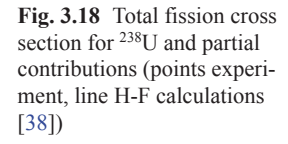
Function $\beta_i(E_0)$ is probability of fission after emission of *i*-neutrons.

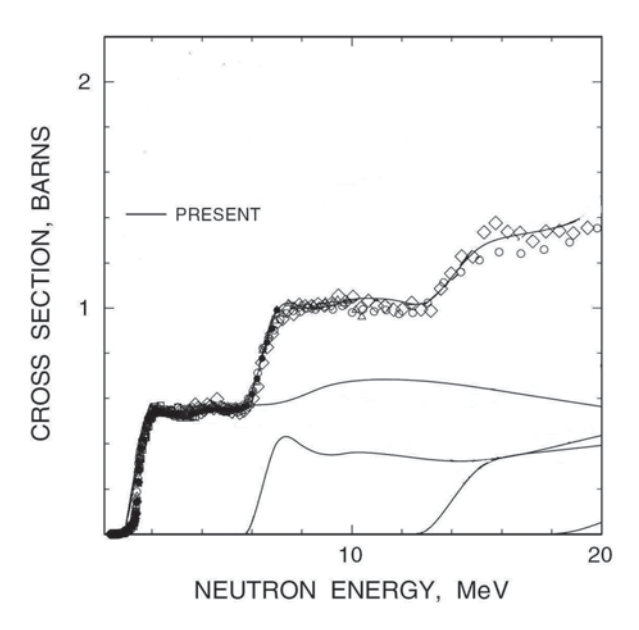
According to this rather short introduction the evaluation of the PFNS for multiple chance fission is a very difficult task. One should predict PFNS and neutron multiplicity for all energy interval $E\!<\!E_0$ and for several fissile nuclei. In an addition, the probability of different fission chances and spectra for all prefission neutrons should be taken into account.

Methods of calculations were developed in several papers [37, 14, 38, 39]. The most important results which demonstrate reliability of this approach will be given here. As an example the 238 U(n, F) reaction will be discussed following to [37, 38].

The contributions of the *i*-th multiple-chance fission reactions to the observed fission cross-section $\beta_i(E_0)$ and prefission neutron spectra $P_{ij}(E,E_0)$, i.e., spectra of the *j*-th prefission neutrons for the *i*-th chance fission, were calculated in a Hauser-Feshbach statistical-model simultaneously with the ²³⁸U(n,F), ²³⁸U(n,2n), and ²³⁸U(n,3n) reaction cross-sections. So we do not have experimental information about the contribution of partial $\beta_i(E_0)$ fission cross sections. However, the comparison of the experimental and calculated results for total fission (n,F) reaction, and (n,2n), (n,3n) reactions cross sections allow us to verify the calculated procedure, and be sure in reliability of the calculated function which are important for PFNS evaluation.

The preequilibrium emission for first-neutron was taken into account, then average neutron energies $\langle E_{ii} \rangle$ Eq. (3.20) were estimated. Contributions of the ²³⁸U($n_i f$),





 238 U(n,nf), and 238 U(n,2nf) fission reactions to the observed 238 U(n,F) fission cross section are shown in Fig. 3.18.

Some parameters of Houser–Feshbach calculation (level density on barrier, structure of barrier, contribution of preequilibrium emission, and so on, see [37, 14, 38, 39]), were slightly adjusted to reach agreement between experimental and calculated results shown in Figs. 3.18, 3.19 and 3.20.

The incorporation of different fissile nuclei, with prefission neutron emission allow us to describe rather complicate PFNS shape at $E_0 > 6$ MeV. First of all this approach explained very large excess of low energy neutrons (see Fig. 3.21 at $E_0 \sim 7$ MeV) and irregularity for average energy of fission neutrons versus of input neutron energy (Fig. 3.22).

The model of multiple chance fission is in reasonable agreement with experimental data (see Fig. 3.21) at low energy but faced with problem at $E_0 > 10$ MeV, which is clearly visible on Figs. 3.22 and 3.23a, b.

This model cannot predict new experimental results for input neutron energies 13–18 MeV. First of all one should highlight that it is not clear nature of the contradiction between old and new results (see Fig. 3.22). One may assume [37] that the most important factors are: low efficiency of FF counting, different orientation of fission chamber electrodes, and problem with extrapolation of the experimental data to low energy range. All these problems were discussed in [37], and conclusion was that recent experimental data seem more realistic, from point of view of experimental procedure. From another side, data from [31] were measured with unique experimental peculiarity—the ²⁵²Cf as a standard neutron source was incorporated in one of the fission chamber electrode.

Fig. 3.19 238 U(n,2n) reaction cross section (experimental data (*points*) and calculated function (*line*))

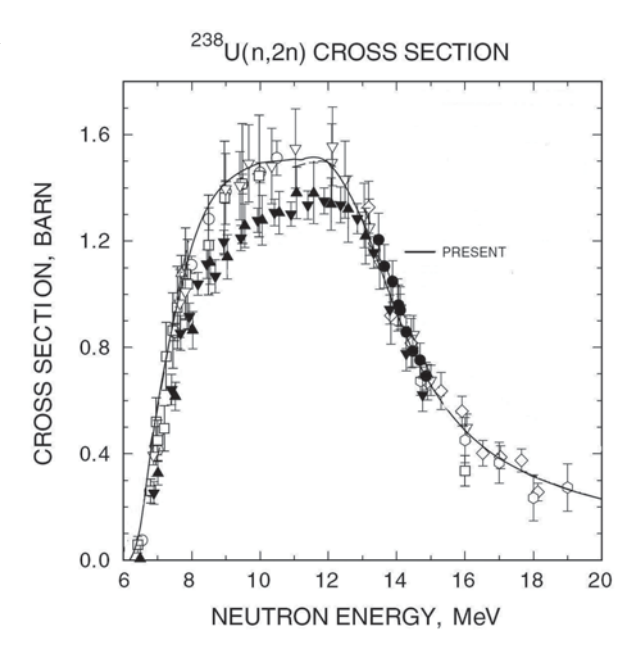
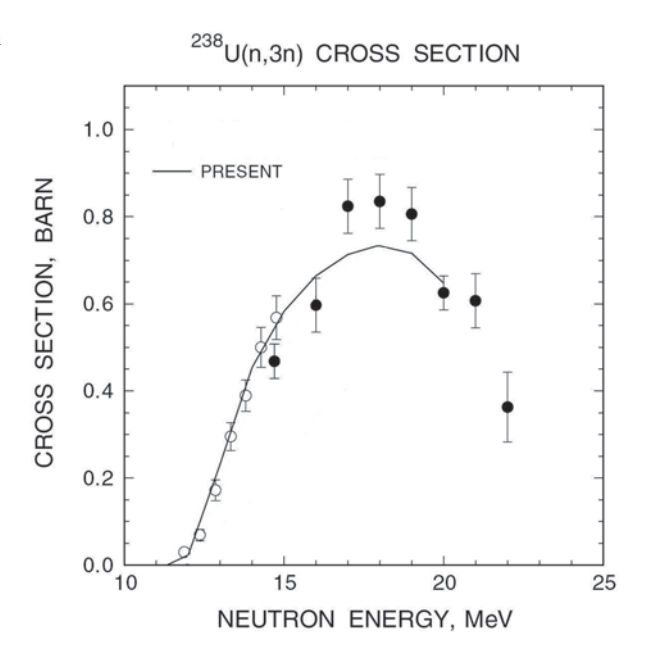


Fig. 3.20 238 U(n,3n) reaction cross section (experimental data (*points*) and calculated function (*line*))



The authors [31] assume that this fact allows them to reduce uncertainties connected with fission fragment counting from thick target of fissile material (²³⁸U) and Cf on separate electrode. However, there are obvious facts which may complicate this simple picture. The contribution of Cf fission dependence on time (due to Cf

Fig. 3.21 Measured [20, 17] and calculated PFNS [37] at $E_0 \sim 7$ MeV relative to Maxwellian with the same average energy $\langle E \rangle = 2.024$ MeV

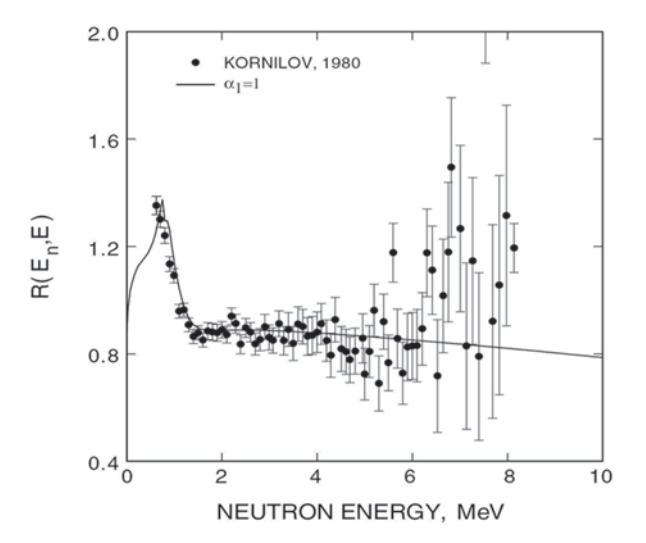
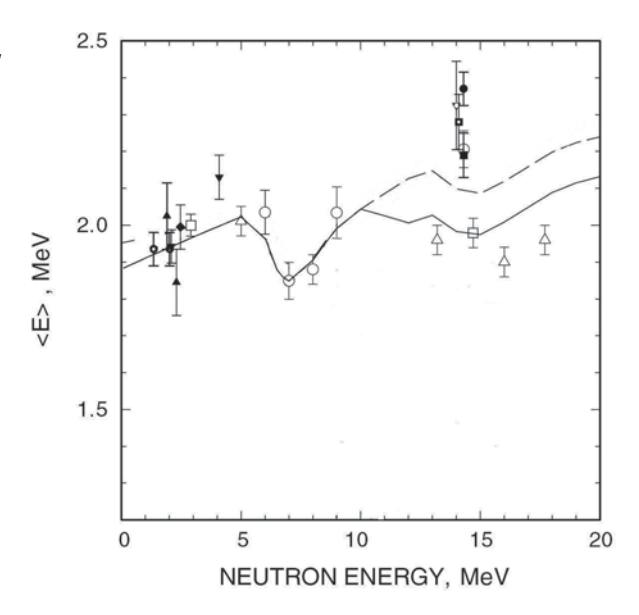


Fig. 3.22 Average energy of PFNS for ²³⁸U [37]. The *solid line* corresponds to α_1 =0.8, the *dashed line* to α_1 =1. *Triangles* give data from [31]



decay) and intensity of induced fission of ²³⁸U. They did not discuss the contribution of induced fission in the Cf electrode count rate, and how they took into account this effect.

The capacitor of U-electrodes even connected to different preamplifiers is much higher, so the pulse shape is different as compared with Cf-electrode, and noise contribution is also different. The average kinetic energy for Cf is higher than for ²³⁸U. This effect may also give the influence on efficiency for U and Cf standard. There

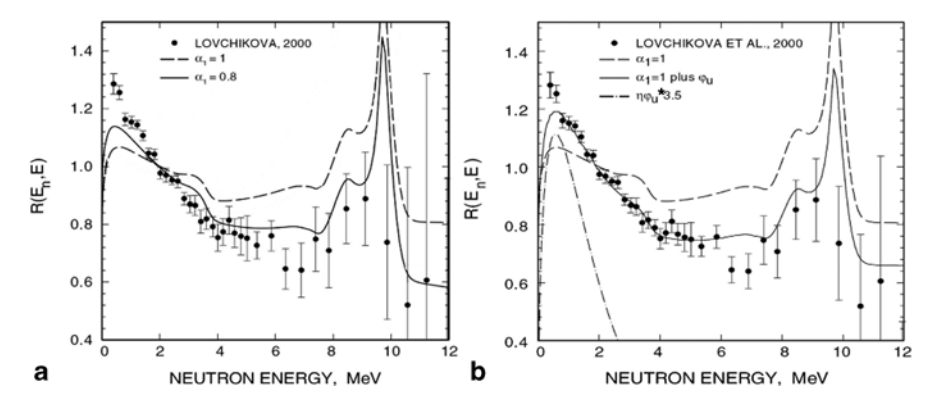


Fig. 3.23 a Measured [31] and calculated PFNS [37] at E_0 =16 MeV relative to Maxwellian with the same average energy $\langle E \rangle$ = 2.191 MeV . **b** The same as in **a** but with incorporation of an additional neutron source

are not strong arguments that experimental data of [31] are correct. However, if made this assumption, a rather big difference between experimental and calculated data (Figs. 3.22 and 3.23) should be explained.

It was discussed in many papers [48, 25, 11, 35, 24] that for excitations higher than ~20 MeV prompt fission neutrons could be emitted from the fragments before their full acceleration. It means that for $E_0 \sim 14$ MeV or higher, the neutron emission time might be comparable with the 238 U(n_s f) fission fragments' acceleration time of ~ 10^{-20} s; in other words, some neutrons could be emitted during fragments acceleration. Consequently, the CMS energy and average neutron energy in the LS would be reduced. This idea was used in TWS evaluation; however, it was used as an additional free parameter without deep "scientific sense." One may assume that the CMS energy per one nucleon E_{vij} could be further reduced see Eq. (3.9) as:

$$\tilde{E}_{vij} = \alpha_1 \times \alpha \times E_{vij} \tag{3.23}$$

here α_1 =1 for E_0 <10 MeV and α_1 =0.8 for E_0 >12 MeV, it is linearly interpolated for $10 \le E_0 \le 12$ MeV. This correction was made for the $^{238}\text{U}(n,f)$, $^{238}\text{U}(n,nf)$, and $^{238}\text{U}(n,2nf)$ multiple-chance fission reactions. The relevant calculated $\langle E \rangle$ and PFNS are shown in Figs. 3.22 and 3.23 by *solid lines*. This additional lowering of average energy of PFNS due to the reduced fission fragment velocity at the moment of neutron emission removes the major discrepancy between calculated spectra and measured data. This hypothesis roughly describes the reduction of the average energy and changes calculated PFNS shape at neutron energy >5 MeV in an agreement with experimental results.

At the same time one may suggest another explanation of this difference. There is stable excess of neutrons in the energy range <2 MeV for experimental data for $E_0>13$ MeV. This effect is clearly visible in Fig. 3.23. This contradiction may be reduced introducing an additional source of soft neutrons, emitted from nonacceler-

ated fragments, as was proposed in [44], or during the scission (Scission neutrons). The PFNS can be represented as:

$$S_s(E, E_0) = \eta \varphi_s + (1 - \eta) \tilde{S}(E, E_0)$$
 (3.24)

here $S(E, E_0)$ is the spectrum of PFNS from fission fragments, defined by Eq. (3.21), parameters are the same as those used without additional neutron source. The spectrum $\phi_c(E)$ of this neutron source is represented as:

$$\varphi_s(E) = \frac{E}{T_s^2} exp\left(-\frac{E}{T_s}\right) \tag{3.25}$$

The calculated spectrum with adjusted parameters η =0.18, T_s =0.64 MeV, $(v_s = \eta v = 0.86 \text{ neutrons/fission}, \langle E \rangle = 2T_s = 1.28 \text{ MeV})$ is shown in Fig. 3.23b by a solid line. The spectrum of these neutrons $\eta \times \phi_s(E)$, multiplied by a factor of 3.5 for convenience, is shown with a dashed-dotted line. Inclusion of this additional neutron source also decreases the discrepancy of calculated PFNS with measured data, but the properties of this neutron source look rather strange.

In work [44], it was found that the yield of these neutrons is ~ 0.5 neutrons/fission and their average energies $\langle E \rangle \sim 0.5-0.7$ MeV. They assumed that these soft neutrons are emitted from separated fragments staying at rest. Then the neutron emission time should be rather short, because emission should occur before full acceleration. The energies of emitted neutrons should be low, which corresponds to low excitation of the fragments. Authors of [44] argued that the excitation energy for each of the fragments is $\sim 5-6$ MeV. A compound nucleus at an excitation energy of $\sim 5-6$ MeV has a neutron emission lifetime of $10^{-18}-10^{-17}$ s. A similar neutron emission time was obtained in [40]. It was also shown in [24, 16] that the TKE reaches ~ 90 % of its maximum value within $\sim 10^{-20}$ s. That means that FF have rather low excitation energy, and neutrons could not be emitted from these fragments (low excitations-long emission time) before acceleration. Hence, if an additional neutrons source exists, it should be rather exotic in nature, i.e., its strength should increase with incident neutron energy.

The second explanation is that this component is so-named scission neutrons which are emitted during the scission of compound. However, it is not clear why we cannot see this type of neutrons at low input energy.

Nevertheless, the incorporation of the low energetic additional source may help in description of experimental data also.

References

 Abramson D, Lavelaine C (1974) Fission neutron spectra of ²³⁵U and ²³⁹Pu, Neitronnaya Fizika (Neutron Physics). Obninsk 3:47 (EXFOR 20997) References 73

 Baba M, Wakabayashi H et al (1989) Measurement of prompt fission neutron spectra and double-diffrential neutron inelastic-scattering sross section for ²³⁸U, and ²³²Th, INDC(JAP)-129/L, EXFOR 22112, 22158

- Baba M, Wakabayashi H, Ito N et al (1990) Prompt fission neutron spectrum measured of ²³²Th, ²³⁸U for 2 MeV neutrons. J Nucl Sci Tech 2(1):601 (EXFOR 22112)
- Blinov MV, Boykov GS, Vitenko VA (1983) New experimental data on the energy spectrum of ²⁵²Cf spontanious fission promt neutrons, Antwerp Conference, 479, Blinov MV, Boykov GS, Vitenko VA, Prompt fission neutron spectrum for spontanious fission of ²⁵²Cf, Report INDC(CCP)-238/L (June 1985)
- 5. Boikov GS, Dmitriev VD, Svirin MI, Smirenkin GI (1994) Neutron spectra in ²³⁷Np induced by neutrons of energy 2.9 and 14.7 MeV. Phys At Nucl 57:2126 (Phys At Nucl 57:2047)
- Boldeman JW, Clancy BE, Culley D (1986) Measurement of prompt fission neutron spectrum from spontanious fission of ²⁵²Cf. Nucl Sci Eng 93:181
- Boldeman JW, Culley D, Cawley RW (1979) Prompt fission neutron spectrum of ²⁵²Cf at low energy. Trans Am Nucl Soc 32:733
- 8. Bottger R, Klein H, Chalupka A, Strohmaier B The neutron energy spectrum from the spontanious fission of ²⁵²Cf in the energy range 2-14 MeV, Antwerp, Conference (1983), 484; Bottger R, Klein H, Chalupka A, Strohmaier B, The neutron spectra of the spontanious fission of Cf-252 (3–12MeV neeutron energy), IAEA-TECTOC-410, 1986, 186
- Boykov GS, Dmitriev VD, Kudyaev GA et al (1991) PFNS from ²³²Th, ²³⁸U, ²³⁵U at neutron energy 2.9 and 14.7MeV (low and upper the threshold for emission fission), Yad. Fyz. 53, 628. EXFOR 41110,41094
- Drosg M (DROSG-2000) Neutron source reactions. https://www-nds.iaea.org/drosg2000. html
- Eismont VP (1965) Neutron emission before total acceleration of fission fragments. At Energy 19:113
- 12. Hawerton RJ, Doyas R (1971) New systematic of temperature parameters for fission neutron spectra. NSE 46:414
- 13. Johanson PI et al (1977) Neutron spectrum of ²³⁵U at 0.5MeV neutron energy. NSE 62:695
- 14. Kawano T, Ohsawa T, Baba M et al (2001) Effect of the preequilibrium process upon rast neutron fission neutron spectra from ²³⁸U. Phys Rev C63:034601
- 15. Knitter H-H et al (1975) Measurement of the energy spectrum of prompt neutrons from the fission of ²³⁹Pu by 0.215 MeV neutrons. Atomkernenergie 26:76 (EXFOR 20576)
- Knitter H-H, Brosa U, Budtz-Jorgensen C (1991) Neutron and gamma emission in fission, The nuclear fission process, edited by C.Wagemans, (CRC Press Inc. 1991) pp 496-553
- Kornilov NV (1991) Prompt fission neutron spectrum of ²³⁸U, INDC(CCP)-336, Vienna, p 71
- 18. Kornilov N (2011) Scale method for evaluation of fission neutron spectra. NSE 169:290-295
- Kornilov N, Hambsch F-J (2011) Absolute ratio ²⁵²CF and ²³⁵U prompt fission neutron spectra. Nucl Sci Eng 168:73
- Kornilov NV, Zhuravlev BV, Salnikov OA et al (1980) PFNS for ²³⁸U at neutron energies 6-9MeV. In: Proceedings of the 5th Conference on neutron physics, Kiev, 15–19 Sept 1980, vol 2 (TsNIIAtominform, Moscow, 1980) pp 44–49
- Kornilov NV, Kagalenko AB, Zolatorev KI (1998) On the contradiction between microscopic and macroscopic data for ²³⁵U fission neutron spectrum at thermal energy, Dubna, Proceedings of ISINN-6, 242
- 22. Kornilov N, Kagalenko A, Hambsch F-J (1999) Computing spactra of prompt fission neutron spectra on the basis of a new systematic of experimental data. Phys At Nucl 62(2):173
- Kornilov NV, Kagalenko AB, Baryba VY et al (2000) Inelastic neutron scattering and prompt fission neutron spectra for ²³⁷Np, ISINN-5, Dubna, 1997, p 304, Ann Nucl Energy 27:1643– 1667
- Kornilov NV, Kagalenko AB, Hambsch F-J (2001) Prescission neutronsin the fission of ²³⁵U and ²⁵²Cf nuclei. Phys At Nucl 64(8):1372–1384. Translated from Yadernaya Fizika 64(8):1427–1433

- Kornilov NV, Kagalenko AB, Poupko SV et al (2001) New evidence of an intense scission neutron sourcein the ²⁵²Cf spontanious fission. Nucl Phys A686:187–203
- 26. Kornilov NV, Fabry I, Oberstedt S et al (2009) Total characterization of neutron detectors with a ²⁵²Cf source and a new light output determination NIMPR A 599:226–233
- 27. Kornilov NV, Hambesh F-J, Fabry I et al (2010) The ²³⁵U(n,f) prompt fission neutron spectrum at 100K input neutron energy. NSE 165:117–127
- Kornilov NV, Zhuravlev B, Salnikov O et al (1980) Prompt fission neutron spectra for ²³⁸U. Neitronnaya Fiz. (Neutron Physics), Moscow, Atominform, 3:104
- Lajtai A, Dyachenko PP, Kutzaeva LS, Kononov VN, Androsenko PA, Androsenko AA (1983) An absolute measurement of ²⁵²Cf prompt fission neutron spectrum at low energy range. Smolenice Meeting, 177
- Lajtai A, Kecskemeti J, Safar J et al (1985) Prompt fission neutron spectra for energy range 30keV -4MeV from ²³³U, ²³⁵U, and ²³⁹Pu induced by trhermal neutrons, TECDOC-335, Vienna, IAEA, p 312; EXFOR 30704
- Lovchikova GN, Trufanov AM, Svirin MI et al (2000) Energy spectra of neutrons accompanying the emission fission of ²³⁸U. In: Proceedings of the XIV international workshop on nuclear fission physics, Obninsk, 12–15 Oct, (State Scientific Center of Russian Federation—Institute for Physics & Power Engineering, (SSC RF IPPE), Obninsk, Russia, 2000) pp 72–82
- 32. Malinovskii VV (1987) Systematic of neutron multiplicity, VANT (Yad. Konstant). 2:25
- 33. Mannhard W (1987) Evaluation of the Cf-252 fission neutron spectrum between 0 MeV and 20 MeV, IAEA-TECDOC-410, p 158
- 34. Marten H, Richter D, Ruben A et al (1988) The neutron spectrum from neutron-induced fission of ²³²Th, Proc. IAEA Cons. Meeting, Mito, 1988; INDC(NDS)-220, p 169; Inter. Symp On Nucl Phys. Gaussig Zfk-638, p 10
- Marten H, Seeliger D (1988) Neutron evaporation during fission fragmment acceleration. J Phys G14:211
- Marten H, Seeliger D, Stobinski B (1983) The high energy part of the neutron spectrum from spontanious fission of ²⁵²Cf, Antwerp Conference, 488, Marten H, Richter D, Seeliger D, report INDC(GDR)-28/L, Sept 1984
- 37. Maslov VM, Poprodzinskij YV, Baba M et al (2003) Prompt fission neutron of ²³⁸U (n,f) above emission fission threshold. Eur Phys J A18:93
- 38. Maslov VM, Porodzinskij YV, Baba M, Hasegava A, Kornilov N et al (2004) Prompt fission neutron spectra of ²³⁸U and ²³²Th above emissive fission threshold. Phys Rev C69:034607
- Maslov VM, Kornilov N, Kagalenko AB et al (2005) Prompt fission neutron spectra of ²³⁵U above emissive fission threshold. Nucl Phys A760:274–302
- 40. Morettor LG (1972) Shell-correction calculations of fission decay widths and probabilities in superheavy nuclei. Nucl Phys A180:337
- Poenitz WP, Tamura T (1983) Investigation of the prompt-neutron spectrum for spontaniously fissioning ²⁵²Cf. Antwerp conference, 465; Poenitz WP, Tamura T, Smolenice meeting (1983), 175
- 42. Starostov BI et al (1984) Measurement of prompt fission neutron specta for some isotyopes, Neitronnaya Fizika (Neutron Phys) 2:285, 290, 294 (EXFOR 40871, 40872, 40873)
- 43. Staples P, Egan JJ, Kegel GHR, Mittler A, Woodring ML (1995) Prompt fission neutron energy spectra induced by fast neutrons. Nucl Phys A591:41
- 44. Svirin MI, Lovchikova GN, Trufanov AM (1997) Features of the spectra of neutrons accompanying the neutron-induced emission fission of ²³⁸U. Yad Fyz 60:818
- 45. Terrell J (1959) Fission neutron spectra and nuclear temperature. Phys Rev 113(2):527
- 46. Trufanov AM, Lovchikova GN, Sukhih SE et al (1992) Energy distribution of ²³⁷Np fission neutrons. Phys At Nucl 52:298
- 47. Trufanov AM, Lovchikova GN, Smirenkin GN (1994) Measurements and estimation of the average energy of neutrons fron the ²³⁵U(n,f) reaction. Yad Fiz 57:606; (Phys At Nucl 57:572)

References 75

48. Vorobyev AS, Sherbakov OA, Pleva YS et al (2009) Measurements of angular and energy distributions of prompt neutrons from thermal neutron-induced fission. NIMPR A598:795–801

- 49. Wapstra AH, Audi G, Hoekstra R (1988) Atomic masses from (mainly) experimental data. At Data Nucl Data Tables 39(2):281
- 50. Watt B (1952) Energy spectrum of neutrons from thermal fission of ²³⁵U. Phys Rev 87(6):1037–1041
- 51. Weigmann H, Hambsch F-J, Mannhart W, Madland DG et al (2003) Fission neutron spectra of Uranium-235, NEA WPEC-9, ISBN-92-64-02134-5, NEA
- 52. Yufeng W, Xixiang L, Anli L et al (1989) Experimental study of the prompt fission neutron spetrum of ²³⁵U fission induced by thermal neutrons. Chin J Nucl Phys 11:47 (EXFOR 32587)
- Zamyatnin YS, Kroshkin NI, Melnikov AK et al Measurement of energy spectra and neutron multiplicities for fission neutrons of actinides. Second international conference on nuclear data for reactors, Vienna, 15–19 June 1970, 2:183

Chapter 4 Physical Models

We selected the process of the Prompt Fission Neutron Spectra (PFNS) analysis into two parts, or separate sections:

- 1. Evaluation on the basis of semiempirical model, which allows us to compare of different experimental data, select wrong results, and give recommendations for data library creation;
- 2. Development of theoretical models, which first of all are addressed for understanding of the nature of prompt fission neutron (PFN) emission, explanation semiempirical relations, and of course made recommendations for data library, if the theoretical model agrees with experimental data in the whole energy range and for all isotopes. Or provide the recommendation for future experimental efforts, to understand problem and explain the mechanism of neutron emission in fission.

This splitting of the problem has very simple explanation: till now we have a problem with theoretical modeling which can predict all sets of experimental data without tuning of model parameters, sometimes outside the reasonable range.

The most important data for practical application are the neutron multiplicity as function of input neutron energy for main isotopes, and the shape of the PFNS. Therefore, main attention was paid for investigations of these data; sometimes very important results were outside the attention of models' creators.

The German "ansatz" is the best word to define modeling of the neutron emission in fission. An ansatz is the establishment of the starting equation(s), the theorem(s), or the value(s) describing a mathematical or physical problem or solution. It can take into consideration boundary conditions. After an ansatz has been established (constituting nothing more than an assumption), the equations are solved for the general function of interest (constituting a confirmation of the assumption).

It is not clear at what time the neutrons are emitted; measured neutron widths at thermal energies, extrapolated to high energies [58], give emission times of the order of 10^{-16} s, and an upper limit of 4×10^{-14} s has been found from angular correlation measurements. However, the neutron emission times may be considerably shorter; the lower limit must be of the order of 10^{-22} s, the time required for a

nuclear particle to cross a fission fragment (FF). If the time is less than 10^{-20} s the FFs will not attain their maximum velocities.

The main idea about emission after acceleration based on the assumption that neutrons are emitted from the fragments in a time lying in the range 10^{-20} – 10^{-14} s, during which the fragments have an essentially constant velocity in any case.

A lot of theoretical works during last 60 years were devoted to the detailed discussions of neutron emission mechanism in fission. The most important papers which may be defined as "mile stones" are mentioned in [22, 34, 36, 38, 39, 41, 43, 58].

According to discussion in [39], an actinide nucleus undergoing fission is characterized by the variables: A—mass, Z—charge, E^* —excitation energy, J—spin, and projection quantum number K. These quantities define its fissility Z^2/A , the fission probability (mainly via E^*), the angular distribution of FFs (depending on J, and K), and the occurrence probability $Y(A,Z,TKE,E^*,J)$. The probability function Y is mainly formed during the descent from the outside saddle point to the scission point. Whereas the potential energy at all deformation stages can be approximated by self-consistent Hartree–Fock calculations or the macroscopic—microscopic method, the time evolution of the fissioning nucleus and all its dynamic features, which is strongly related to nuclear inertia and dissipation, is still one of the most challenging topics in the field.

According to various dynamical calculations, which differ in regard to dissipation mechanism, the transition time between saddle and scission point is in the order of $(2-6) \times 10^{-21}$ s.

Phenomenological, one can assume that the potential energy gain between saddle and scission point is the sum of a dissipative energy $E_{\rm dis}$, and the kinetic energy of collective degrees of freedom, whose translational part appears as prescission kinetic energy of the fragments $E_{\rm pre}$.

The first term gives rise to a scission point temperature influencing the microscopic terms of the potential energy. The definition of a scission point is crucial, since it is not defined by static conditions alone, but can be understood as random neck rupture, since the rather small transition time for the descent from saddle to scission point is required. Scission itself corresponds to a rapid change of nuclear potential. Strong single particle excitations and, consequently, particle emission at scission seem to be possible.

For simplicity, it is, however, useful to formulate a phenomenological energy balance equation for the scission point:

$$Q + E_A^* = E_{\text{pre}} + E_{\text{coul}} + E_{\text{def}} + E_{\text{dis}} + E_B^*, \tag{4.1}$$

where Q is the total energy release for the given fragmentation $(A_1/A_2; Z_1/Z_2)$. The total intrinsic excitation energy:

$$\boldsymbol{E}_{\mathrm{sc}}^* = \boldsymbol{E}_{\mathrm{dis}} + \boldsymbol{E}_{\mathrm{B}}^*$$

is assumed as sum of $E_{\rm dis}$ and the excitation energy $E_{\rm B}^*$ at the second saddle. The variable F is the potential energy at scission:

$$F = E_{\text{coul}} + E_{\text{def}},$$

whose two parts, the Coulomb potential energy $E_{\rm coul}$, and the deformation energies $E_{\rm def}$ of the individual fragments, depend on the deformation (represented by a set of parameters).

Besides the acceleration of the fragments in the Coulomb field starting with the initial condition $E_{\rm pre}$ at scission and resulting in total kinetic energy (TKE):

$$\mathrm{TKE} = E_{\mathrm{pre}} + E_{\mathrm{coul}}.$$

At the beginning of the postscission dissipation, which immediately follows the descent from saddle to scission point with the relevant dissipation, states far from equilibrium conditions are shortly occupied. Accordingly, nonequilibrium particle emission should be expected. In respect to neutron emission during fragment acceleration, the time evolution of the internal fragment dynamics is of high importance. That is, since the neutron emission time (corresponding to a certain fragment kinetic energy) defines emission kinetics and, therefore, the angular correlations between neutron and fragment.

Due to the dynamic processes discussed above, the probability function, or FF yield $Y(A,Z,\mathrm{TKE},E^*,J)$ depends on time. However, it is useful to define "asymptotic" conditions achieved after fragment acceleration (effectively finished at about $3\times 10^{-20}\,\mathrm{s}$ after scission) as well as dissipation of E_{def} into intrinsic excitation energy distributed among the single particle degrees of freedom according to equilibrium. These conditions hold before any de-excitation process. Hence, we have:

$$U = E_{\rm def} + \alpha E_{\rm sc}^*,$$

where α —the fraction of scission point excitation energy coming to FF back. In regard to the probability function Y, it is emphasized that for a given nucleon number partition $(A_1/A_2;Z_1/Z_2)$ resulting in a defined Q-value, a distribution in TKE and U appears, where the constraint must be met. For fixed $(A_1/A_2;Z_1/Z_2)$ and TKE, the ratio U_1/U_2 is distributed around an average value due to phase space conditions. Obviously, the "asymptotic" distribution $Y(A,Z,\text{TKE},E^*,J)$ and energy distribution:

$$Q + E_A^* = \text{TKE} + U, \tag{4.2}$$

are starting points for traditional model calculation—"Neutron Emission After Fully Accelerated fragments" (NEAFA).

4.1 Basis for Theoretical Modeling

Three well-known experimental facts were discussed in introduction: (1) strong angular dependence of PFN yield relative to FF direction, (2) "exponential slope" at high energy, and (3) $(E)^{1/2}$ dependence of neutron energy < 1 MeV. First two facts stimulate assumption (ansatz) that neutrons are emitted from moving fragments.

Let us remind the reader the main relations used for modeling of neutron emission and experimental evaluation procedure. The experiments which may give the most physical information about mechanism on neutron emission investigate the "energy-angular" distribution of neutrons relative FF direction in Laboratory System (LS). All experiments used (and are using now) the same relations for data evaluations. The similar equations are applied for modeling of the neutron emission, if the NEAFA assumption is true.

In this case, the neutron yield at cosine angle μ , energy E in the LS, and the neutron energy-angular distribution $N(E, \mu)$ are determined by the following equations for any fixed fragment:

$$N(E, \mu^{l}) = \varphi(\mu^{c}) \Phi\left(\varepsilon(E, \mu^{l}, E_{v})\right) \frac{\sqrt{E}}{\sqrt{\varepsilon}}, \tag{4.3}$$

$$\varphi(\mu^c) = (4\pi)^{-1} (1 + bP_2(\mu^c)), \tag{4.4}$$

$$\mu^{c} = \frac{\mu^{l} \sqrt{E} - \sqrt{E_{\nu}}}{\sqrt{\varepsilon}},\tag{4.5}$$

$$\varepsilon = E + E_{\nu} - 2\mu^{l} \sqrt{EE_{\nu}}, \qquad (4.6)$$

where the indices l,c denote the value in the LS and in the center-of-mass system (CMS), respectively; E_{ν} —fragment CMS energy per nucleon; μ —cosine of angle between FF and neutron; ε —neutron energy in CMS; $P_2(\mu)$ —second-order Legendre polynomial; b—anisotropy of neutron emission in CMS; and $\Phi(\varepsilon)$ and $\varphi(\mu)$ —neutron spectrum and angular distribution in the CMS. These equations were given in many papers [see for example 58, 26].

FF with excitation energy $U\sim15$ MeV is very good object for application of the compound decay approach [66, 4]. The relative intensity distributions of outgoing particles (neutron) in Eq. (4.3) may be described:

$$\Phi(\varepsilon) \sim \sigma_{abs}(\varepsilon) \times \varepsilon \times \rho(U_B - \varepsilon), \tag{4.7}$$

where ρ is level density for excitation energy $U_{\rm B} = U - B_{\rm n}$ after emission zero energy neutron and $\sigma_{\rm abs}(\epsilon)$ —absorption cross section estimated with optical model.

To demonstrate the spectrum shape (according to text in [4]) author introduces the following Taylor expansion:

$$\rho(U_{\scriptscriptstyle B}-\varepsilon)\sim e^{S(U_{\scriptscriptstyle B}-\varepsilon)}, \text{ if } U_{\scriptscriptstyle B}>>\varepsilon; \ S(U_{\scriptscriptstyle B}-\varepsilon)\sim S(U_{\scriptscriptstyle B})-\frac{dS(U_{\scriptscriptstyle B})}{d\varepsilon}\varepsilon,$$

where S(U) is entropy function. Taking into account that for Fermi-gas model $U=aT^2$ (a—level density parameter and T—"temperature") one may find:

$$\Phi(\varepsilon) \sim \sigma_{abs}(\varepsilon) \times \varepsilon \times \rho(U_B - \varepsilon) \sim \sigma_{abs}(\varepsilon) \times \varepsilon \times e^{-\varepsilon/T}, \ T^2 = U_B / a. \tag{4.8}$$

This is a traditional, so-named Weisskopf-Ewing approach for PFNS calculation.

However, first researchers who started the application of Eqs. (4.3)–(4.8) for PFNS calculation, Watt [65], Feather [unpublished], Terrell [58], were faced with the problem. All measured PFNS exhibit property that at low energy in LS the spectrum is proportional to $E^{1/2}$. According to Eq. (4.3) this dependence in LS will appear immediately if one assumes the $E^{1/2}$ dependence in the CMS, however, there is not any realistic explanation for Maxwellian shape in CMS.

The spectrum which uses Eq. (4.8) and proper transformation in LS (Feather) "is not in accord with experiment for any single set of parameters Ev and T, ... and the use of two values of Ev corresponding to light and heavy fragment velocities does not much improve the fit" [58].

It is interesting that researchers in 1950s–1960s did not discuss that $E^{1/2}$ dependence may be a sign for different reaction mechanism. All attention was addressed which additional factors should be included in model to "move" the Weisskopf's evaporation spectrum Eq. (4.8) closer to square root dependence in LS.

After Terrell [58] the attention was concentrated on:

- Multiple neutron emission with its simple simulation with triangle distribution of *T*-"temperature";
- The incorporation of angular anisotropy effect [see Eq. (4.4)]. The *b* parameter should be ~ 0.1 to increase the neutron yield at < 2 MeV neutron energy in LS;
- Detail investigation of absorption cross sections. The energy dependence $\sigma_{abs}(\epsilon) \sim 1/\epsilon^{1/2}$ should help very much.

Researchers assumed that different mechanism of neutron emission may exist. According to Marten [38 and references therein] the following mechanisms, placed with increasing the time of the process mentioned about during long history of investigations:

- 1. Scission neutron emission due to rapid nuclear potential changes close to scission;
- 2. Neutron emission (equilibrium, nonequilibrium?) during fragment acceleration (strongly correlated with the mechanisms of dissipation of deformation energy;
- 3. Neutron emission from neutron-unstable light charged particles (⁵He, ⁶He,...) after ternary fission;

4. Neutron evaporation from fully accelerated fragments (predominant mechanism).

The following types of fission neutron models were used in past and are used now: *Hauser–Feshbach models* [7, 12, 16, 50, 57] (HFM) including the spin dependence of neutron emission in competition to gamma-ray and charged particle release.

Cascade evaporation models [1, 29, 31, 40, 49, 58] (CEM) based on the Weisskopf formula [Eq. (4.7)], i.e., neglection of spin effects on emission spectra.

Temperature distribution models [35, 42, 61] (MNM) assuming a distribution in rest-nucleus temperature instead of a fragment distribution versus energy.

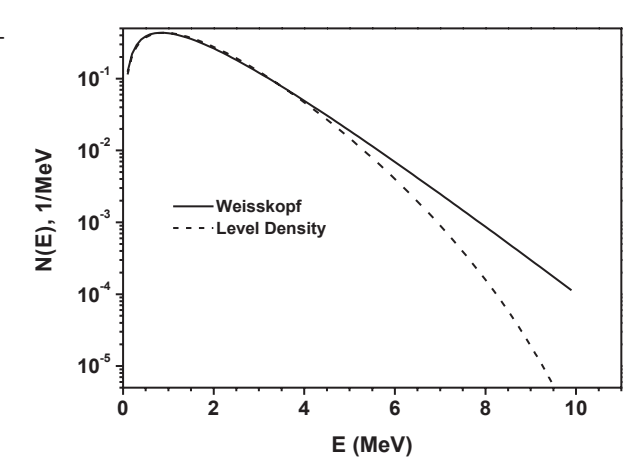
All models are based on the following assumptions and input data:

- NEAFA from excited fragments;
- Detail information for FF yield Y(A,Z,TKE,E*,J), or more simple selection of FF from this distribution;
- Detailed simulation of neutrons emitted from excited fragments, using evaporation model, or Hauser–Feshbach equations;
- Triangle "temperature distribution" is applied in case of Madland–Nix Model (MNM) instead of cascade emission with detailed information about binding neutron energy;
- Absorption cross section estimated from optical model;
- Level density parameter was adjusted to experimental data. Parameter *a* is applying for *T* calculation;
- The thermo-equilibrium or semiempirical relations for splitting of excitation energy between FFs;
- The constant "temperature" assumption [Eq. (4.8)] was applied in all these models;
- Angular dependence of neutron emission simulated with Eq. (4.4) (or similar [58])

4.2 True or Plausible Results?

The author of [39] concluded (1991): "In summary, it is emphasized that mechanisms of neutron emission in low-energy fission other than evaporation from fully accelerated fragments are really secondary. Deviations of differential experimental data from Statistical Model Approaches (SMA) predictions are commonly a consequence of nonadequate assumptions concerning the fragment distribution Y (in particular, drastic variable averaging), sometimes neglection of fission mode influences, and rough CMS (Centre of Mass Spectrum) approximations. Only after clarifying these circumstances, one should draw definite conclusions about any secondary mechanisms. The derivation of CMS spectrum parameters from experimental data and the application of such (rough) spectrum ansatzes to describe differential LS emission probabilities as done in several previous works must be evaluated. Chances to get more information about fission neutron mechanisms should be seen

Fig. 4.1 Neutron spectra calculated with Weisskopf and level density approaches



in combining further precise exclusive measurements of multiparameter fission neutron data with detailed theoretical descriptions on the basis of full-scale fragment distributions."

Terrell highlighted [58]: "Although the fission neutron spectrum calculations must, of course, conform to experimental data, the only adjustable constant determined from fission spectrum data is the nuclear temperature coefficient." So one may understand that without parameter adjusting (in a particularly *T*) to fission neutron spectra we cannot create correct model!

More ~ 20 years after Marten [39], we cannot demonstrate demonstrate "precise exclusive measurements of multiparameter fission neutron data with detailed theoretical descriptions" moved us very strong to understanding of mechanism of neutron emission in fission. However, some conclusions and approaches which were used before seem as "plausible result" now.

The "constant temperature" approach stimulated by big differences between experimental and calculated results at high energy range, and motivated by Weisskopf-Ewing simplification is "unique" approach for PFNS calculation to describe the experimental data.

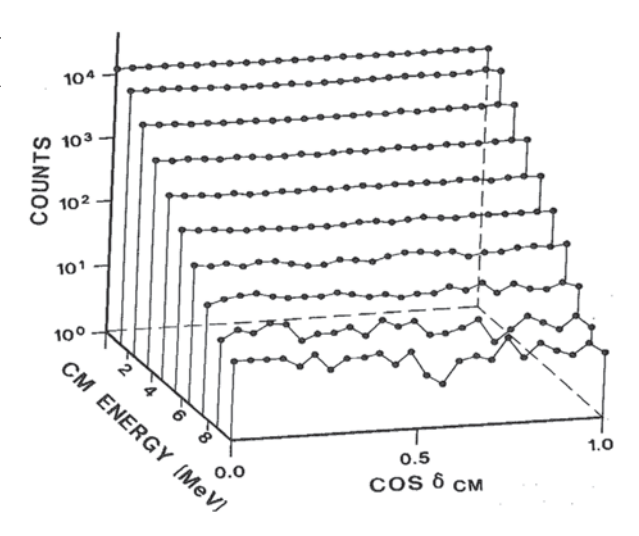
It is interesting to understand how is the spectrum shape changing after transition from original "evaporation spectrum shape [Eq. (4.7)]" to "*T*-constant" (4.8) approach.

The spectrum shape was calculated with well-known formula for level density $\rho(U)$:

$$\rho(U) \approx \exp(2\sqrt{aU}) / U^{1.25}.$$

And T=constant approach with Eq. (4.8). Both spectra with Level Density and Weisskopf assumptions, calculated with parameters a = A/10, A = 140, $U_B = 10$ MeV, $\sigma(E) = const$ are demonstrated in Fig. 4.1.

Fig. 4.2 Neutron angular distribution in CMS according to [8] for ²⁵²Cf(sf). *CM* center of mass



The average neutron energies are very close, so the experimental data like a neutron multiplicity may be predicted with similar accuracy. However, the spectrum shape in particular for high energy range may be overestimated very much with Eq. (4.8).

In [53], it was shown that incorporation of angular anisotropy in CMS emission β =0.1 increases the neutron yield for energy range E<1 MeV up to ~10%. They used equation for CMS emission:

$$\varphi(\mu^c) = \frac{1 + \beta(\mu^c)^2}{4\pi(1 + \frac{\beta}{3})}.$$
(4.9)

Parameters b [Eq. (4.4)] and β [Eq. (4.9)] are connected by formula:

$$b = \frac{2\beta}{3+\beta}.\tag{4.10}$$

So for $\beta = 0.1$, b = 0.065.

Terrell did not have experimental data when suggesting this dependence for correction of low energy part of the CMS spectrum. The angular distribution of neutrons in CMS was investigated in [8]. The Fig. 4.2 demonstrate anisotropy for energy range 1–8 MeV. The energy integrated angular distribution was described by Eq. (4.8). It was found that:

$$b = 0.01 \pm 0.02$$
.

Author concluded that this result means complete isotropy within experimental uncertainties.

The same experimental data after correction for multiple scattering were analyzed in [24]. Anisotropy parameters were fitted for light and heavy fragments: b_1 =0.022±0.003, b_h =0.015±0.03. So one may conclude experimental data for ²⁵²Cf (in any case) do not confirm the anisotropy on the levels used in theoretical models.

The NEAFA assumption is traditionally applied for experimental data analysis. Neutron energy distributions measured in LS are transformed to CMS. These data are described by equation:

$$\varepsilon^{\lambda} \exp\left(-\frac{\varepsilon}{T}\right),$$
 (4.11)

with fitted parameters λ , T. After this the data return back to LS with following conclusion about reliability of NEAFA assumption. It seems this procedure may provide wrong conclusion. Facts demonstrated here may illustrate this problem.

After the transformation to CMS system the average energy of neutrons estimated in [5, 8] are in reasonable agreement (Fig. 4.3a). There are not any problems for light FF. CEM predicts $\langle \varepsilon \rangle$ for mass range A < 130 reasonably well. Author [39] explained the difference for heavy fragment due to contribution of different fission modes [6]. The "fission mode" model predicts (this is parameter sensitive case) two modes around $A \sim 132$ —"standard 1" and "standard 2" with much higher excitation energy. It is difficult to predict with high accuracy the contribution of "standard 2" mode. However, the appearance of this mode according to [39] gives possible explanation of the old discrepancy between measured average CMS neutron energy and evaporation calculation around $A \sim 132$ (252 Cf).

This conclusion seems rather optimistic. An additional excitation energy due to "standard 2" should increase neutron multiplicity and average energy together.

However, the experimental data demonstrate rather strange case, the multiplicity v(A) < 1, but average energy is rather high. If evaporation theory is correct, the high average energy means high excitation, but at the same time high excitation do not allow the multiple neutron emission at all. So the result predicted by CEM is in agreement with fundamental basis of this theory. The experimental results measured by different teams are in agreement, and the contradiction cannot be explained with systematic experimental mistakes. This conflict also exists for another fissile target. The similar problems were discussed in [16, 29] for 235 U(th) (see Fig. 4.3b).

It means that experimental data evaluated in framework of NEAFA contradict to CEM, based on the same assumptions, and this conflict may be connected with the procedure of experimental data analysis.

There are big contradictions between estimations of "secondary mechanism of neutron emission." According to experimental data analyzed in [25, 26, 39], the intensity of Scission Neutron Emission is very small <1%, or reach \sim 20%. What is the reality? As an example, let us analyze the evaluation procedure [8] where it was concluded that SCission Neutron (SCN) yield <1% and [8] \sim 10%. Both work used the same experimental data.

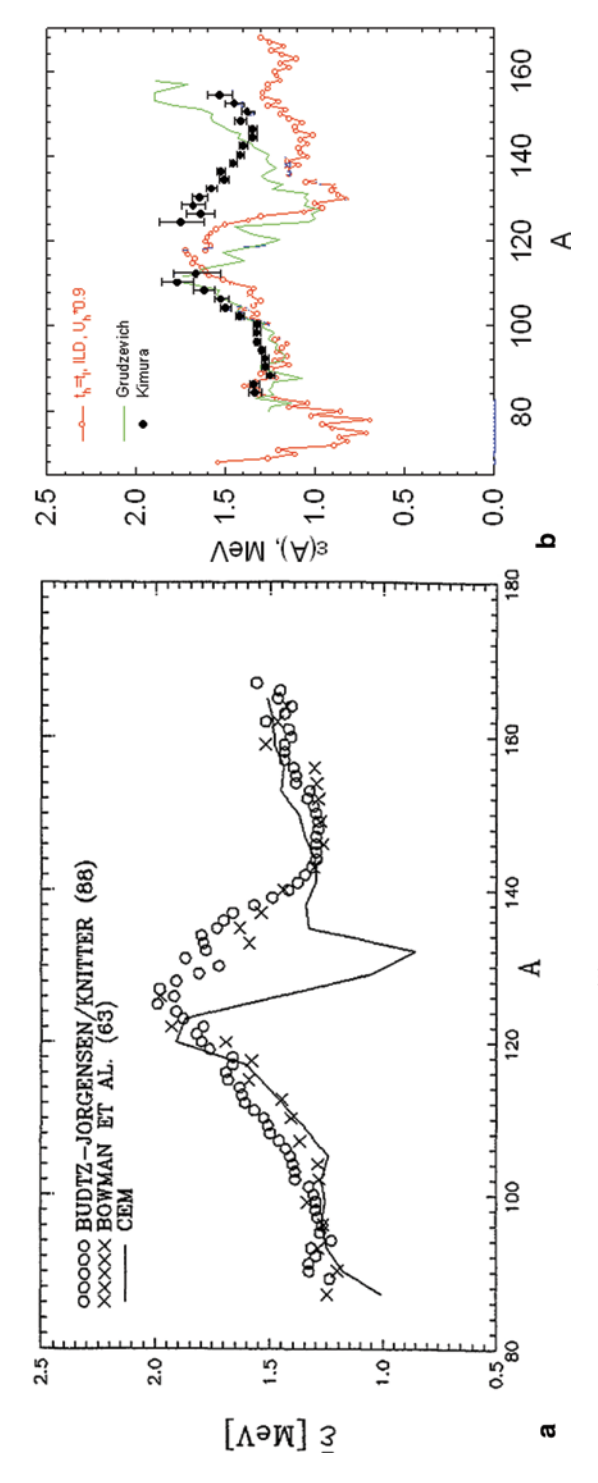


Fig. 4.3 a Average energy of neutron in CMS for ²⁵²Cf(sf) (circle [8] and crosses [5]). Solid line—cascade evaporation model [39]. **b** The same as in **a** for ²⁵⁵U(th). Experimental data [46]. Lines give calculated result from [16] (green) and from [28]

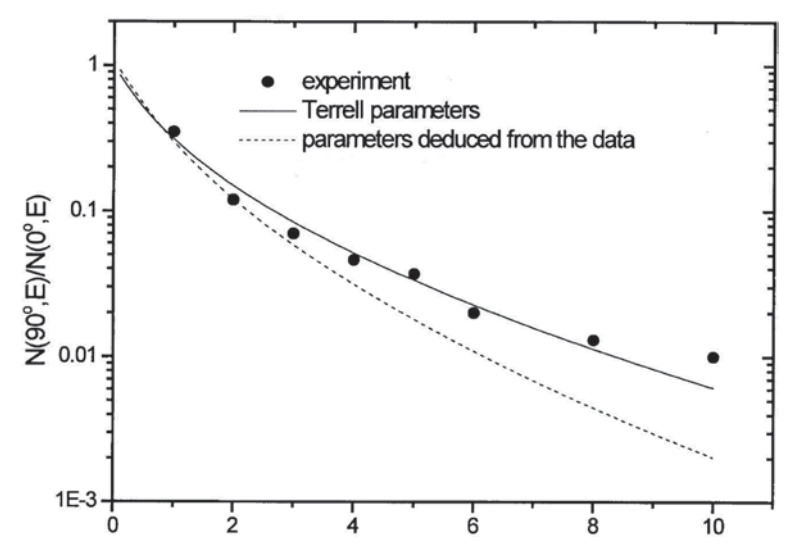


Fig. 4.4 Experimental [8] and calculated anisotropy with Terrel's parameters [59] (solid) and parameters estimated with parameters [8] (dashed)

The fragment direction, their masses, and kinetic energies were measured with a double Frischgridded ionization chamber [8]. Neutron spectra were measured by the time-of-flight (TOF) method. This experiment had very advanced characteristics: mass resolution $\sim\!0.5$ u, the resolution of the cosine of the fragment emission angle $\sim\!0.05$, time resolution $\sim\!0.7$ ns, and high statistical accuracy due to the integration over the azimuth angle. Such parameters as fragment mass, kinetic energy, angle between fragment, and neutron emission and the neutron energy were measured for each counted event.

The authors [8] tried to define which procedure of data analysis they may apply. Is it possible NEAFA assumption? They evaluated the angular anisotropy (the ratio $N(90^{\circ})/N(0^{\circ})$) as a function of the neutron energy, and compared this experimental result with calculated one using relations and parameters from paper [59].

The rather good agreement, stimulated the conclusion: "the energy dependence of the present $N(90^\circ)/N(0^\circ)$ intensity ratio is in agreement with the assumption that all neutrons are emitted from fully accelerated fragments." In the following paper [22], it was demonstrated that only a small amount of additional neutrons (~1%), with an average energy of ~0.4 MeV should be incorporated to describe the evaluated data for 252 Cf.

However, Terrell [59] did not make any difference between the CMS neutron energies and "temperatures" for light and heavy fragments. The calculated anisotropy based on the experimental parameters from [8] is shown in Fig. 4.4 by the *dashed line*.

Now we have got an obvious disagreement between the data points and the theoretical calculation assuming neutron emission from fully accelerated fragments that

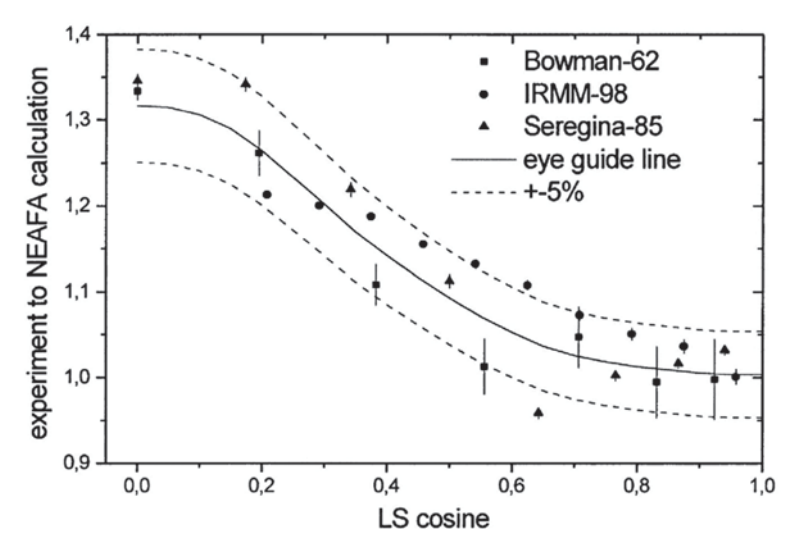


Fig. 4.5 The ratio of the experimental integrals from 1 to 5 MeV and calculated results. The spectra of IRMM-98 at abs (μ) =0.958 have been used for the transformation to the CMS and the calculation of the NEAFA integrals at abs (μ) <0.958. *LS* Laboratory System

requires an additional explanation. Understanding this disagreement stimulated a reevaluation [26] of the experimental data of Ref. [8].

There are two differences between analysis the same experimental data set: (1) correction for scattering in FF counter was done in [26], (2) after the positive conclusion about NEAFA approach, all data were transformed to CMS in [8]. In [26], only data at small angle with small contribution of SCission Neutron (SCN) (assumption) was transformed in to CMS. The parameters of Eq. (4.11) were found separately for light and heavy FF, and were used for calculation of energy angular distribution in framework of NEAFA model.

The comparison of experimental and calculated angular distribution in LS as a ratio is given in Fig. 4.5. This approach gave opposite result—contribution SCission Neutron (SCN) emission increased in order of magnitude.

So the main conclusion on the basis the results presented in Figs. 4.4 and 4.5 is the experimental data analysis used this scheme "LS dada \Rightarrow CMS dada \Rightarrow LS comparison" with conclusion about reality NEAFA assumption may give wrong understanding of the neutron emission mechanism.

Watt spectrum which describes reasonably the experimental data is an additional example of "plausible" result. This shape has very good physical basement in framework of traditional assumption. The Maxwellian distribution with parameter T emitted in the CMS moving with energy per nucleon $E_{\rm v}$ will be transformed to Watt function.

It is not important now that we cannot explain (exactly) the nature of the Maxwellian spectrum, and that Watt spectra may be agreed with experimental data only after fitting parameters.

It seems the most important that we understand the nature of this shape and origin of the second parameter E_v —the movement of the neutron source. In case of 252 Cf $E_{vl} = 0.958$ MeV, $E_{vh} = 0.557$ MeV, and average $E_v = 0.758$ MeV.

Frohner [11] analyzed experimental PFNS ²⁵²Cf and used Watt formula to describe practically the same data array as Mannhart did [37].

Maxwellian fit to the data gave $T=1.400\pm0.001$ MeV, with chi-square per degree of freedom $\chi^2=1.9$. On other hand, a Watt fit gave:

$$T = 1.175 \pm 0.005 \text{ MeV}, E_v = 0.359 \pm 0.009 \text{ MeV}, \rho(T, E_v) = -0.984 \text{ with } \chi^2 = 1.04.$$

The correlation coefficient $\rho(T, Ev)$ shows almost complete anticorrelation between the two parameters. Utilization of *two superposed Watt spectra* did not improve this very satisfactory fit, the spectrum, and chi-square changing only by fractions of a percent.

A Watt spectrum fitted to Mannhart's evaluation yielded in excellent agreement with the results given above:

$$T = 1.174 \pm 0.008 \text{ MeV}, \quad E_v = 0.361 \pm 0.014 \text{ MeV}.$$

The similar results were calculated with ²³⁵U(th) using experimental data set prepared for "scale method" evaluation:

$$T = 1.031 \pm 0.005 \text{ MeV}, E_v = 0.427 \pm 0.008 \text{ MeV}, \text{ with } \chi^2 = 0.798.$$

Analysis with two Watt's spectra gave:

$$T_1 = 1.24 \pm 0.02 \text{ MeV}, \ E_{v1} = 0.1 \pm 1.0 \text{ MeV}, \ T_2 = 0.93 \pm 0.02 \text{ MeV}, \ E_{v2} = 0.59 \pm 0.01 \text{ MeV}, \ \chi^2 = 0.789.$$

The E_{v} parameter has very clear physical meaning, but it is difficult to understand:

- Why incorporation of the second source (light and heavy fragments) did not increase the quality of the fit?
- Why parameter $E_{\rm v}$ fitted with high accuracy (2.5%) two times less its physical value?
- Why (in any case for 235 U) $E_{\rm v}$ for second moving source very close to zero?

4.3 Model Realized in Code FINE (FIssion Neutron Emission)

The FINE code based on the same assumption—NEAFA—as all previous models. The particular attention was addressed to the following points:

1. All available parameters and function were calculated in the LS, and these data were compared with experimental data: total PFNS, PFNS for separate fragment

masses A and TKE, energy-angular distribution for separate A and TKE, neutron angular distribution integrated over energy for different combination A, TKE, neutron multiplicity ν versus mass and TKE, so any combination available in experiment may be simulated;

- 2. For all isotopes two dimensions FF yield, Y(A,TKE) was constructed on the basis of one dimension Y(A), TKE(A) experimental data, and multimodal fission model;
- 3. For each mass split, A_1/A_2 estimated energy release and binding energy for all neutrons in cascade (up to 10);
- 4. Monter Carlo method was applied for simulation of neutron emission from excited FF, so it is not necessary to apply the simplification like "triangle T distribution" for simulation of multiple emission;
- 5. Evaporation approach was used for neutron spectra calculations;
- 6. Level density functions were verified with neutron spectra from (p, n) reactions;
- 7. Energy dependence of absorption cross section was used;
- 8. The code was verified relative to well-known distributions.

4.3.1 Estimation of the Two-Dimensional Y(A,TKE) Distribution

The idea of application of one dimension distributions Y(A), TKE(A) to estimate Y(A, TKE) was suggested in [27], and was used for multiplicity calculations [29].

For the correct calculation of the neutron multiplicity versus fragment mass and TKE, the two-dimensional distribution Y(A, TKE) should be known. Experimental data for Y(A, TKE) are only available for the major fissile isotopes.

The FF yield was calculated in the framework of the multimodal fission model [6]. Model parameters were adjusted iteratively by comparing the calculated with the experimental one-dimensional distributions for Y(A) and TKE(A). We assumed four fission modes—one symmetric mode, $S_{\rm sym}$, and three asymmetric modes, S_j , j=1.3. The question of fission mode existence and their sheer number is not point for discussion. This approach was used to parameterize the experimental data and to reconstruct the "two-dimensional model" distribution.

The least square method was applied for the minimization of the function $S(\vec{p})$ defined as:

$$S(\vec{p}) = \frac{\left(1 - \sum_{j} Y_{0j}\right)^{2}}{\sigma_{n}^{2}} + \sum_{i} \frac{\left(Y_{i} - \sum_{j} Y_{0j} G_{ij}\right)^{2}}{\sigma_{yi}^{2}} + \sum_{i} \frac{\left(\text{TKE}_{i} - \frac{\sum_{j} Y_{0j} G_{ij} \text{TKE}_{ij}}{\sum_{j} Y_{0j} G_{ij}}\right)^{2}}{\sigma_{\text{TKE}_{i}}^{2}}, \quad (4.12)$$

where Y_i and TKE_i are experimental data for the mass yield and TKE of the fragments for a given mass split with the heavy fragment mass A_i and the parameter vector being $\vec{p} = \{Y_{0j}, A_j, \sigma_j, \delta_j\}$. In this model, we take into account four parameters

for each fission mode: $Y0_j$ —yield of the mode, A_j —average mass, σ_j —variance of the mass distribution, and δ_j —distance between touching fragments. The uncertainties of the experimental data for normalization, mass yield, and TKE are denoted as σ_n , $\sigma_{\rm X}$, $\sigma_{\rm TKE}$, respectively.

The dependence of TKE as a function of fragment mass was calculated according to:

$$TKE(A_{i}, \delta_{j}) = TKE_{ij} = \frac{1.442(Z - Z_{i})Z_{i}}{\delta_{j}} + V_{\text{nucl}}(A_{i}, \delta_{j})$$

$$V_{\text{nucl}} = 4\pi\gamma_{0}\phi(0)\frac{b_{1}^{2}b_{2}^{2}}{a_{1}b_{2}^{2} + a_{2}b_{1}^{2}}, \rho_{1,2} = \frac{b_{1,2}^{2}}{a_{1,2}}.$$
(4.13)

Spheroidal fragments with semiaxis a, b were assumed.

As an additional assumption the distance between the fragment centers δj was kept *const* and independent of mass split. The nuclear attraction force is calculated as for two touching spheroids. We have only three equations to estimate four spheroidal parameters:

$$\delta_{j} = a_{1} + a_{2}$$

$$r_{0}^{3} A_{1} = a_{1}^{2} \rho_{1}$$

$$r_{0}^{3} A_{2} = a_{2}^{2} \rho_{2}.$$
(4.14)

An additional assumption is that in the touching point both fragments have the same curvature radius $\rho_1 = \rho_2$ at the tips of the spheroids. $\varphi(0) = -1.7817$ fm is the proximity potential function for zero distance between the surfaces, and γ_0 is the surface tension coefficient:

$$\gamma_0 = 0.9517 \left[1 - 1.7828 \left(\frac{N - Z}{A} \right)^2 \right] \text{MeV fm}^{-2}.$$
 (4.15)

All these equations and parameters were taken from [6].

We also assumed that the TKE distribution is limited by the Q-value for separate mass splits. This has as consequence that the total yield of the FFs with mass A is reduced with the share of the TKE distribution that is outside of the available range (TKE>Q). Due to this, the mass distribution for a separate fission mode G_{ij} has no simple Gaussian shape.

The variance of the TKE distribution for each fission mode was taken from Refs. [17, 54] with minor corrections. All fitted parameters are given in Table 4.1 for ²³⁵U [54], ^{244,248}Cm [21], and ²⁵²Cf [17]. The similar analysis was done for following nuclei and input energies: ²³⁹Pu at thermal and 5.5 MeV neutron energies [55], ²³²Th [51], ²³³U [52], and ²³⁵U [9] for Eo < 5 MeV.

Mode	Y_{oj} (%)	$\left\langle A_{j} ight angle \qquad \qquad \sigma_{j}$		δ_{j} (fm)	$\sigma_{TKE}^{}\left(MeV\right)$	
^{235}U			,			
SL	0.21	118.00	13.00	16.99	7.6	
S1	21.05	133.42	2.44	13.71	10.9	
S2	36.75	140.66	4.13	14.00	7.0	
S3	42.00	141.10	5.34	15.16	7.0	
²⁴⁴ Cm						
SL	1.14	122.00	8.00	16.27	10.0	
S1	9.42	132.58	3.34	14.65	7.5	
S2	46.06	138.76	4.77	14.72	7.5	
S3	43.37	141.34	9.02	15.32	8.0	
²⁴⁸ Cm						
SL	0.30	124.00	8.00	17.00	10.0	
S1	14.57	133.14	2.20	14.61	7.5	
S2	47.49	140.54	4.42	15.10	7.5	
S3	37.65	145.27	6.58	15.75	8.0	
²⁵² Cf						
SL	3.36	126.00	13.00	15.90	10.0	
S1	12.02	136.51	3.06	15.05	9.5	
S2	53.90	144.15	4.65	15.54	8.1	
S3	30.71	149.08	7.48	16.21	9.1	

Table 4.1 Fission mode parameters

Figure 4.6 shows the experimental data (*symbols*) for Y(A) and TKE(A) for 235 U(n_{th} , f) [54] together with the respective contributions (*dashed lines*) of the fission modes and their sum (*full line*). The similar good description one may see on Figs. 4.7 and 4.8 for 252 Cf and 239 Pu.

The two-dimension distribution constructed with this approach for ²³⁵U(th) is given in Fig. 4.9.

4.3.2 Neutron Emission from Excited Fragments

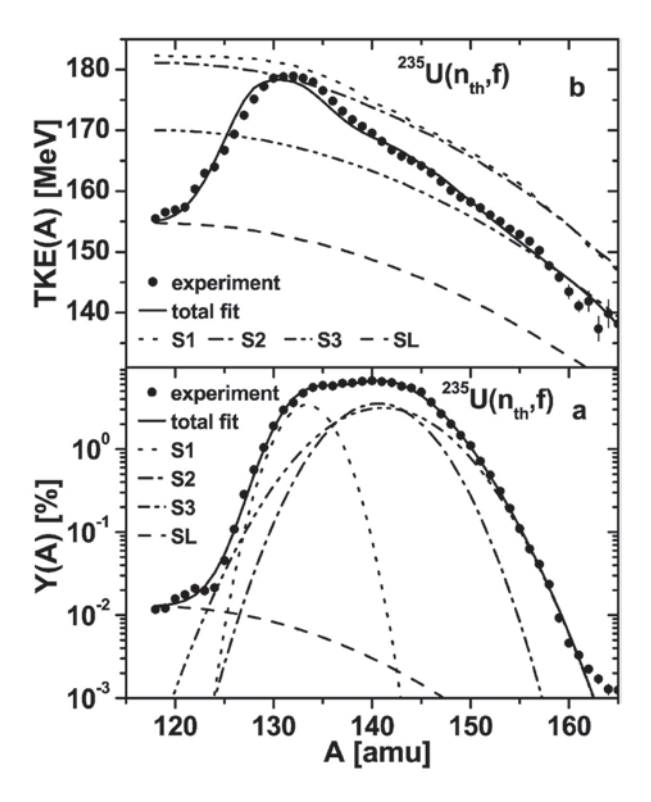
After the Y(A,TKE) distribution was found, the calculation of the neutron emission is a rather simple task consisting of the following steps:

1. For any TKE and mass split the Total Excitation Energy (TXE) was estimated as:

$$TXE(Z,A) = Q(Z,A) - TKE(Z,A).$$
(4.16)

The Q(Z,A) values were calculated with the Audi–Wapstra experimental mass tables [2] for the UCD (unchanged charge distribution) value $Z_0 = A \times Zc/Ac$ and $Z_0 \pm 1$, Zc, Ac being the compound nucleus charge and mass, respectively. If the masses did not exist in the experimental file, the theoretical data of Ref. [44]

Fig. 4.6 a Experimental neutron multiplicity for 235 U(n_{th} f) of Ref. [54] compared to model calculations (full line). b The same for TKE(A) experimental average neutron energy (full symbols) compared to our model calculation (full line). TKE total kinetic energy



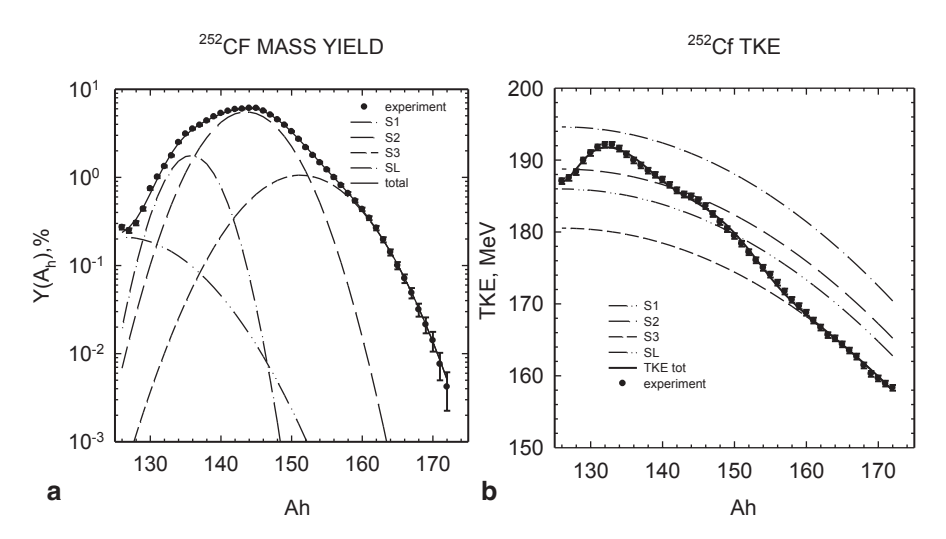


Fig. 4.7 a Experimental yield for ²⁵²Cf [17] (*solid symbols*) and multimodes description (*lines*). b The same as in a for TKE versus heavy fragment mass. *TKE* total kinetic energy

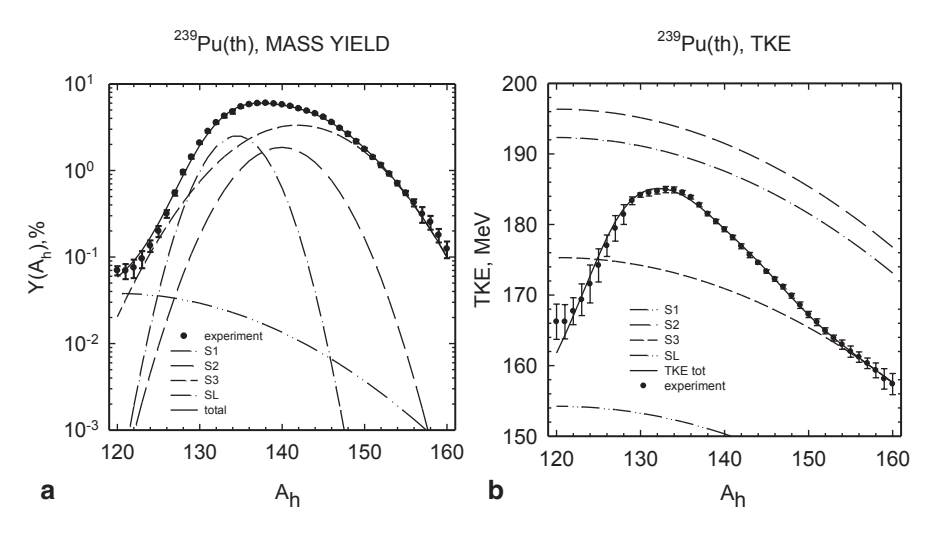


Fig. 4.8 a Experimental yield for ²³⁹Pu [55] (*solid symbols*) and multimodes description (*lines*). **b** The same as in **a** for TKE versus heavy fragment mass. *TKE* total kinetic energy

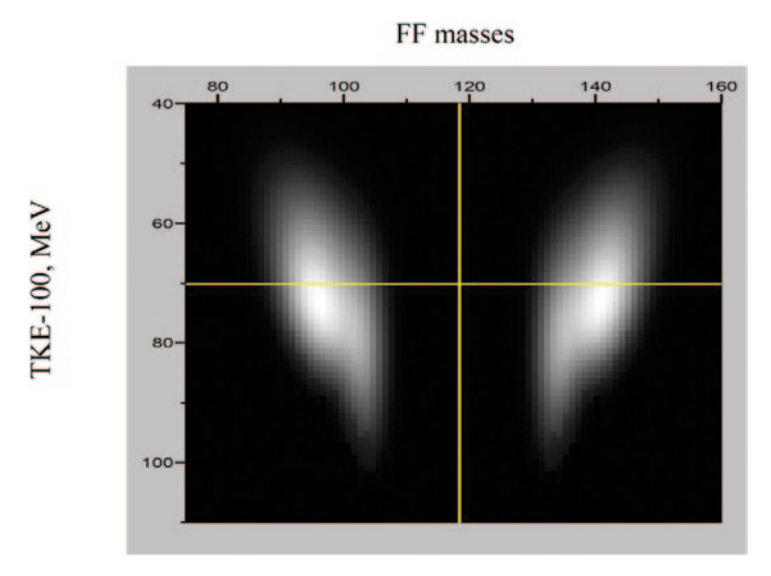


Fig. 4.9 Two-dimension distribution for Y(A,TKE) estimated from single dimension analysis for ²³⁵U(th). *FF* fission fragment, *TKE* total kinetic energy

were used. The charge yield was assumed to be the same for all fissile nuclei and FF masses— $\rho(Z_0)=0.584$, $\rho(Z_0\pm 1)=0.208$.

2. The $TXE = U_h + U_1$ was distributed between the light and heavy fragments based on a thermodynamical-equilibrium assumption. An additional correction

Target	TKE (MeV)		ν		E_{γ} (MeV)	
	Exp. [13]	Adjusted	Exp. [47]	Calc.	Exp.	Calc.
²³³ U	170.1 ± 0.5	168.8	2.488 ± 0.004	2.486	6.69 [10, 18]	6.89
$^{233}U(\lambda=1)$		168.8		2.267		7.22
^{235}U	170.5 ± 0.5	169.7	2.416 ± 0.004	2.412	6.70 ± 0.32 [68]	6.30
²⁵² Cf	184.1 ± 1.3	184.0	3.756 ± 0.005	3.723	6.99 ± 0.29 [68]	6.82

Table 4.2 Experimental and calculated average results: TKE, neutron multiplicity, and average energy of gamma-rays

TKE total kinetic energy

(without any scientific background) may be used to get agreement between calculated and experimental results for the dependence in v(A).

3. A neutron with energy ε is emitted if $U > B_n + \varepsilon$ (B_n the neutron binding energy). If this condition is wrong, the energy U was added to gamma-ray emission.

At the first stage of the model investigation, the simple Weisskopf–Ewing assumption with T-constant was applied for calculation of average energy, without neutron spectrum simulation. In this case, the spectrum shape was described with Eq. (4.11). The average energy $\langle \varepsilon \rangle = (\lambda + 1) \times T$ was applied only for estimation of neutron multiplicity. The value for $\lambda = 0.5$ was adjusted by fitting the calculated result to the experimental data of the total energy of fission γ -rays, E_{γ} , and average neutron multiplicity, v. The temperature parameter T was estimated by level density calculations. The level densities for this analysis were calculated on the basis of Phenomenological Superfluid model with Collective Enhancement (PSCE) [19] (subroutine may be found in www-nds.iaea/org/RIPL). So, in the beginning of the model development, the λ is the only free parameter for the v(A, TKE) calculation. All other data, namely Y(A, TKE), TKE(A), Y(A), Q-values, and B_n were taken from experiments or systematical investigations.

The calculated and experimental results supporting the choice of model parameters are given in Table 4.2. The experimental average TKE were slightly corrected (<1%, see column 3) to describe the experimental average ν , and E_{γ} . All calculations were made with λ =0.5. The value λ =1 (see row 4) cannot describe the whole data set. The assumption λ =0.33 (λ +1=4/3) contradicts the experimental data too.

4.3.3 Monte Carlo Simulation of Energy-Angular Distribution. Verification

As it was mentioned above for each mass split A_1/A_2 , TKE and charge Z, $Z\pm 1$, TXE(Z, A), and array of binding energies were found for each A_1 , A_2 , $A_1+A_2=A$. One may incorporate average binding energy B, average neutron energy ϵ , and average gamma-ray energy ϵ .

With this simplification average neutron multiplicity ν is connected with energy component by equation:

$$TXE(Z,A) = Q(Z,A) - TKE(Z,A) = v^*(B+\varepsilon) + E_{\gamma}.$$
 (4.17)

Having in mind the verity of input parameters (see Fig. 4.9) the Monte Carlo (MC) method is most attractive method for detailed simulation of neutron emission.

The neutron spectrum in LS was calculated for each angle, starting with energy simulated in CMS, angle in CMS, and angular distribution, Eq. (4.4), used as a "weight" of this event. The Y(A,TKE) was used for each FF splitting as another "weighting function." In reality, MC randomization applied for energy distribution only.

The energy split of TXE between light fragment (LF) and heavy fragment (HF) was defined by the "termo-equilibrium" condition between two fragments. However, any semiempirical correction for distribution of energy is possible.

The energy of emitted neutron was found with equation similar to Eq. (2.11), with "evaporation function" in integral:

$$rand(NN) = \int_{0}^{\varepsilon} \Phi(x) dx \tag{4.18}$$

where $\Phi(x)$ is defined by Eq. (4.7). At each cascade, $\Phi(x)$ was normalized to unit. The process was repeated until excitation energy of last residual nucleus was less than binding energy.

The procedure and subroutines prepared for energy simulation was verified with the following approach. If we assume that the energy distribution of the emitted particle is proportional to 1/E, the spectrum shape for n-th particle may be calculated with simple Eq. (4.19):

$$N_n(E) = \frac{(\ln(E_0) - \ln(E))^{n-1}}{(n-1)!Eo}.$$
(4.19)

Results of MC simulation and calculations with Eq. (4.19) for E_0 =10 MeV are shown in Fig. 4.10.

Model results may be calculated for selected LS angle, or like an angular integrated spectrum. This approach allows us reduce the time of calculation. So we started from cosine of angle in LS— μ^l and simulated CMS energy ε and angle of neutron emission in CMS. On the basis of these parameters, neutron energy in LS was estimated. In this approach, only $\frac{d\mu^c}{d\mu^l}$ should be incorporated as "weight" of emitted neutrons, together with "weight" due to "angular anisotropy" [Eq. (4.4)]. The vector diagram for transformation from CMS to LS is shown in Fig. 4.11. We have several cases which should be investigated separately. There is only one possibility for estimation of energy in LS for $\varepsilon > E_v$ and simple formula for derivative calculation.

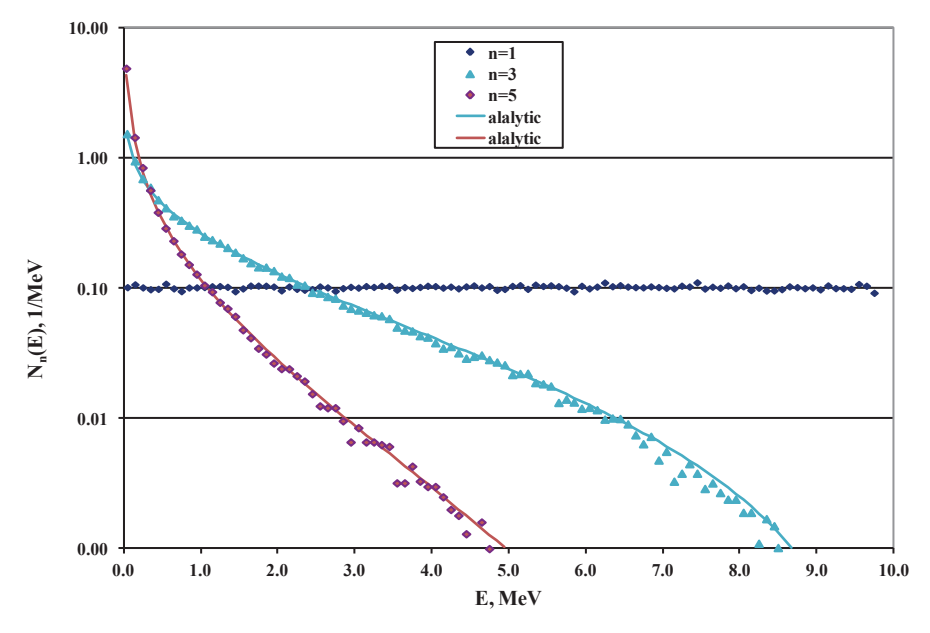


Fig. 4.10 The verification of MC simulation for 1/E distribution. *Points*—MC calculations, *lines* are Eq. (4.19) for n=1, 3 and 5

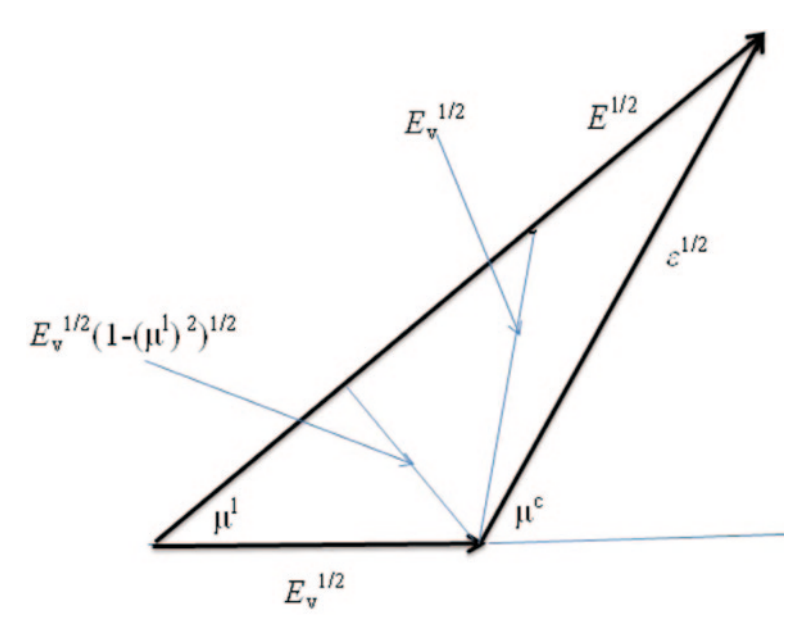


Fig. 4.11 Vector diagram for transformation from CMS to LS

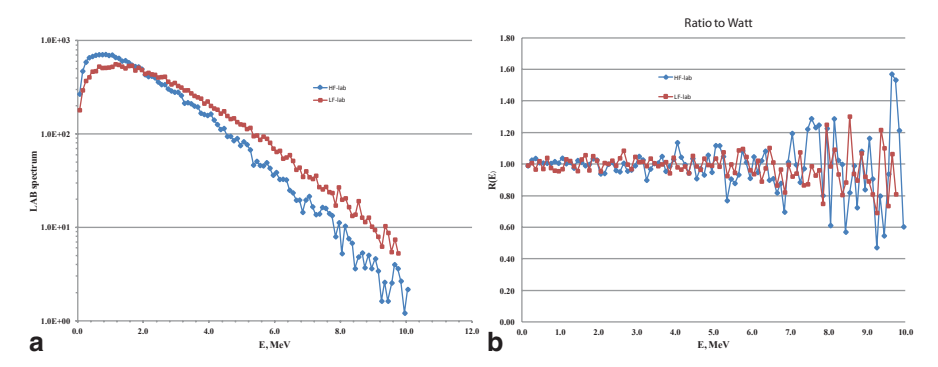


Fig. 4.12 a MC simulated Watt distributions for HF and LF (A_h =139, A=236, TKE=170 MeV, T=1 MeV). **b** The same as in **a** plotted as a ratio to Watt

$$X = \varepsilon - E_{..}(1 - \mu^{12}), \tag{4.20}$$

$$E = (\sqrt{X} + \mu^{l} \sqrt{E_{v}})^{2}, \tag{4.21}$$

$$\frac{d\mu^{c}}{d\mu^{l}} = \operatorname{abs}\left(\frac{2\sqrt{E_{v}}\mu^{l} + \sqrt{X} + (\mu^{l})^{2} E_{v}/\sqrt{X}}{\sqrt{\varepsilon}}\right). \tag{4.22}$$

The cosine of angle in CMS μ^c is estimated with Eq. (4.5) for estimation of "weight" according to Eq. (4.4).

For different CMS energy intervals $\varepsilon < E_v$, and $\varepsilon > E_v (1 - (\mu^l)^2)$ two cases are possible, depending on sign between square root.

$$E = (\pm \sqrt{X} + \mu^{l} \sqrt{E_{v}})^{2}$$
 (4.23)

$$\frac{d\mu^{c}}{d\mu^{l}} = abs \left(\frac{2\sqrt{E_{\nu}}\mu^{l} \pm \sqrt{X} + (\mu^{l})^{2} E_{\nu} / \sqrt{X}}{\sqrt{\varepsilon}} \right)$$
(4.24)

The sign (\pm) in Eqs. (4.21) and (4.23) is also selected by MC randomization.

In case of $\varepsilon < E_v (1 - (\mu^l)^2$, the neutron with selected CMS energy cannot give any contribution at angle μ^l in the LS.

The fact that Maxwellian function, Eq. (3.1), is transformed into Watt [Eq. (3.6)] was applied for verification of the transformation algorithm and accuracy of prepared subroutines.

At first stage, the angular integration was produced with MC randomization (Fig. 4.12).

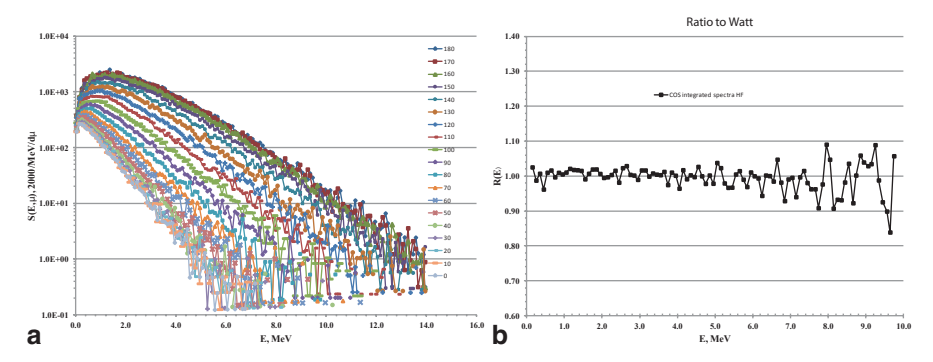


Fig. 4.13 a MC-simulated angular energy distribution in LS. Spectra for selected angles calculated for HF (A_h =139, A=236, TKE=170 MeV, T=1 MeV). LF oriented at 0°. **b** Integrated spectrum plotted as a ration to Watt function

At the second step, the energy-angular distribution of neutrons relative to HF with the same parameters was calculated with step $d\theta = 10^{\circ}$. All these results are given in Fig. 4.13a.

These spectra were numerical integrated over emission angle. The integrated spectrum as a ratio to Watt function is given in Fig. 4.13b. The conclusion is: the simulated procedure and subroutines for its realization do not have any systematical mistakes.

4.3.4 Level Density Verification

The neutron spectra from (p, n) reactions at $E_p = 5 - 30$ MeV is very fruitful for understanding properties of compound emission. Contribution of the direct and pre-equilibrium processes is rather small, and may be estimated in frame of well-known model, or applying semiempirical relations.

The following experimental data available with EXFOR data library were analyzed:

 $^{53,54}{\rm Cr}(p,\,n),\,E_{\rm p}\!=\!11.2\,\,{\rm MeV}\,\,[69],\,^{94}{\rm Zr}(p,\,n);\,E_{\rm p}\!=\!8,\,11\,\,{\rm MeV}\,\,[71],\,^{109}{\rm Ag}(p,\,n);\,E_{\rm p}\!=\!7,\,8,\,9,\,10\,\,{\rm MeV}\,\,[32],\,^{113}{\rm Cd}(p,\,n);\,E_{\rm p}\!=\!7,\,8,\,9,\,10\,\,{\rm MeV}\,\,[33],\,^{118}{\rm Sn}(p,\,n);\,^{124}{\rm Sn}(p,\,n),\,E_{\rm p}\!=\!10.2,\,11.2\,\,{\rm MeV},\,^{165}{\rm Ho}(p,\,n)\,\,[70];\,^{181}{\rm Ta}\,E_{\rm p}\!=\!11.2\,{\rm MeV}\,\,[3],\,^{181}{\rm Ta}(p,\,n);\,E_{\rm p}\!=\!6,\,7,\,8,\,9,\,10\,\,{\rm MeV}\,\,[30]\,\,({\rm Institute}\,\,{\rm for}\,\,{\rm Physics}\,\,{\rm and}\,\,{\rm Power}\,\,{\rm Engineering},\,{\rm Russia}),\,^{103}{\rm Rh}(p,\,n),\,^{104}{\rm Pd}(p,\,n),\,^{105}{\rm Pd}(p,\,n),\,^{106}{\rm Pd}(p,\,n),\,^{107}{\rm Ag}(p,\,n),\,^{108}{\rm Pd}(p,\,n);\,^{109}{\rm Ag}(p,\,n),\,^{110}{\rm Pd}(p,\,n),\,^{110}{\rm Pd}(p,\,n)\,\,{\rm at}\,\,E_{\rm p}\!=\!18,\,\,22,\,\,{\rm and}\,\,25\,\,{\rm MeV}\,\,[15],\,^{51}{\rm V}(p,\,n),\,E_{\rm p}\!=\!18,\,\,20,\,\,22,\,\,24,\,\,26\,\,{\rm MeV}\,\,[14],\,^{159}{\rm Tb}(p,\,n),\,^{169}{\rm Tm}(p,\,n),\,E_{\rm p}\!=\!25\,\,{\rm MeV}\,\,[20]\,\,({\rm Lawrence}\,\,\,{\rm Livermore}\,\,\,{\rm National}\,\,\,{\rm Laboratory},\,{\rm USA}),\,{\rm and}\,\,^{92-100}{\rm Mo}(p,\,n),\,E_{\rm p}\!=\!25.6\,\,{\rm MeV}\,\,[45]\,\,({\rm Un}\,\,{\rm Hamburg},\,{\rm Germany}).$

All experiments have been done by TOF method, with hydrogen scintillator as neutron detectors.

Cyclotron or tandem generator EGP-10 M with pulse mode was used as proton source in IPPE experiments. Neutron detector was placed in moving collimator with

flight path \sim 2 m. Angular distributions were measured by rotating collimator with neutron detector around (p, n) target. Time resolution was 2–3 ns. The efficiency of neutron detector was measured with "monoenergetic" D(d, n) T(p, n) reactions or relative to 252 Cf neutron source operating in time mode.

In works [14, 15, 20] protons were accelerated by LLL cyclo-graaff. Neutron detector was placed outside the target hall. Several detectors (10 angles between 9 and 159°) at flight path 10.8 m were used in these experiments. Neutron detector efficiency was calculated with simple analytical function, and was verified with D(d,n) reaction.

The experiment [45] has been carried out at the Hamburg Isochronous Cyclotron with 25.6 MeV energy of protons. Neutron TOF (flight path 7.5 m) array of eight detectors was designed. Total time resolution was ~ 1.5 ns. Efficiency of neutron detector was calculated with MC code.

Total analysis was summarized and published in [23]. During this investigation a rather interesting (*N-Z*) odd–even effect for spectrum shape and cross section fluctuations for direct emission was found. Now I will not discuss the physical basis of this phenomenon, here. The main goal of this discussion is the demonstration of evidences, which level density, developed in previous works is the "best" for our application—neutron emission from excited FFs, and can be applied Weisskopf–Ewing evaporation assumption for this task.

The compound spectrum for reaction A(p, n)B was calculated according to Eq. (4.25):

$$\sigma_c(E) \sim \sigma_{abs}(E) \times E \times \rho(U_B - E)$$
 $\sigma_{abs}(E)$ —absorption cross section for reaction (B+n);
 $\rho(U_B - E)$ —state density for target B;
$$U_c = E_p \frac{A}{A+1} + B_p$$
—excitation energy of compound (A+1);
$$U_B = U_c - B_p$$
—highest energy of emitted neutron

Level densities for this analysis were calculated on the basis of Phenomenological Superfluid model with Collective Enhancement (PSCE) model. All parameters for level density calculation were fixed for all isotopes and input energies. The $\sigma_{abs}(E)$ was calculated with optical model parameters from [67]. Multiple neutron emission was simulated by MC method, with the same code as was used in FINE. The calculated spectra from compound emission have intrinsic normalization to neutron multiplicity.

"Direct" components were described by the equation:

$$\sigma_n(E) = \frac{(n+2)(n+1)}{(U_B - \delta_n)^{n+2}} E \times (U_B - \delta_n - E)^n$$

$$\delta_n - \text{energy"shift"} \times \delta_1 = 0.$$
(4.26)

The experimental data $S_{\text{exp}}(E)$ were compared with calculated spectrum S(E) which was found according to Eq. (4.27):

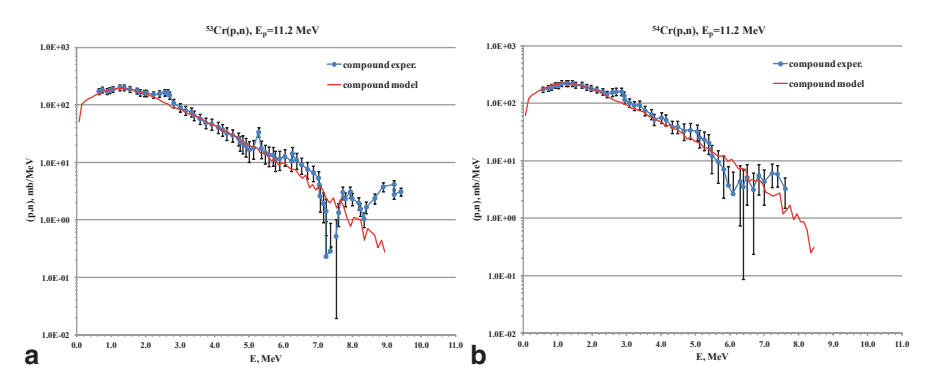


Fig. 4.14 a Experimental and calculated data for compound emission, 53 Cr(p, n) reaction. **b** Experimental and calculated data for compound emission, 54 Cr(p, n) reaction

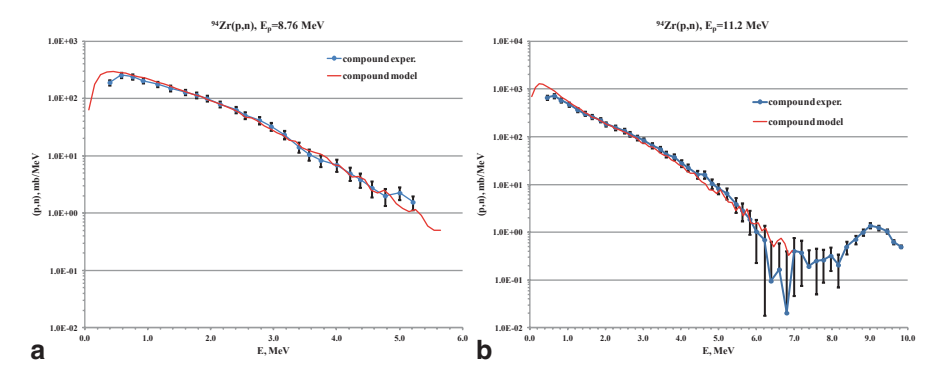


Fig. 4.15 a Experimental and calculated data for compound emission, 94 Zr(p, n) (8.76 MeV). **b** Experimental and calculated data for compound emission, 94 Zr(p, n) (11.2 MeV)

$$S(E) = \sigma_{0c} \times \sigma_{c}(E) + \sigma_{01} \times \sigma_{1}(E) \times \sigma_{02} \times \sigma_{2}(E). \tag{4.27}$$

Parameters σ_{0c} , σ_{01} , σ_{02} , δ_2 were fitted to produce agreement between experimental and calculated results.

The experimental compounds spectra were found with Eq. (4.28):

$$S_{\text{exp}c}(E) = S_{\text{exp}}(E) - \sigma_{01} \times \sigma_{1}(E) - \sigma_{02} \times \sigma_{2}(E).$$
 (4.28)

These spectra are shown in Figs. 4.14, 4.15, 4.16, and 4.17 with results of MC simulations. The level density subroutine presented in RIPL library may describe all experimental data for input proton energy 6–26 MeV and for mass number A=50–181 without any an additional corrections of input parameters.

In Ref. [66], Weisskopf and Ewing suggested a simple approach for nuclear reaction calculations. One may separate two steps of this simplification. In first one they demonstrated the transition from Hauser–Feshbach formulas to a simpler equation,

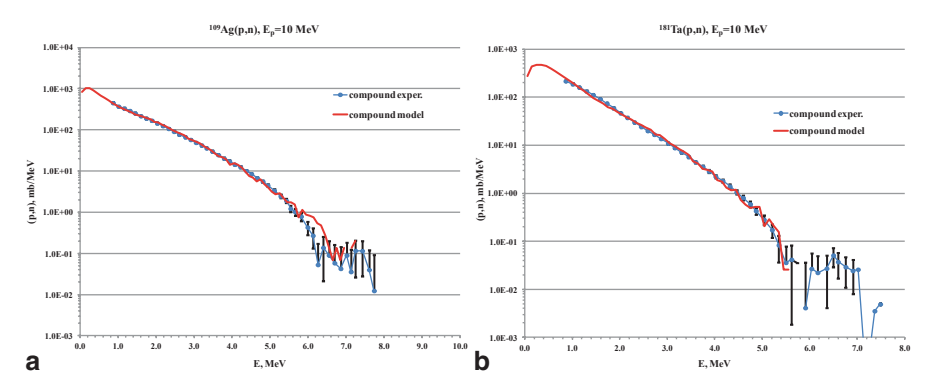
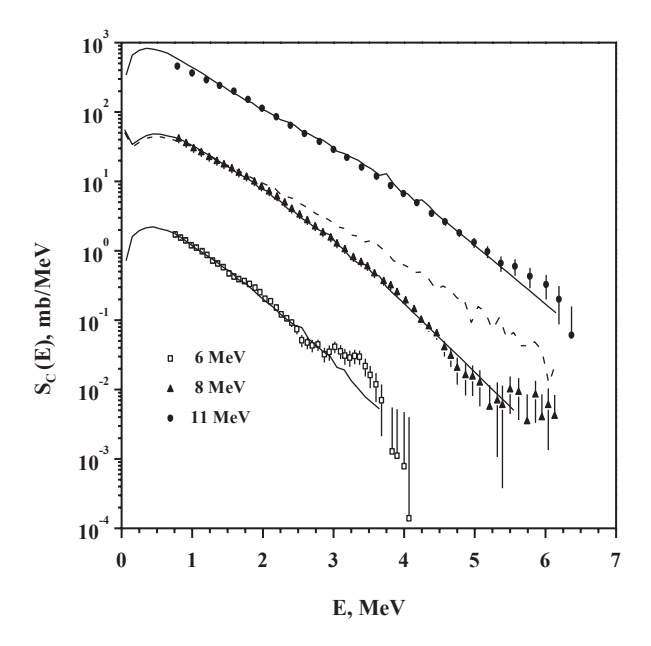


Fig. 4.16 a Experimental and calculated data for compound emission, 109 Ag(p, n) (10 MeV). **b** Experimental and calculated data for compound emission, 181 Ta(p, n) (10 MeV)

Fig. 4.17 Experimental compound spectra for ¹⁸¹Ta(*p*, *n*) reaction and calculated results with Phenomenological Superfluid model with Collective Enhancement (PSCE) model (*solid*) and Weisskopf–Ewing's assumption *T*-constant (*dash*)



so-named "evaporation spectrum" [Eq. (4.7)]. At the second step, they suggested that the level density in Eq. (4.7) may be replaced with series expansion, and finally appeared *T*-constant formula in Eq. (4.8).

The constant temperature dependence for neutron spectra in CMS is the traditional way to describe the total (integrated over masses, TKE, and emission angle) PFNS.

The motivation of this approach with reference to Weisskopf simplification [Eq. (4.8)] was discussed above.

Authors [48] motivated the T=constant law as an experimental fact which was found from analysis of low-lying levels and resonance spacing [63], for excitation energy 6–7 MeV, and was supported in [62] with analysis of spectra from different nuclear reactions. Results of the last paper [62] allow authors [48] to extrapolate this law up to ~20 MeV.

Analysis of (*p*, *n*) reactions summarized in [23] and partly submitted here, reveals rather interesting facts. The prediction of the Phenomenological Superfluid model with Collective Enhancement (PSCE) model in frame work of Weisskopf-Ewing assumption (first step) is in very good agreement with experimental neutron spectra for compound emission in the excitation energy range <20 MeV. This model for Level Density (LD) calculation and evaporation model itself may be applied for calculation of FINE. This conclusion is illustrated in Figs. 4.14, 4.15, 4.16, and 4.17. Similar agreement was found for all reactions and input energies investigated in [23].

For the excitation energy <15 MeV the condition $U_{\rm B}>>E$ is not true. Therefore, the second step of assumption [Eq. (4.8)] overestimates very much the neutron yield at high energy range (see Fig. 4.17 for $E_{\rm p}=8$ MeV) and its application may provide a wrong conclusion about mechanism of neutron emission in fission. This simplification may be used for estimation of average energy but not for spectrum shape.

Only two energy points (low-lying levels and resonances) were used in [63]. So result of this work cannot be used as an argument for motivation of T-law—any function may be drawn through two points. So the only argument is the result and conclusion of [62], based on the energy distribution of reaction products, and assumptions about nuclear reaction mechanism.

Experimental results for A>90 may be treated in the frame of common model: compound emission with the same level density model, added by two components' direct mechanism with strong (N-Z) odd—even effect [23].

There are two possibilities for $A \sim 50$ (Cr-isotopes): (1) the neutron spectrum can be described with T= constant law without any an additional reaction mechanism, (2) the same as for A > 90 model, the same N–Z odd–even effect, with contribution of noncompound emission ~ 25 %, and the same level density. What is the real physics?

All FF are neutron reach isotopes placed rather close to neutron drip line. So, the properties of these isotopes may be different in comparison with stable nucleus verified with (p, n) reaction. However, one should clearly demonstrate the nature of this difference, give the explanation why Level Density (LD) transformed to constant temperature law, and tool how to calculate this temperature.

4.4 Comparison Experimental and Calculated Results

Let us summarize the main assumptions, input parameters, and function for FINE model:

- NEAFA assumption;
- Two-dimension distribution Y(A,TKE);
- Optical model for inverse reaction cross section;

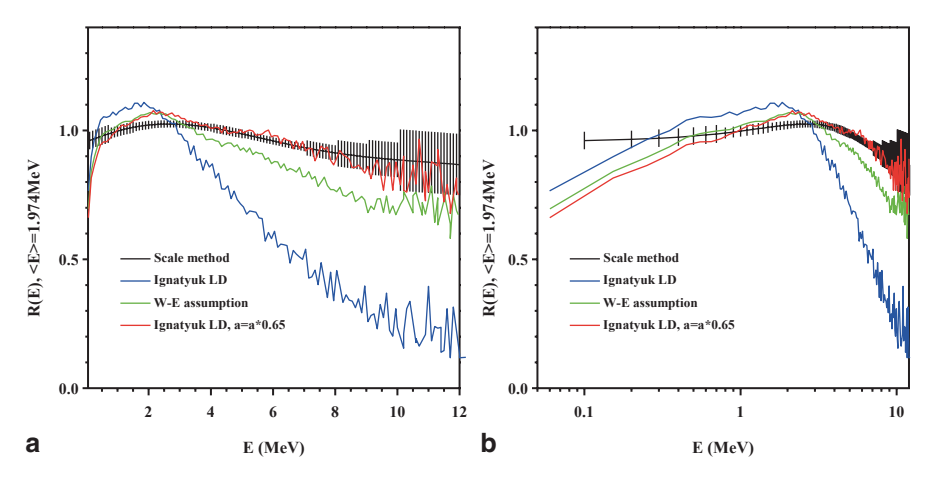


Fig. 4.18 a Evaluated and calculated ²³⁵U(th) PFNS in linear scale. **b** The same as in **a** in logarithmic scale W-E assumption means T-constant

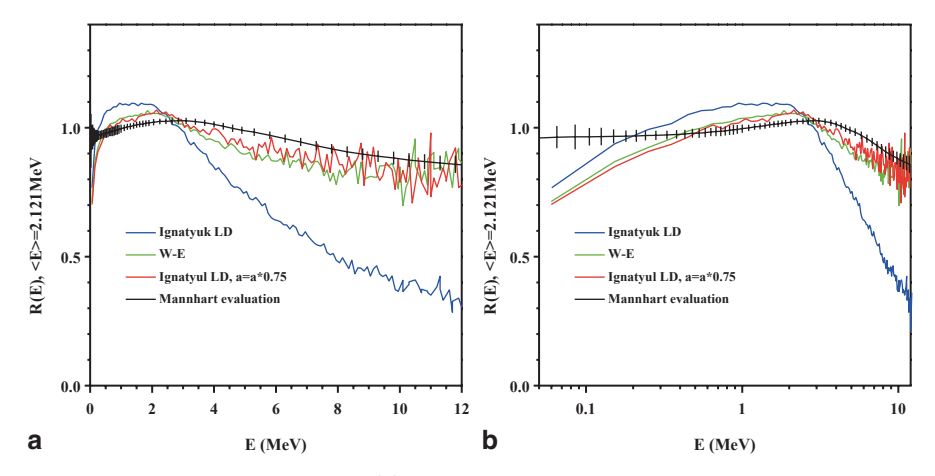


Fig. 4.19 a Evaluated and calculated 252 Cf(sf) PFNS in linear scale. b The same as in a in logarithmic scale

- Level density from Phenomenological Superfluid model with Collective Enhancement (PSCE);
- Thermo-equilibrium for energy splitting between LF and HF (correction is possible);
- Energy release and binding energy from systematic.

The PFNS for ²³⁵U(th) and ²⁵²Cf(sf) are shown in Figs. 4.18 and 4.19.

As it was mentioned more than 50 years ago, high energy part cannot be described without special "tuning" of the "hardness" of evaporation spectra. Terrell's conclusion is valid till now: "although the fission neutron spectrum calculations must, of course, conform to experimental data, the only adjustable constant determined from fission spectrum data is the nuclear temperature coefficient."

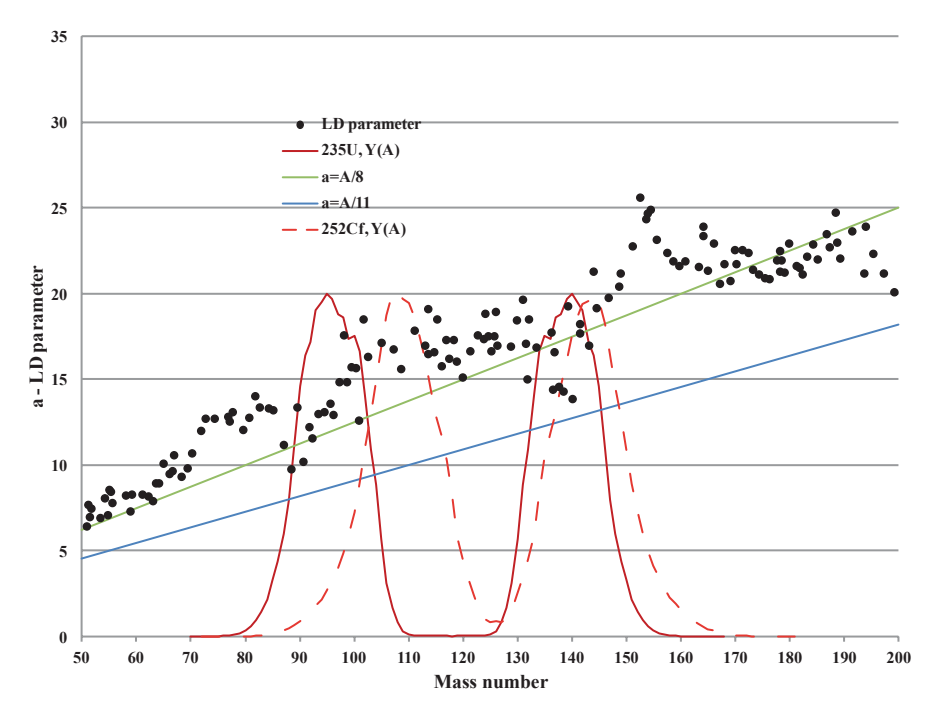


Fig. 4.20 Level density parameters from resonance counting (*points*) and different dependencies applied for PFNS calculation. FF yield for ²³⁵U and ²⁵²Cf are shown by *lines*

We may agree calculated and experimental results due to very strong changing of level density parameter (0.6–0.7) or (and) incorporating constant temperature assumption. The motivation of this incorporation addressing to Weisskopf–Ewing simplification cannot be applied. They demonstrated this formula to simplify calculation and suggest the simple method for average energy calculations.

Of course, properties of FF may be different from isotopes close to stable line. However, this also cannot be used as a motivation for applying *T*-constant assumption instead of level density formula.

Another strange point is connected with a-parameters used for PFNS in different model including MNM. The parameter for successful description of experimental data for 252 U (a=A/11) and 252 Cf (a=A/8) are different in more simple model (MNM, Point-by-Point model [61]), and they are different in our attempts to describe evaluated experimental PFNS with FINE model (Figs. 4.18 and 4.19). The nature of this difference is not clear. In any case, the difference in mass distribution cannot explain this fact (see Fig. 4.20).

The energy dependence of absorption cross section and multiple neutron emission (as was expected in papers of 1950s) may fill the gap at low energy but cannot describe evaluated function. I would like to highlight that evaluated spectrum shape for ²³⁵U and ²⁵²Cf contradict to model calculation even with adjusted parameters level density. The difference is higher than estimated uncertainties of evaluated PFNS.

106 4 Physical Models

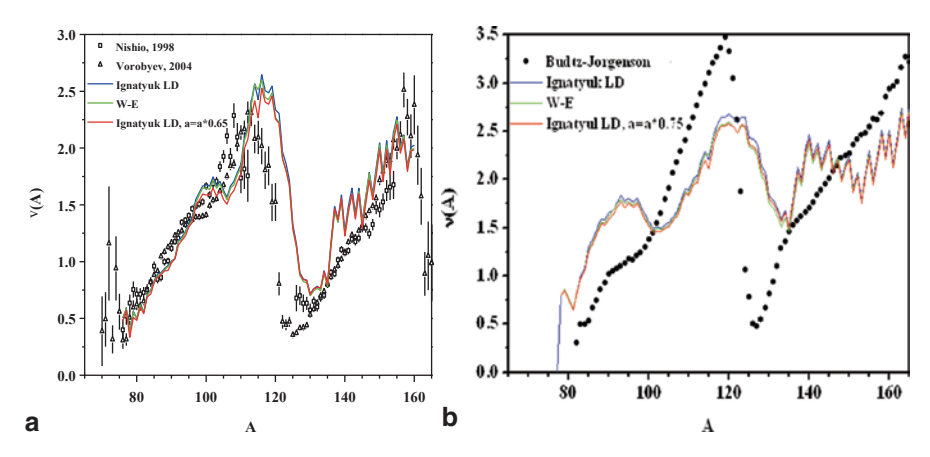


Fig. 4.21 a Neutron multiplicity as function of FF masses for ²³⁵U(th) and calculated results. **b** The same as in Fig. 4.20a for ²⁵²Cf. Experimental results from [8]

The other important characteristic which may gave additional information about mechanism of neutron emission in fission is the dependence of neutron multiplicity versus mass number of FF. The agreement between experimental and calculated data for some isotopes [²³⁵U (Fig. 4.21a) and ²³⁹Pu (Fig. 4.24b)] is reasonably good without any semiempirical correction for shearing excitation energy for LF and HF.

Situation is not so good for ²³³U (Fig. 4.23b) in particular for LF. The agreement for HF is still reasonable.

Real problem there exists for ²⁵²Cf (and ^{244,248}Cm [29]). The experimental multiplicity requires other then thermoequilibrium law for distribution of excitation energy between LF and HF. This function is different for Cf and Cm isotopes. What is the reason for this peculiarity: -U-Pu isotopes at thermal point are in equilibrium, but Cf-Cm isotopes are not?

The PFNS is the only experimental data which is very sensitive to assumption about model parameters like the selection of the level density, *T*-constant simplification, and the absorption cross section. The neutron multiplicity according to Eq. (4.17), depends on these assumptions via average energy of neutrons, and big variation in the PFNS shape provide very moderate influence on amount of neutrons ($\Delta \varepsilon << B_p$).

The MC simulation including all varieties of TXE and Bn confirms the result which is clear from simple Eq. (4.17). For all multiplicity function v(A) and v(TKE) the influence of parameters which provide very strong changing for the PFNS is very small (Figs. 4.21, 4.22, 4.23, and 4.24).

The relation between TKE and neutron multiplicity is defined by Eq. (4.17) and this is the basis of the model if we assume the formation of kinetic energy as a first step, which defines the total excitation energy of FF. This Eq. (4.17) allows us to estimate expected slope for v(TKE).

The binding energy and energy release [Q] in Eq. (4.17) are collected in Table 4.3. The average binding energy for heavy fragment and complimentary light

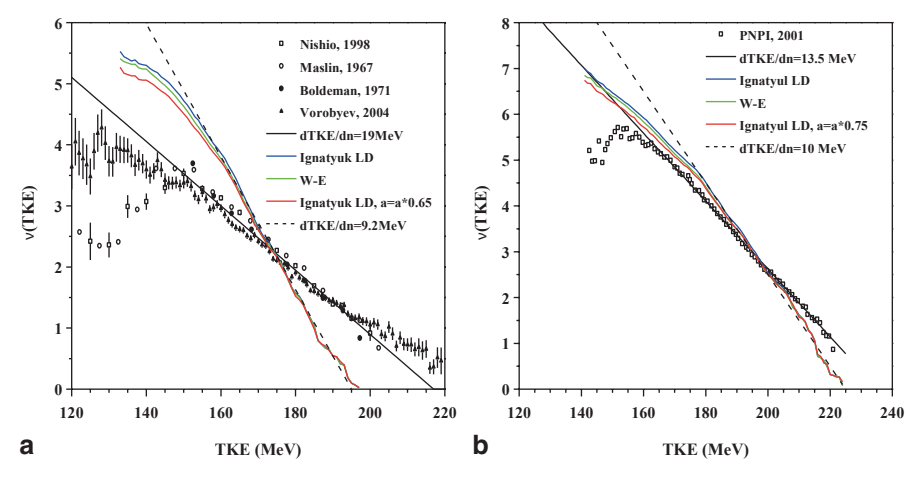


Fig. 4.22 a Neutron multiplicity as function of TKE for ²³⁵U(th). EXFOR numbers are: Nishio-22464, Boldeman-14087, Vorobyev-41502. **b** The same as in Fig. 4.21a for ²⁵²Cf. Experimental data from [21]. *TKE* total kinetic energy

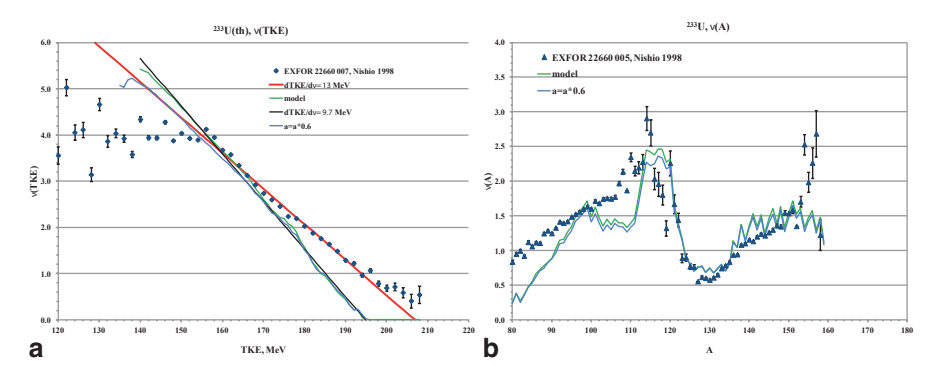


Fig. 4.23 a Neutron multiplicity as function of TKE for 233 U(th). EXFOR 22660, [46]. *Green line* calculated result. *Blue line* with Level Density (LD) parameter $a=a\times0.6$. **b** Neutron multiplicity as function of mass number for 233 U(th) [46]. *Green line* is calculated function. *Blue line* with Level Density (LD) parameter $a=a\times0.6$. *TKE* total kinetic energy

fragment, and three neutron cascade is \sim 6 MeV. If we place this value, $v\sim2.5$, $E_{\gamma}\sim0.5\mathrm{B}_{\mathrm{n}}$, and $<\varepsilon>\sim1.5$ MeV in Eq. (4.17) we may estimate that theoretical slope should be \sim 9 MeV/n.

This simple estimation allows us to understand the nature of calculated slope if the main assumptions are correct. Calculated slope for all isotopes taking into account all variety of FF parameters is ~ 10 MeV/n. This slope (Figs. 4.22, 4.23a, and 4.24a) is practically insensitive to model parameters like Level Density (LD), absorption cross section, energy release, and so on. The same slope was calculated with LANL model [56].

108 4 Physical Models

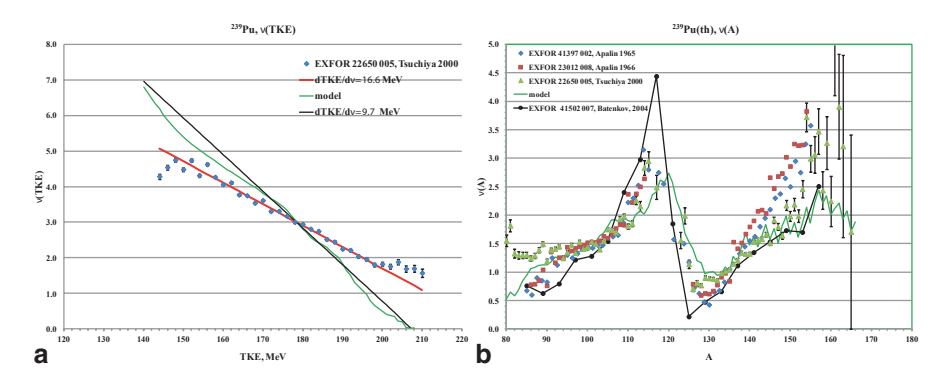


Fig. 4.24 a Neutron multiplicity as function of TKE for ²³⁹Pu(th). EXFOR 22650, [60]. *Green line* calculated result. **b** Neutron multiplicity as function of mass number. *Green line* is calculated function. *TKE* total kinetic energy

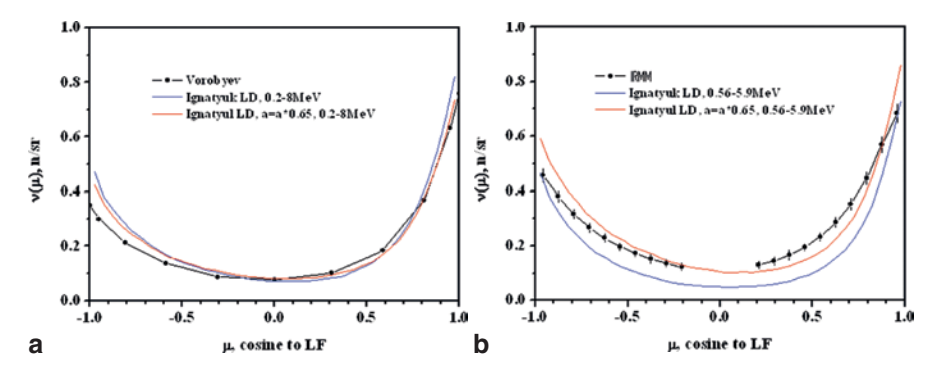


Fig. 4.25 a Angular distribution of neutrons emitted in the energy range 0.2–8 MeV for ²³⁵U. Points from EXFOR-41502 [64]. *Lines* give calculated results. **b** The same as in Fig. 4.22a for ²⁵²Cf. Experimental data from [8, 26]. Energy range 0.57–5.9 MeV. *LF* low frequency

The experimental slope of v(TKE) is much higher than calculated one. The dependence on S=(N-Z)/A parameter is visible: dTKE/dv=19 MeV/n (^{235}U , S=0.217), 16.5 MeV/n (^{239}Pu , S=0.213), and 13 MeV/n (^{233}U , S=0.210). But for ^{252}Cf , S=0.222, and the slope is 13 MeV/n.

The difference is most strong for ²³⁵U. Experimental results measured by different methods are in agreement (see Fig. 4.22a). So this difference is unlikely connected with experimental systematical uncertainties.

The angular distribution of fission neutrons relative to FF direction is rather sensitive to spectrum shape. Therefore, model result should be calculated in the same energy interval as given for experimental data. In case 235 U [64], the low energy limit is small E_1 =0.2 MeV, therefore, the shape of angular distribution changes a bit for original Level Density (LD) parameter and for reduced a=a×0.65 to agree with experimental PFNS. In case 252 CF the E_1 =0.56 MeV and the result is more sensitive to input parameters.

Table 4.3 Parameters for HF and LF (TXE and B_i in [MeV], 235 U(th), TKE=170 MeV). Results of Q-calculator are shown by italic

HF						
ΔZ	A_{h}	Z_{h}	TXE	B_1	B_2	B_3
-1	120	46	29.712	6.814	4.628	7.006
0	120	47	25.695	5.163	7.062	5.372
			25.337	5.163	7.063	5.372
1	120	48	28.013	8.138	5.269	8.355
-1	130	50	35.489	7.687	5.365	7.900
0	130	51	28.270	5.839	8.087	5.973
1	130	52	26.038	8.419	6.083	8.776
-1	140	54	24.936	5.418	3.602	5.812
0	140	55	17.255	4.421	5.885	4.413
			17.267	4.421	5.885	4.413
1	140	56	15.291	6.428	4.724	8.612
-1	150	57	11.847	4.159	6.042	3.999
0	150	58	14.520	6.267	4.444	6.317
1	150	59	6.390	5.087	6.574	5.087
-1	160	61	0.000	4.476	5.799	4.820
0	160	62	1.445	6.264	5.079	6.550
			1.545	6.275	5.072	6.551
1	160	63	0.000	5.386	6.914	5.815
LF						
ΔZ	A_1	Z_1	TXE	B_1	B_2	B_3
-1	116	46	29.712	7.629	4.981	7.872
0	116	45	25.695	4.729	6.881	4.880
				4.599	6.648	5.020
1	116	44	28.013	6.348	4.056	6.712
-1	106	42	35.489	6.989	5.078	7.555
0	106	41	28.270	4.107	6.698	4.981
1	106	40	26.038	5.408	4.094	6.038
-1	96	38	24.936	5.908	4.347	6.826
0	96	37	17.255	3.447	5.359	3.996
				3.442	5.372	4.007
1	96	36	15.291	5.062	2.969	5.187
-1	86	35	11.847	5.101	8.906	6.839
0	86	34	14.520	6.184	4.550	8.681
1	86	33	6.390	3.954	5.509	4.272
-1	76	31	0.000	5.810	8.482	6.422
0	76	30	1.445	7.646	4.831	8.371
				7.739	4.832	8.370
	76	29	0.000	4.075	6.674	4.616

The comparison of experimental and calculated results (Fig. 4.25) demonstrates common (U and Cf) tendency. The experimental shape of angular distribution is more symmetric. The model predicts more neutron yield for heavy fragments and more strong dependences for both fragments.

110 4 Physical Models

References

 Arnold K, During I, Kalka H et al (1989) Modes of de-exitation of fission fragments. Nucl Phys A502:325

- Audi G, Wapstra AH (1993) The 1993 atomic mass evaluation. Atomic mass table. Nucl Phys A565:1, 66. www-nds.iaea.org/ndspub/masses
- 3. Birjukov NS, Zhuravlev BV, Rudenko AP et al (1988) Neutron spectra and angular distributions from the (p, n) reactions on 165-Ho, 197-Ta, 197-Au, 209-Bi nuclei at Ep=11.2 MeV. J Izveatia Acad Nauk 52:180 (EXFOR A0367)
- 4. Blatt J, Weisskopf V (1979) Theoretical nuclear physics. ISBN 0-387-90382-8
- Bowman HR, Milton JCD, Thompson SG et al (1963) Further studies of the prompt neutrons from the spontaneous fission of ²⁵²Cf. Phys Rev 126(1962):2120; Phys Rev 129(1963):2133
- Brosa U (1990) Multimodal fission and neutron evaporation. Phys Rev C38(1988):1944;
 Brosa U, Grosman S, Muller A. Phys Rep 197(1990):167
- Browne JC, Dietrich FS (1974) Hauser-Feshbach calculation of the ²⁵²Cf spontaneous fission neutron spectrum. Phys Rev C10:2545
- Budtz-Jorgensen C, Knitter H-H (1988) Simultaneous investigation of fission fragments and neutrons in ²⁵²Cf(sf). Nucl Phys A490:307
- 9. Djachenko PP, Kuz'minov BD, Lajtai A (1969) Kinetic energy of fragments at the fission of ²³⁵U by neutrons in the energy range 0–0.6 MeV. R, YFI-8,7,1969 (EXFOR 40017)
- Frehaut J (1989) Physics of neutron emission in fission. In: Proc. of Consultants Meeting, Mito City, Japan, 24–27 May 1988, ed. Lemmel HD. INDC(NDS)220
- Fronher FH (1987) Watt spectrum fit to ²⁵²Cf prompt fission neutron data. IAEA-TEC-DOC-0483, 12–16 Oct 1987, p 160
- Gerasimenko BF, Rubchenya VA (1985) Prompt neutrons from the low-energy fission of atomic nuclei. At Energy 59:335
- 13. Gönnenwein F (1991) In: Wagemans C (ed) The nuclear fission process. p 287
- 14. Grimes SM, Anderson JD, Davis JC, Wong C (1973) Nonequilibrium contribution to the 51 V(p, n) 51 Cr reaction for $18 < E < \tau \beta p > 26$ MeV. Phys Rev C8:1770
- 15. Grimes SM, Anderson JD, Wong C (1976) Odd-even effects in pre-equilibrium (p, n) reactions. Phys Rev C 13:2224
- Grudzevich OT (2001) Neutron and gamma-emission from fission fragments, VANT, Nuclear data, 1, 2000, 27, INDC(CCR)-430, p 39
- Hambsch F-J, Siegler P, Van Aarle J, Vogt R (1994) Investigations of fission modes. In: Proceedings of 11th international seminar on neutron interaction with nuclei, (ISINN-3), Dubna, p 299
- 18. Hoffman DC, Hoffman MD (1974) Fission gamma-rays. Ann Rev Nucl Sci 24:151
- 19. Ignatyuk AV, Istekov K, Smirenkin GN (1979) The role of collective effects in the systematic of nuclear level densities. Sov J Nucl Phys 29:450 (RIPL library of IAEA)
- 20. Kalbach C, Grimes SM, Wong C Comparison of proton and neutron spectra: the extended Griffin model, pairing and isospin. Z Phys A275:175
- 21. Kalinin VA, Dushin VN (2001) Measurements of the multiplicity distributions for fission neutrons emitted in spontanious fission of Cf-252, Cm-244, and Cm-248. In: Proc. 5th Conf. Costa-Papernika, Slovak Republic, 23–27 Oct 2001, p 252
- 22. Knitter H-H, Brosa U, Budtz-Jorgensen C (1991) Neutron and gamma emission in fission. In: Wagemans C (ed) The nuclear fission process. CRC Press Inc., Boca Raton, pp 496–553
- Kornilov NV (2014) (N-Z) odd-even effect for non-equilibrium mechanism of (p, n) reactions. J Phys Sci Appl 4(4)
- Kornilov NV, Kagalenko AB, Pupko SV et al (1993) On the mechanism of neutron emission in fission. Conf. Proc. Nuclear data for sci. and tech, Reffo G, Ventura A, Grandi C (eds). Ital Phys Soc 1:179

References 111

 Kornilov NV, Kagalenko AB, Hambsch F-J (2001) Prescission neutronsin the fission of ²³⁵U and ²⁵²Cf nuclei. Phys At Nucl 64(8):1372–1384. (Translated from Yadernaya Fizika 64(8):1427–1433)

- Kornilov NV, Kagalenko AB, Poupko SV et al (2001) New evidence of an intense scission neutron sourcein the ²⁵²Cf spontanious fission. Nucl Phys A 686:87–203
- Kornilov NV, Kagalenko AB (2003) How many fission modes do exist? In: Proceedings of 11th international seminar on neutron interaction with nuclei, (ISINN-11), Dubna, 2003, p 144
- 28. Kornilov NV, Kagalenko AB, Lunev AP (2004) The conflict between small multiplicity and high average energy of fission neutrons. In: Proceedings of 12th international seminar on neutron interaction with nuclei. (ISINN-12), Dubna
- Kornilov NV, Hambsch F-J, Vorobyev AS (2007) Neutron emission in fission. Nucl Phys A789:53
- Kotel'nikova GV, Lovchikova GN, Sal'nikov OA et al (1980) Mechanism of ¹⁸¹Ta(p, n)181W reaction at proton energies below 10 MeV. J At Nucl 31:1127 (EXFOR A0077)
- 31. Litaize O, Serot O (2011) Investigation of prompt fission neutrons and gamma-rays by Monte Carlo simulation. ND2010. J Korean Phys Soc 59(2):991
- 32. Lovchikova GN, Kotel'nikovz GV, Trufanov AM et al (1980) The investigation of (p, n) reaction on silver isotopes preprint FEI-999 (EXFOR A0224)
- 33. Lovchikova GN, Trufanov AM, Sal'nikov OA et al (1981) Study of the (p, n) reaction on ¹¹³Cd at proton energies below 10 MeV. J At Nucl 33:41 (EXFOR A0261)
- Madland DG (1991) Theoretical descriptions of neutron emission in fission. INDC(NDC)-251, p 201
- Madland DG, Nix JR (1982) New calculation of prompt fission neutron spectra and average promt neutron multiplicities. Nucl Sci Eng 81:213
- Madland DG, Labauve RJ, Nix JR (1989) Recent improvements in the calculation of prompt fission neutron spectra. Physica of Neutron emission in Fission, Mito, Japan, 24–27 May 1988, INDC(NDS)-220, p 259
- 37. Mannhard W (1987) Evaluation of the Cf-252 fission neutron spectrum between 0 MeV and 20 MeV. IAEA-TECDOC-410, 1987, p 158
- 38. Marten H (1987) Theoretical models and computer programs for the calculation of prompt fission neutron spectra. IAEA-TECHDOC-0483, 12–18 Oct 1987, p 148
- 39. Marten H (1991) Mechanism of fission neutron emission. Nuclear data for neutron emission in the fission process, Vienna, Austria, 22–24 Oct 1990, INDC(NDS)-251, p 23
- Marten H, Seeliger D (1984) Analysis of the prompt-neutron spectrum from spontanious fission of ²⁵²Cf. J Phys G10:349
- Marten H, Seeliger D (1988) Neutron evaporation during fission fragmment acceleration. J Phys G14, 211
- Marten H, Seeliger D (1989) Description of the ²⁵²Cf neutron spectrum in the framework of a generalized Madland-Nix model. In: Proceedings International Conference "On 50 years with nuclear fission", Gaithergurg, 25–28 April 1989, ed. By Behrens JW, Cralson AD, ANS vII, 1987, p 743
- 43. Marten H, Ruben A, Seeliger D (1989) Theory of prompt fission-neutron emission. Physics of neutron emission in fission, Mito, Japan, 24–27 May 1988, INDC(NDS)-220, p 47
- Moller P, Nix JR, Mayers WD, Swiatecki WJ (1995) Nuclear ground-state masses and deformation. At Data Nucl Data Tables 59:185–381
- 45. Mordhorst E, Trabant H, Kaminsky A et al (1986) Pairing effect and multistep direct and compound emission in the 92–100Mo(p, xn) reactions. Phys Rec C34:103 (EXFOR 00517)
- 46. Nishio K, Nakashima M, Kimura I et al (1998) Multi-parametric measurement of prompt neutrons and fission fragments for ²³³U(nth, f). J Nucl Sci Tech 35:631 (EXFOR 22660)
- 47. Nuclear Standard file (1991) NEANDC/INDC, NEA-OECD, 1992
- 48. Schmidt K-H, Jurado B (2010) Entropy driven excitation energy sorting in superfluid fission dynamics. Phys Rev Lett 104:212501

112 4 Physical Models

 Schmidt K-H, Jurado B (2013) Prompt-neutron spectra from a general description of the fission process. INDC(NDS)-0608, Vienna, Sept 2013, p 47

- Seeliger D, Kalka H, Marten H et al (1989) Prompt neutron emission in nuclear fission. INDC(GDR)-056/L
- 51. Sergachev AI, Vorob'eva VG, Kuz'minov BD et al (1968) Mass and kinetic energy distribution of fission fragments J, YF,7,(4):778 (EXFOR 40173)
- 52. Sergachev AI, Djachenko NP, Kovalev AM, Kuz'minov BD et al (1972) Influence of intermediate states of fissioning ²³³Th nucleus on the mass and kinetic energy distribution of fission fragments J, YF,16,(3):475 (EXFOR 40106)
- 53. spectrum, IAEA, TECHDOC-335, Vienna 1985, p 255
- Straede C, Budtz-Jorgensen C, Knitter H-H (1987) ²³⁵U (n, f) fragment mass-, kinetic energyand angular distributions for incident neutron energies between thermal and 6 MeV. Nucl Phys A 462:85
- 55. Surin VM, Sergachev AI, Kuzminov BD et al (1971) Yields and kinetic energies of fragments in the fission of ²³³U, and ²³⁹Pu, by 5.5 MeV and 15 MeV neutrons. J Nucl Phys 14:935
- 56. Talou P (2013) Report for GAMMA-2 workshop, Sept 2013, (private communication) in press
- 57. Talou P, Kawano T, Lynn JE et al (2011) Recent advances in nuclear fission theory: pre- and post-scission physics. ND2010. J Korean Phys Soc 59(2):797
- 58. Terrell J (1959) Fission neutron spectra and nuclear temperature. Phys Rev 113(2):527
- 59. Terrell J (1962) Neutron yield from individual fission fragments. Phys Rev 127:880
- Tsuchiya C, Nakagone Y, Yamana H et al (2000) Simultaneous measurement of prompt neutrons and fission fragments for ²³⁹Pu (nth, f). J Nucl Sci Technol 37(11):941 (EXFOR 22650)
- Tudora A, Vladuca G, Morilon B (2004) Prompt fission neutron multiplicity and spectrum model form 30–80 MeV neutrons incident on ²³⁸U. Nucl Phys A740:33
- 62. Voinov AV, Oginni BG, Grimes SM et al (2009) Nuclear excitation at constant temperature. Phys Rev C79:031301
- 63. von Egidy T, Bucurescu D (2005) Systematic of nuclear level density parameters. Phys Rev C 73:044311
- Vorobyev AS, Sherbakov OA, Pleva YS et al (2009) Measurements of angular and energy distributions of prompt neutrons from thermal neutron-induced fission. Nucl Instrum Methods Phys Res A598:795–801
- 65. Watt B (1952) Energy spectrum of neutrons from thermal fission of ²³⁵U. Phys Rev 87(6)
- 66. Weisskopf VF, Ewing DH (1940) On the yield of nuclear reactions with heavy elements. Phys Rev 57:472
- 67. Young P, Herman M, Koning A et al (2006) Handbook for calculations of nuclear raction data. RIPL-2, IAEA-TECDOC-1506, RIPL number 2405
- Zamyatnin YS, Konovalov VY (2000) Nuclear fission, low energy neutron physics, I/16, chapter 9. Shopper H (ed). Landolt-Börnstein
- 69. Zhuravlev BV, Biryukov NS, Rudenko AP et al (1990) Neutron spectra from (p, n) reactions on ⁵²Cr, ⁵³Cr, ⁵⁴Cr, ⁵⁶Fe, ⁶²Ni, ⁹⁰Zr nuclei and nuclear level density EXFORA0837. J BAS (Bull Rusian Acad Sci) 56:742(1992); J SNP (Sov J Nucl Phys) 51:3338
- Zhuravlev BV, Lychagin AA, Titarenko NN et al (2003) Nuclear level densities from neutron spectra in reactions induced by protons on tin, lead, and bismuth isotopes. J Izvestia Acad Nauk 67:98 (EXFOR D0522)
- 71. Zhuravlev BV, Lychagin AA, Titarenko NN et al (2004) Level densities in 90 Nb and 94 Nb nuclei from neutron evaporation spectra. J Izv Acad Nauk 68:1170 (EXFOR A0809)

Chapter 5 Achievements and Still Open Problems

5.1 Real Achievements

Summarizing previous discussion one may conclude about achievements and the current stage of fission neutron emission investigations.

First of all were developed experimental methods which allow us to increase the accuracy of neutron emission investigation. There are a lot of experimental Prompt Fission Neutron Spectra (PFNS) for main fissile isotopes in the energy range 0–20 MeV. Main part of these data is available via EXFOR library, and may be applied for data analysis and evaluation.

Several semiempirical methods (including Madland–Nix model) with parameters adjustable to experimental data were developed and may be used for data evaluation and practical application—data library preparation. The data including PFNS may be extrapolated with this model to uninvestigated energy range. However, the poor theoretical basis for these models does not allow us to extrapolate calculated results to uninvestigated isotopes.

The ²⁵²Cf(sf) PFNS is known with high accuracy in the energy range 0.1–10 MeV, and it was recommended as a standard. This evaluation was verified by macroscopic experiments. The Fig. 5.1 taken from [1] demonstrates the conclusion that microscopic experimental results confirm evaluated spectrum shape in the energy range up to 15 MeV. The only problem for application of this spectra as a standard is low intensity of neutrons with energy > 10 MeV.

The combination of semiempirical models for PFNS calculation together with standard compound, preequilibrium neutron emission, penetration over fission barrier, and competition between fission, neutron, and gamma-ray emissions demonstrates rather realistic results for prefission neutron emission. It seems that physics of the first stage of this process (neutron emission before fission) was understood reasonably well. The calculated functions such as PFNS shape at incident energy >6 MeV, the dependence of average energy of fission neutrons are in good agreement with experimental data. The deviation at >10 MeV neutron energy may be explained in framework of reasonable physical assumptions.

The PFNS for ²³⁵U(th) is also known with high accuracy for energy range 0.1–10 MeV. At higher energy, the uncertainties of the evaluated spectrum increases

essentially. The average energy estimated directly from microscopic data at thermal energy is $\langle E \rangle$ = 1.974±0.002 MeV. This value is in perfect agreement with tendency estimated on the basis of PFNS analysis in the energy range 0–5 MeV. So, there are not any doubts that this is correct value.

Recently [2, 3, 8], dynamical model of behavior of each neutron state in nucleus that undergoes scission was developed. This evolution is followed from the moment when the neck cracks until the neck is completely absorbed by the nascent fragments.

The authors investigated the nucleus 236 U, at two mass asymmetries defined by the light fragment (LF) mass A_1 =96 and A_h =140. The number of neutrons that leave a sphere of radius R=30 fm (a test is done with R=40 fm) around the fissioning nucleus in a solid angle $d\Omega$ and in a time interval dt, $dv_{sc}/d\Omega$, was calculated.

The integration in time of this quantity from 0 to ∞ gives the angular distribution. The $T_{\rm max}=4\times10^{-21}$ s was reached in discussed calculations. At this time, however, the majority of the scission neutrons (SCNs) left the sphere. The SCN emission is found to take place mainly along the fission axis (Fig. 5.2) with a small preference for the LF similar with what is experimentally observed for all prompt neutrons. A ratio v_1/v_h close to the experimental value 1.41 was obtained.

The neutron emission in fission may be explained in the following way. During the neck rupture neutrons are released (become unbound) due to the nonadiabaticity of this process. They leave the fissioning system during the next few 10^{-21} s after scission, i.e., during (or before) the acceleration of the fission fragments (FFs). Even if the neutrons are released predominantly in the neck region, they do not move perpendicular to the fission axis but instead they are focused (by the fragments) along the fission axis. This feature is unexpected. The resulting angular distribution of these neutrons with respect to the fission axis resembles with the experimental data for all prompt neutrons.

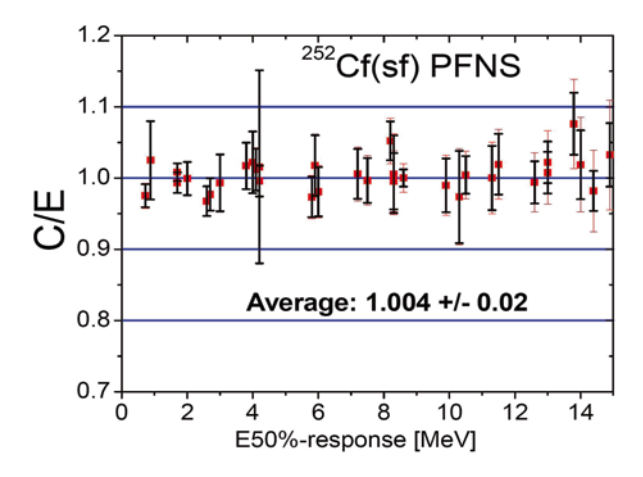
This research re-opens the 50 years' old debate on the origin of the fission neutrons. The model was realized with numerical integration of two-dimension Schrodenger equation with time-dependent potential. This is rather difficult for realization, and "simple" relations for its application are not found now. However, one may conclude, that the distinction between scission and evaporated neutrons, based on their angular distribution, is more challenging than expected.

5.2 Mechanism of Neutron Emission in Fission

The list of achievements is rather short in comparison with what we did not understand.

The PFNS calculated with traditional assumption contradicts to experimental data very much. All FF are neutron-rich isotopes rather close to neutron drip line and the properties of these isotopes may be different from the stable nucleus verified with the (p,n) reaction. So, the correction of level density parameter, the application of T-constant dependences may be explained by this fact. However, one should

Fig. 5.1 Dependence of the *C/E* ratio for the spectrum-average cross sections on the energy E50%-response in ²⁵²Cf(sf). *PFNS* Prompt Fission Neutron Spectra



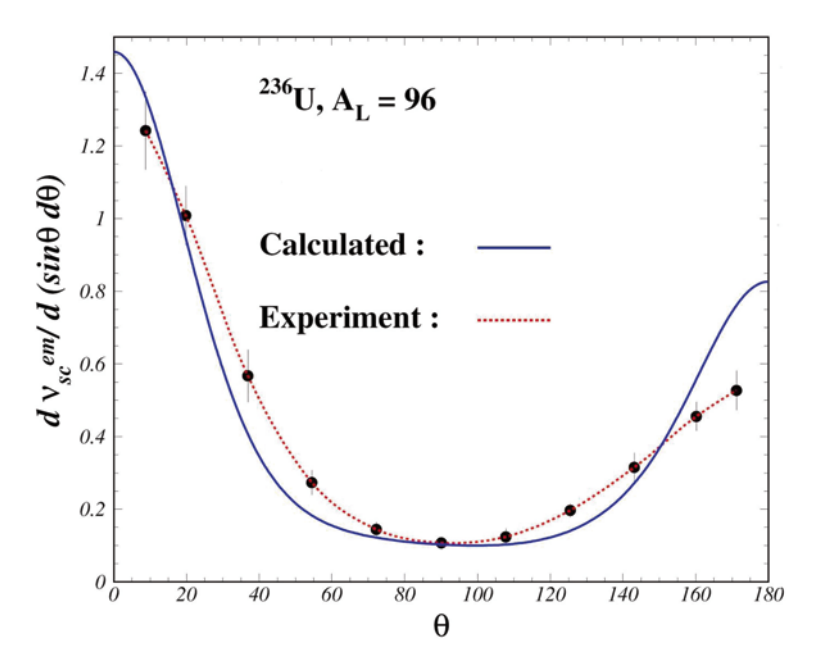


Fig. 5.2 Experimental data A_1/A_h =96/140 and calculated angular distribution for scission neutron emission for ²³⁵U thermal fission

clearly demonstrate the nature of this difference, give the explanation why LD transformed to constant temperature law and tool how to calculate this temperature.

The neutron emission along the fission axis may be produced with the fast scission emission, so due to this fact the mechanism of NEAFA is not dominant process. Hence, the difference between experimental and calculated PFNS may have another explanation—contribution of SCN emission. In previous papers (see, for example

[11] and references within), it was assumed that there are three sources of fission neutrons: neutron emission due to fission of compound nucleus $A+1-N_{A+1}(E)$, neutron emission from fission of nucleus $A-N_{\rm A}(E)$, with smaller excitation due to SCN emission, and SCN spectrum itself $N_{\rm SCN}(E)$. According to investigations [2, 3, 8] rather big amount of SCN may be emitted.

So, one should consider two separate ways (methods) of fission: fission of compound and traditional neutron emission accompanying of this way of fission N_{A+1} and fast fission together with emission of SCN— $N_{\rm SCN}(E)$. The excitation of these FF is rather small for an additional neutron emission.

One may assume that more than one neutron may be emitted as SCN. So the total neutron spectra N(E) may consist of two independent "fission neutron sources":

$$N(E) = N_{441}(E) + N_{SCN}(E)$$
 (5.1)

 Neutrons from fragments after fission of the compound nucleus A+1 (traditional NEAFA):

$$N_{4+1}(E) = (1 - \alpha) \times W_{4+1}(E) \tag{5.2}$$

where α is the share of scission process (neutrons) and W_{A+1} is the spectrum which describes the neutron emission from accelerated fragments.

2. SCNs itself:

$$N_{scn}(E) = \alpha \times E \times \left(\frac{\varsigma}{T_1^2} \exp\left(-\frac{E}{T_1}\right) + \frac{1-\varsigma}{T_2^2} \exp\left(-\frac{E}{T_2}\right)\right),\tag{5.3}$$

where ζ is the share of the low energy component. The results of this analysis are given in Figs. 5.3 and 5.4.

Parameters are collected in Table 5.1. The incorporation of SCN according to Eq. (5.3) allows us to describe the experimental data both for ²³⁵U and ²⁵²Cf inside the uncertainties of evaluated spectra. It is interesting that parameters are rather close for both fissile systems, in particular the share of SCN component—44% for both isotopes.

The SCN was described with two Maxwellian distributions also. However, the agreement with experimental results was much worse.

The agreement between calculated with SCN component and experimental PFNS for ^{235}U and ^{252}Cf may stimulate the conclusion that including rather big amount of SCN emission does not contradict to experimental spectra. Now we do not have specific approach (angular anisotropy) for data analysis which allows us to separate neutron emission mechanisms. Only different methods of data analysis, all available experimental data (N(E), v(A), v(TKE), $N(E,\theta)$) should be included in data evaluation procedure to define emission mechanism.

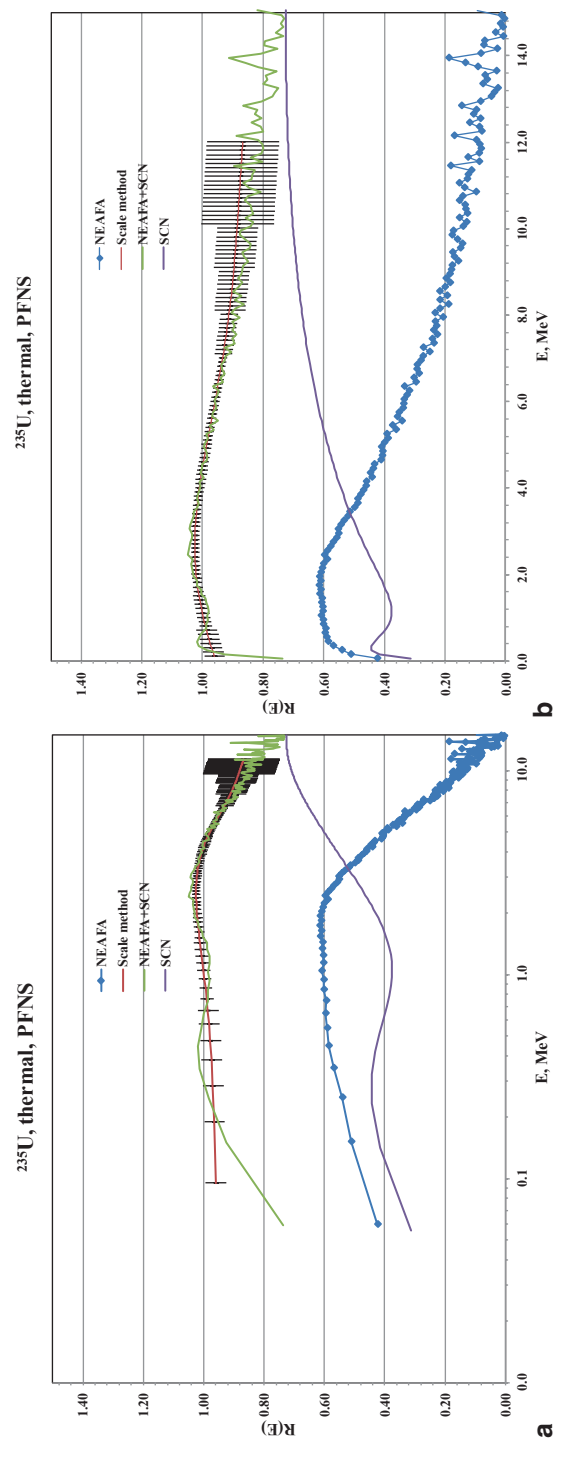


Fig. 5.3 a Evaluated and calculated with FINE code PFNS, together with SCN spectrum for 235U(th) in logarithmic scale. b The same as in Fig. 5.1a in linear scale. PFNS Prompt Fission Neutron Spectra, SCN scission neutron

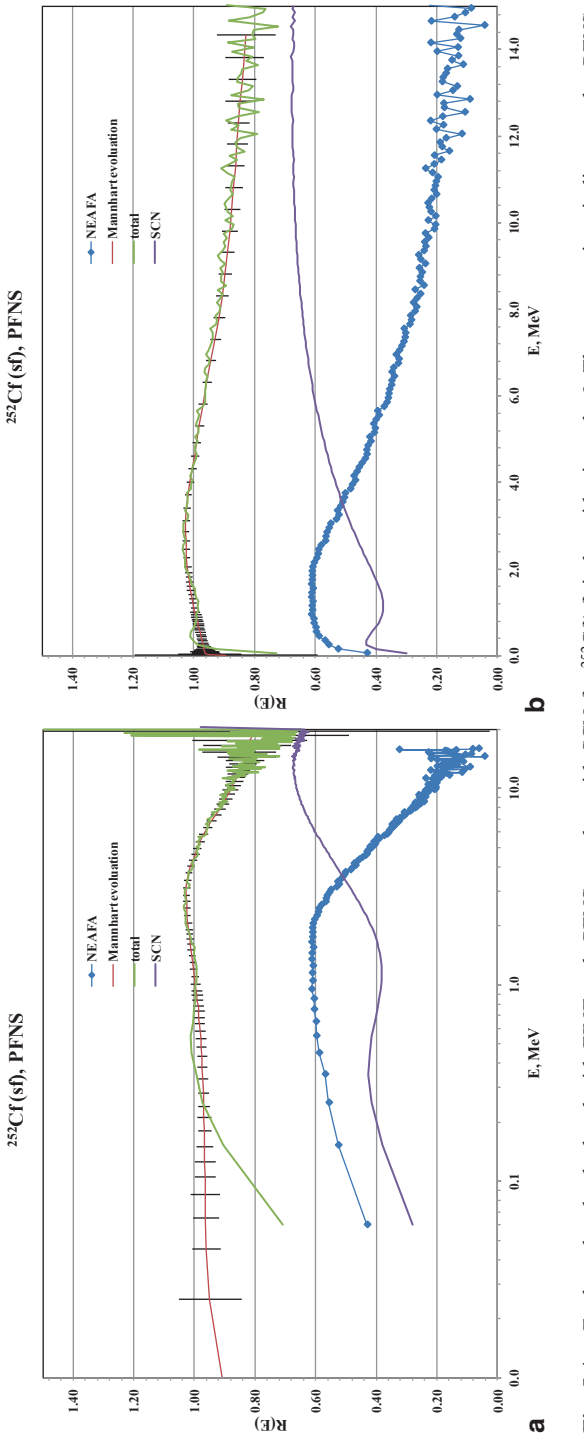


Fig. 5.4 a Evaluated and calculated with FINE code PFNS together with SCN for ²⁵²Cf(sf) in logarithmic scale. **b** The same as in **a** in linear scale. *PFNS* Prompt Fission Neutron Spectra, *SCN* scission neutron

Parameters	²³⁵ U	²⁵² Cf	
α	0.44	0.44	
ζ	0.16	0.15	
T_1 (MeV)	0.29	0.32	
T_2 (MeV)	1.26	1.34	
$\langle E \rangle$ (MeV)	1.976	2.120	

Table 5.1 Parameters of Eqs. (5.1)–(5.3)

Practically we do know nothing about SCN emission. The Eqs. (5.1)–(5.3) assumed that there are two independent ways of final stage of fission and neutron emission. However, "fast" SCN emission and "slow" NEAFA may be consequent steps of single process. Fission neutron may be emitted at any time of nucleus evolution. "Fast neutron emission," neutron emission at scission is the first stage of the process. The residual, after emission of some amount of SCN will have broad energy distribution according to spectrum of SCN. If the excitation energy is higher than binding energy for some FF, an additional amount of neutrons will be emitted with NEAFA. So the correct model may be constructed if we will understand the properties of emitted neutron at each stage of evolution.

What is the multiplicity of SCN and its dependences on mass number and total kinetic energy (TKE)? What is the possible energy store? According to NEAFA calculations (Figs. 4.22, 4.23, and 4.24) the neutron emission is not possible at high TKE (190–200 MeV) due to energy conservation law. But we have rather big experimental amount of neutrons emitted in this TKE range. In addition, not only high energy part, but neutron multiplicity versus TKE is the crucial dependence for understanding of mechanism of neutron emission in fission. All calculated results predict the slope $\sim\!10$ MeV/n, and this value is not sensitive to input parameters like the PFNS. In the framework of traditional assumption, the origin of this value is clearly visible, but the strong contradiction with experiment ($\sim\!19$ MeV/n for 235 U) is also obvious.

It seems that some of the fissions happened due to simultaneous emission several particles (two FFs and neutron(s)), providing continuous energy distribution. In this case, a lot of energy is available for neutron emission, and this process may change dTKE/dv slope also. However, we do not have enough facts to support this assumption.

Now one may conclude that in spite of more than 50 years' efforts, the mechanism of neutron emission in fission is unknown. New experimental and theoretical efforts are extremely necessary to clarify the problem, to suggest new model, and to formulate new experiments for its investigation.

5.3 Left-Right and Angular Effects for Fission Neutron Emission at 0.5 MeV Input Energy

The several experiments for investigation of PFNS 235 U at E_0 =0.5 MeV have been realized in JRC-IRMM [4, 8, 9] during 2004–2008. Based on the very high counting statistics and, hence, small statistical uncertainty, a very unusual result, never

observed before, was found in this investigations. The left-right and angular asymmetry effect was demonstrated in these papers.

This fact may give the evidence that not only different emission mechanism but a different mechanism of the fission process should be assumed for its explanation. Therefore, this discussion was not included in previous section.

The demonstration of the validity and precision of the experimental procedure was the main goal for the authors [8, 9], to provide arguments that the observed effects are not artifacts. I repeated here most interesting facts and arguments, with hope that new discussion will be stimulated.

Three experiments were carried out at the 7 MV Van de Graaff accelerator of the IRMM in Geel, Belgium, using the fast neutron time-of-flight (TOF) technique. A pulsed proton beam of about 1.0–1.5 ns full width at half maximum (FWHM) at 1.25–2.5 MHz repetition rate and 0.2–0.8 μ A average current was used. Monoenergetic neutrons of 0.52 MeV average energy were produced using the ⁷Li(p,n) reaction. A metallic ²³⁵U sample (93.15% enrichment, 161.28 g) and a similar sized lead sample were applied for foreground and background measurements, respectively.

In the first run (Jul06), an angular dependent effect was found. The neutron yield is $\sim\!10\,\%$ higher and the average secondary neutron energy $\sim\!80$ keV higher at 120° compared to 90° . The result was discussed at the Nice ND2007 conference [8]. This unusual finding stimulated new investigations to verify and to estimate the nature of this effect. In the second experiment (Apr07), we used three identical neutron detectors at a flight path of $2.24\!\pm\!0.01$ m placed at $90^\circ, 150^\circ,$ and $120^\circ.$ The distance from the neutron production target to the sample was $\sim\!8$ cm.

In the third experiment (Jan08), the same detectors were applied. Two of them were placed at 90° to the left (L90) as well as to the right (R90) side relative to the proton beam direction. The third detector was placed at 150° to the right side (R150). Flight paths were of 2.25 ± 0.01 m. The sample was placed at 8.5 ± 0.2 cm from the neutron target (0° position) and was moved also along the axis between detectors R90 and L90 at ±3 cm and ±7 cm. The plus sign means that the sample was moved towards the R90-detector and the minus sign in opposite direction towards the 90° L detector. The third detector can see the sample only in the 0° position. In every experiment, the neutron detectors were shielded against direct and room-scattered neutrons.

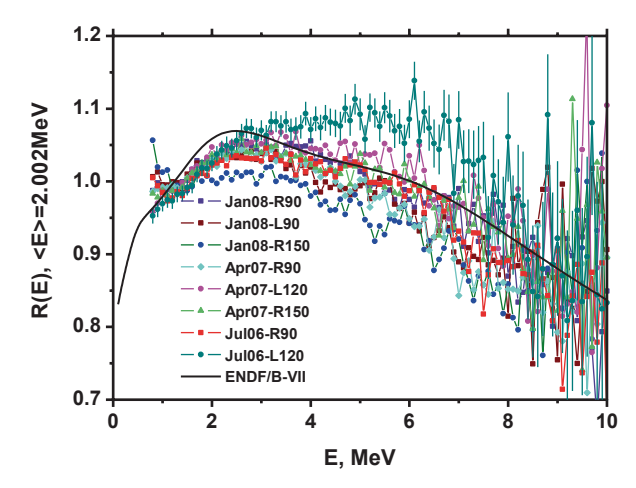
The traditional pulse-shape analysis was applied to reduce the gamma-ray background. A small Pilot-U scintillator was used as a proton pulse-shape monitor. The data were collected in list mode for offline analysis. The detector efficiencies were measured relative to the ²⁵²Cf standard spectrum. A specially designed low mass, fast ionization chamber (see Sect. 5.2) was put at the place of the U-sample keeping the same geometry as during the experiments. The energy spectra were corrected:

- For detector efficiency;
- For neutron multiple scattering in the sample;
- For time resolution, including neutron energy spread on the sample;
- Time shift versus pulse height.

Angle (deg)	$\langle E \rangle$ (MeV)	$\langle E \rangle$ (MeV)	$\langle E \rangle$ (MeV)	
	Jul06	Apr07	Jan08	
R90	2.004	2.002	2.021	
L90			2.007	
L120	2.076	2.050		
R150		2.026	1.975	
a The letters show	ws left-L and right-R	sides of the detector	r relative to the proton	beam.

Table 5.2 Average energies of the PFNS for all angles and runs^a

Fig. 5.5 Comparison between all our results (*full symbols*). ENDF/B-VII spectrum is given as *full line*



The special efforts were done to estimate zero-time and investigation of the possible time correlated background (Pb sample run).

The pulse mode operation of the VdG was not the same during these experiments. The FWHM was between 1 and 1.5 ns in all experiment. However, some tailing is observed, which could not be removed completely. The worst tailing was observed during the Jul06 experiment. The best beam quality was eventually realized during the third experiment, with an FWHM ~ 1 ns and a FW(1/1,000) M < 10 ns. The authors recalculated the time resolution correction for the measured spectra from the Jul06.

The experimental PFNS were normalized to unity and the average secondary neutron energy was calculated. A Maxwellian spectrum was fitted in the energy range of 0.7–1.5 MeV and 9–11 MeV to the measured spectrum and an extrapolation to zero and to 20 MeV performed. Based on detailed analysis of all incorporated corrections and possible uncertainties, authors conclude that the average energy is estimated with an accuracy of ± 0.010 MeV. The average energies measured in all experiments are given in Table 5.2.

The PFNS at all investigated angles and for all runs are shown in Fig. 5.5 as a ratio to a Maxwellian distribution with the average energy $\langle E \rangle = 2.002$ MeV.

^a The letters shows left-L and right-R sides of the detector relative to the proton beam, $\delta < E > = 0.010 \text{ MeV}$

$E_1 - E_2 (MeV)$	$\langle R \rangle \pm \delta R$	$E_1 - E_2 (MeV)$	$\langle R \rangle \pm \delta R$
0.8–2	0.999 ± 0.003	5–6	1.009 ± 0.005
2–3	1.010 ± 0.002	6–8	1.051 ± 0.006
3–4	1.020 ± 0.005	8-10	0.970 ± 0.032
4–5	1.034 ± 0.004		

Table 5.3 Average spectral ratios $\langle R \rangle = N(E,R90) / N(E,L90)$ and their errors for different energy intervals

The following peculiarities are highlighted:

- 1. The data demonstrate the variety of the prompt neutron spectrum shape. The difference exists not only for various detector angles but for detectors at 90° placed at left and right sides (see Jan08 R90, L90 in Fig. 5.5 and Tables 5.2 and 5.3);
- 2. The normalized spectra are fixed at low and high energies (see Fig. 5.5). The yields integrated between 1.3–2.3 MeV and 8–10 MeV are constant. The standard deviations of eight spectra measured in these runs are 0.6% and 3%, respectively, in these energy intervals;
- 3. Among these data one may find a result which agrees perfectly with one of the old experiments or evaluations.

Before starting any scientific discussion about the nature of this strange behavior of the PFNS one should answer the main question: is this a real effect or an experimental artifact?

The experiments were carried out relative to the standard 252 Cf spectrum measured in the same experimental conditions. Therefore, a lot of mistakes such as flight path differences, uncertainties in the time channel width, a possible time reference shift (T_0 value) connected with the detector operation, a distortion of the spectrum due to scattering in the collimator were drastically reduced or even canceled.

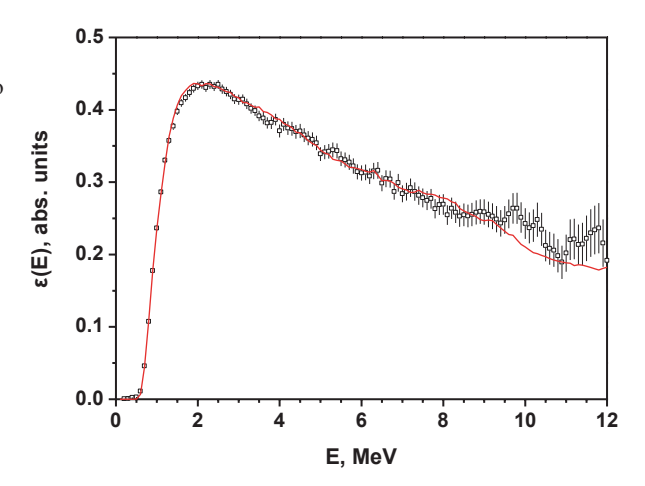
The shift of T_0 (zero time for channel scale calibration) versus pulse height was investigated. After an additional correction as a function of pulse height, the shift was < 0.1 ns (Analog to Digital Convertor (ADC) channel width was 0.117 ns).

A possible change of the ²⁵²Cf spectrum due to different emission angles of the neutrons relative to the electrode plates in the ionization chamber was investigated. The ionization chamber was rotated relative to its vertical axis and the neutron spectra were measured by two detectors at 90° and 120°. No influence was found.

The spectrum shape may be distorted due to the proton pulse shape (VdG pulse mode operation) and a possible mistake in the time resolution correction. In this case, the high energetic part of the spectrum (most sensitive to the time resolution) should be distorted. Since the same integrals for the energy interval 8–10 MeV was observed, this argument is not valid. In addition, this factor is common for all detectors and cannot explain the observed difference between them.

So the most sensitive factor is the stability of the detectors and the correct estimation of the T_0 value. The detector efficiency might be arbitrary changed in between the Cf and U measurements.

Fig. 5.6 The efficiency of one detector (Jan08, R150 detector) measured relative to ²⁵²Cf and calculated with the NEFF7 code (*full line*)



The influence of both factors was simulated. Authors calculated the spectrum with the nominal parameters, with a shifted T_0 by 1 ns and with a distorted detector efficiency by the function $1\pm0.1\cdot(1.7-E)$, E<1.7 MeV.

The influence of these factors may provide an effect comparable with the data spread shown in Fig. 5.5, the average secondary energy varied by \pm 70 keV. However, a shift of T_0 by 1 ns changed the integral in the energy range 8–10 MeV by 28% which is \sim 10 times higher than the real data spread in Fig. 5.5, so this factor was excluded.

Another possibility would be that the distortion factor is connected with instabilities of the threshold and neutron-gamma discrimination parameters. The detector efficiencies were measured before, in the middle, and after the U run in each experiment. The U-spectra shown in Fig. 5.5 are sums of several (5–7) runs measured during 10–20 h, so the direct comparison of the separate spectra may answer this question about the detector stability. According to this analysis there is no evidence for a detector instability which may provoke the change in the measured results. In addition, the detector efficiencies are in very good agreement with calculated results Fig. 5.6 (Monte Carlo simulation with NEFF7 code [13]).

These arguments are valid for each of the experiments, and the final conclusion was the real effect and no experimental artifact was measured!

On the basis of the above discussion, one may conclude that a factor exists which has a rather strong influence on the PFNS shape and asymmetry effects but was not fixed in IRMM's investigations and in all available experiments performed during the long history of fission investigations.

One may assume that this factor is the neutron polarization. In the preparation stage of any PFNS experiment it was assumed that this factor is not important or by definition should be equal to zero. If this explanation is true, the transmission mechanism of the information from the incident neutron to the secondary fission neutron should be found. The only possibility might be SCN emission, a fast process without formation of the compound nucleus. This may provide the link between the

incident neutron and the secondary fission neutron. We should have in mind that three particles (two FFs and a SCN) are emitted at the same time which complicates the problem a lot.

The information about SCN emission is very poor (see discussion above). However, the most important question for current analysis is: which parameters should be changed to provide the variety of results given in Fig. 5.5.

The following possible assumption was applied for analysis, in case of SCN emission, fission neutrons should be emitted from three sources:

1. Neutrons from fragments after fission of the compound nucleus A + 1

$$N_{4+1}(E) = (1-\alpha) \times W_{4+1}(E) \tag{5.4}$$

where α is the share of SCNs emission and W_{A+1} is the spectrum which describes the neutron emission from accelerated fragments;

2. Neutrons from accelerated fragments after fission of the nucleus A, which is formed after the emission of one SCN:

$$N_{A}(E) = \alpha \times (\nu - 1) \times W_{A}(E) / \nu \tag{5.5}$$

SCNs itself:

$$N_{scn}(E) = \frac{\alpha}{\nu} \times E \times \left(\frac{\zeta}{T_1^2} \exp\left(-\frac{E}{T_1}\right) + \frac{1-\zeta}{T_2^2} \exp\left(-\frac{E}{T_2}\right)\right)$$
(5.6)

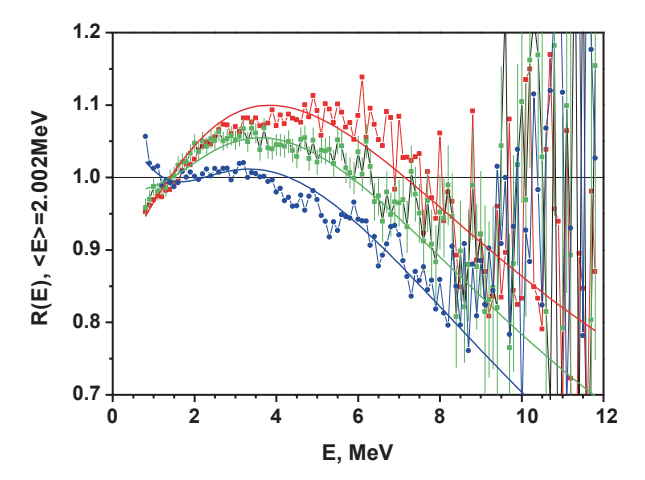
where ζ is the share of the low energy component and v is the average neutron multiplicity.

The spectra W_A , W_{A+1} were calculated with a Watt distribution for Light Fragments (LF) and heavy fragments (HFs) with masses A_h =140 and A_l =A-140. The center-of-mass system (CMS) energy E_l =1.054 MeV, E_h =0.495 MeV were the same for W_{A+1} and W_A . The total excitation for A nucleus was reduced due to B_n and average energy of SCN. The ratio of the neutron multiplicity for light and HFs was $v_l/v = v_h/v = 0.5$ for both fissile nuclei. Temperature parameters were found based on the Fermi-gas relation and the thermal-equilibrium assumption with an additional correction of cor=0.9 for the excitation of the HF U_h = U_{0h} cor [10]. The level density parameter was calculated as a=A/c, c=8.4, TKE=170.5 MeV, and v=2.45.

The equation for $N_{\rm scn}(E)$, and the corresponding parameters α , T_1 , T_2 were taken from [6, 7] introducing minor corrections: α =0.4, T_1 =0.4 MeV, and T_2 =1.35 MeV. The parameters are rather close to ones given in Table 5.1.

Changing only ζ from ζ =0.2 to ζ =0.6 allowed us to describe the spectrum shape with reasonable accuracy from the highest average secondary neutron energy $\langle E \rangle$ = 2.070 MeV to the lowest $\langle E \rangle$ = 1.967 MeV (Fig. 5.7).

Fig. 5.7 Some experimental data and their description with a "3 source model." Blue line— ζ =0.6, green— ζ =0.4, red— ζ =0.2 (for details see text)



The authors of [9] concluded: "Presently, there is no model, able to explain this result. We may assume that a different mechanism of the fission process and of neutron emission should be incorporated. For the moment we may only conclude, that the measured effect is not an experimental artifact. We should assume the existence of an additional factor (parameter), for example the neutron polarization which may be responsible for the measured peculiarities. However, we did not demonstrate the direct link between this unknown parameter and the fission neutron spectrum, the left-right and angular asymmetry. At present, we cannot answer the very important question, why the parameters of prompt fission neutrons changed so drastically and what is happening inside nuclear reactors. Evidently, a new type of experiments are urgently needed. In this respect, experiments with polarized thermal neutrons might be very interesting."

5.4 Contradiction Between Microscopic and Macroscopic experiments (Mic–Mac Problem)

An obvious achievement which was discussed above for the PFNS investigation is the high accuracy of evaluated spectrum for ^{252}Cf which was confirmed by macroscopic experiments (Fig. 5.1). The ration of calculated to experimental average cross sections is $\langle R \rangle = C \, / \, E = 1.004 \pm 0.020$.

In the case of ²³⁵U, the situation is very different. The PFNS evaluated for ENDF/B-VII data library with special selection of parameters, and applying "average high energy" experimental data at 0.5 MeV input energy confirms the average cross section (macroscopic results) with high accuracy comparable with ²⁵²Cf (see Fig. 5.8 and 5.1). The problem may exist only for high energy range > 11 MeV. (Fig. 5.8)

However, ENDF/B-VII PFNS contradict to evaluated spectrum, estimated on the basis of the "microscopic result" only (Fig. 3.16). And besides, the PFNS with

Fig. 5.8 Dependence of the C/E ratio for the spectrum-average cross sections on the energy E50%-response in ²³⁵U(th). The PFNS from ENDF/B-VII. PFNS Prompt Fission Neutron Spectra

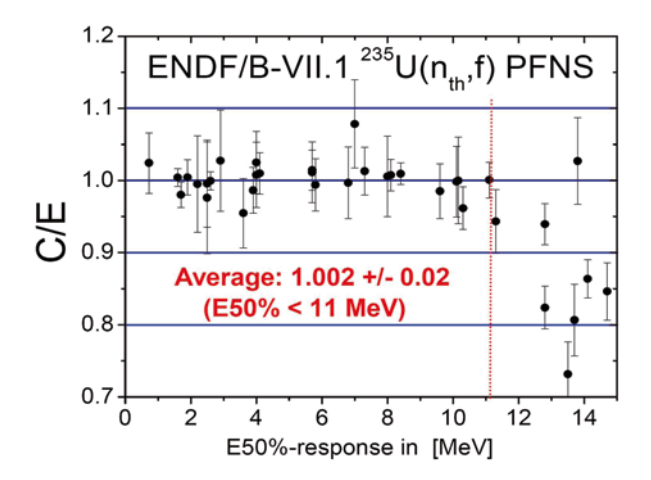
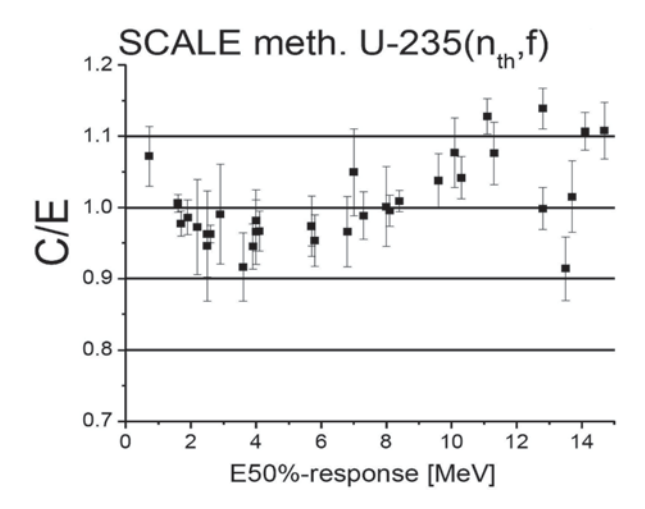


Fig. 5.9 Dependence of the C/E ratio for the spectrum-average cross sections on the energy E50%-response in ²³⁵U(th). The PFNS from "scale-method"



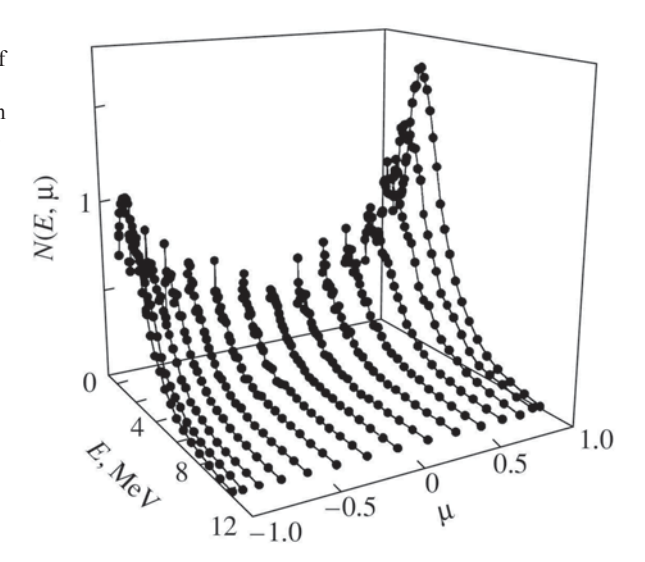
"low energy" corresponding to "microscopic data" cannot predict benchmark experiments also (see Fig. 5.9).

This is very old problem, named as Mic–Mac problem—the contradiction between microscopic and macroscopic experimental data for PFNS for ²³⁵U at thermal energy. As a rule, this difference was explained due to experimental uncertainties for microscopic (differential) experiments.

However, analysis demonstrated above, stimulated another conclusion: both data "microscopic" and "macroscopic" are correct. The possible explanation was discussed in [5].

This contradiction may appear due to strong energy-angular dependence of fission neutrons emission relative to FF direction and its possible influence on macroscopic experimental results.

Fig. 5.10 Experimental energy-angular distribution of fission neutrons in Laboratory System relative to fission fragment axis for thermal fission of 235 U. Light fragment moves in μ =1 direction



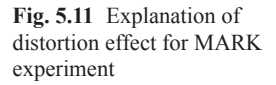
In the process of fission, the compound nucleus (traditional assumption) splits into two FFs which have double bump distribution over mass and close to Gaussian distribution of their kinetic energy. Let us assume that we have only two fragments—LF and HF. These fragments move along the line in opposite direction with different kinetic energy per nucleon. Assume that all PFNs have an isotropic distribution in the CMS of FF and they are emitted from fragments after full acceleration. Due to the movement of the CMS, the neutrons in Laboratory System are emitted (mainly) along the direction of LF and HF.

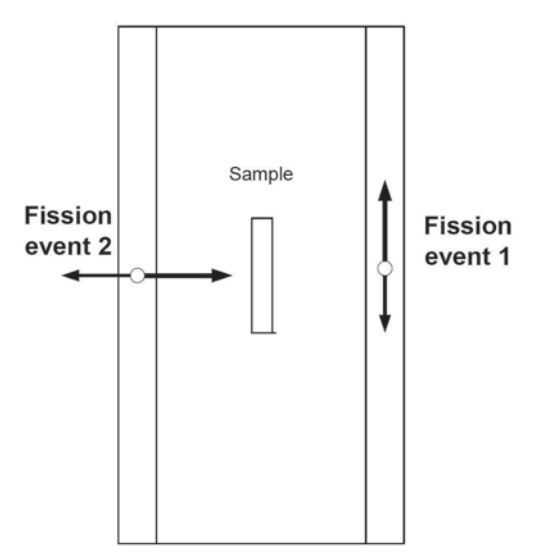
The experimental energy-angular distribution of PFN for ²³⁵U fission at thermal energy in the LS is shown in Fig. 5.10. Calculated spectra at 90°, 0°, and 180° are shown in Fig. 2.12b. The experimental angular distribution for ²⁵²Cf spontaneous fission for both LF and HF after integration in the energy range 1–5 MeV is shown in Fig. 2.12a.

These data illustrate the well-known experimental fact: average neutron energy and neutron yield are much higher along FF direction (abs(μ)~1) than in an orthogonal direction μ ~0.

As a rule, there is not strong angular dependence of the FF emission. Therefore, the traditional assumption is that FF emission is isotropic. The consequence of this assumption is that PFN have an isotropic angular distribution also. The energy spectrum of PFN is angular integrated distribution of neutrons emitted relative to fixed FF direction. These data are tabulated in data libraries and are used for practical applications.

The same assumption is used for preparation of the neutron source for experiments in ²³⁵U neutron field, and for treatment of experimental results. The diagram of well-known MARK source is shown in Fig. 2.28. The motivation for this construction is very simple. The thermal neutrons induce fission in which angular





integrated PFN spectrum is emitted. These neutrons interact with materials of the source and create the "experimental" neutron field. The correction for interaction with environment is rather small and may be calculated on the basis of angular integrated PFNS.

In reality, after fission we have the pair of FF which emit neutrons with particular energy-angular distribution, and effect of interaction with environment depends on direction of the FF and peculiarity of environment in this direction.

Effects which can increase average energy on the sample Let us consider two fission events shown in Fig. 5.11. Low energetic neutrons with small intensity are moving in direction of the sample in first event. Main component of PFN from this event with much higher energy and intensity (~7 times higher) is moving along wall of the source, and after scattering will reach activated sample.

In second fission event, the sample is exposed by high energetic neutrons and contribution of scattering neutrons is rather small due to small intensity of the PFN emitted in orthogonal direction.

So, one may conclude that component of the neutron field produced due to multiple scattering in the sample environment will have higher average neutron energy in comparison with isotropic emission of average neutron spectrum.

Effect which can reduce average energy on the sample If "weighting functions" for scattering or return of neutrons moving in to different directions inside the sample are the same for any direction of FF the final result will be the same as for emission of "average" spectrum. This case is realized in experiments with ²⁵²Cf source.

Let us estimate the "weighting functions" for spectra shown in Fig. 2.12b, having in mind that the average energy for 0° and 180° is higher but for 90° the neutron intensity is less than for angular integrated PFNS.

In case of neutron emission along the "wall," the total cross section will be less for event 1, than for event 2. So the probability of interaction with "wall" will be less for event 1 and higher for event 2 in comparison with integrated PFNS. In addition, elastic scattering has higher asymmetry for higher energy of neutrons (0°, 180° emission). These facts reduce amount of high energetic neutrons returned back to the sample for event 1.

At the same time, inelastic scattering (first level on Al has energy 0.843 MeV) is bigger for event 1. As a consequence, the contribution of low energetic neutrons after the scattering is higher for event 1 than for event 2.

So one may conclude, multiple scattering of neutrons inside the sample environment in macroscopic experiment can provide "effect of angular-energy selection due to anisotropy of fission neutron emission in non-homogeneous environment."

It is very difficult to predict the sign of this effect. It is clear only that combination of real experimental setup and strong energy-angular distribution of neutron relative to FF direction may be responsible for the difference between microscopic and macroscopic experiments.

Very important conclusions about scale (sign) of the discussed effect and its responsibility for old conflict can be made only after detail simulation by Monte Carlo method. I hope that this publication will stimulate these investigations.

The effect discussed above is connected with multiple interactions inside the source. The consequence of this selection for "macroscopic" experiment is also visible. At the same time it is rather difficult to understand how this effect will work in "benchmark" assembly, and real reactor.

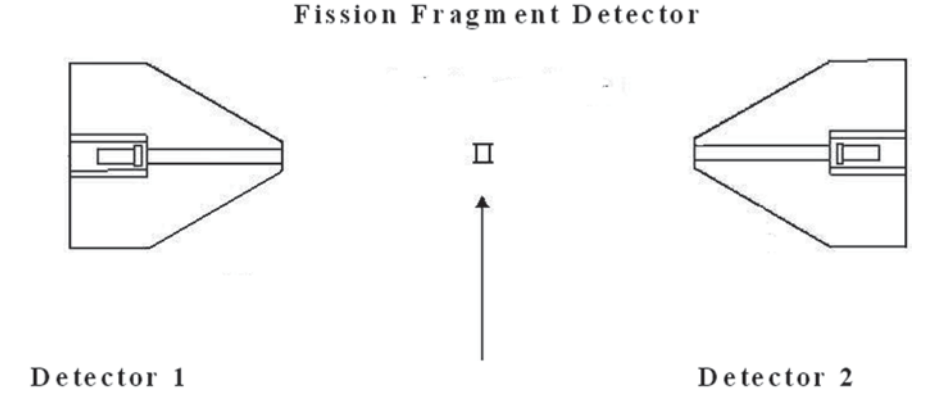
Therefore, an assumption about changing of the PFNS due to unknown interaction in the bulk material, as was discussed in Sect. 5.3, looks rather interesting.

If the parameter ζ (Eqs. 5.4–5.6) is changing in such a way to reach value ζ =0.31, the PFNS of 235 U(th) extrapolated to thermal energy will describe integral experiments. The average ratio of the calculated cross sections to the experimental ones ([11, 14], IRDF-2002) is $\langle R \rangle$ = C/E = 0.997 ± 0.008 . The average energy of the PFNS at thermal energy is $\langle E \rangle$ = 2.038 MeV .

5.5 New Experimental Proposals

One may compress the numerous problems and misunderstandings, which were discussed above, into two points:

There is "Mic-Mac problem" which was not solved during previous 50 years' efforts. Both experimental data sets are correct. The possible explanation due to energy-angular selection inside inhomogeneous environment was not verified yet. There is an assumption that this contradiction may be connected with wrong understanding of the mechanism of neutron emission in fission and fission process itself;



Thermal neutrons

Fig. 5.12 Experimental setup for investigations of unknown properties of fission neutron emission

 There is obvious misunderstanding of the mechanism of neutron emission. NEAFA model cannot explain a lot of experimental facts. The traditional approach that parameters of the model for accurate description of experimental data are unknown is not correct. The assumption was made (supported by theoretical calculations) that many neutrons are emitted at scission during rather short time ~10⁻²⁰ s, and they are emitted along fission axis.

Let us start with the investigation of the nature of emission mechanism. In experiment, we cannot differ 10^{-15} or 10^{-20} s for neutron emission to confirm the source of neutrons. However, the estimation of correlations between energies of neutrons emitted from LF and HF may be realized.

The experimental setup for investigation of "Energy correlations of fission neutrons and mechanism of their emission" is shown in Fig. 5.12. The experiment may be realized by TOF methods, with flight path ~ 2 m. Neutron detectors are traditional hydrogen scintillators with pulse shape analysis. We should use two neutron detectors for counting neutron mainly from one type of FF (light or heavy). For this task, the detectors are placed on the FF axis.

The "grid ionization" chamber or similar detector for FF counting should provide: good time resolution ~ 1 ns, information about FF angle, and total energy for each fragment. The experimental conditions should be similar to ones described in [11]. In this experiment, the neutron flux was $\sim 5\times 10^7$ 1/cm²/s. As target a $^{235}\text{UF}_4$ foil (97.7% enrichment in ^{235}U , Ø=30 mm) of 112 µg/cm² thickness evaporated onto a thin (24 µg/cm²) gold (40 µg/cm²) coated polyimide foil was used. The target was placed in the center of an ionization chamber. The fission count rate was 5×10^4 1/s. Neutron detectors should be placed in shielding collimators to reduce the scattering on the detector environment.

The investigation of energy correlation (anticorrelation) between neutrons, which are emitted from different FF, is the goal of this experiment. Neutron events detected by both neutron counters should be placed in two-dimensional plane—energy measured in one detector versus energy measured in opposite detector. There are two possibilities:

- 1. We will not see any energy correlation between neutrons emitted from complementary fragments;
- 2. Energy correlations will be detected.

In case of NEAFA there is not any correlation between energy of neutrons emitted by complementary fragments. So the first case may support NEAFA assumption, or another mechanism with similar properties.

The second case is more interesting—it means that NEAFA is not the option for fission neutrons. If some amount of correlated events will be detected one may estimate the share of this SCN emission process.

This experiment never was realized before. Therefore, it is difficult to predict, and give any recommendation for its realization. It seems it will be rather useful to measure following observables: "energy correlation" for different FF emission angles, "energy correlation" for different FFs TKE, and masses.

The measured correlations should be compared with model calculations in framework of traditional assumption.

The second experiment which may be realized with the same setup is "Investigation left-right and angular effect with polarized neutrons." In this case, polarized neutron beam will expose U-layer placed inside the same FF counter, as was described above. This experiment was discussed already in [12].

Neutron spectra will be measured with different orientation of the spin of input "thermal" neutrons. According to results presented above one may expect the difference of the PFNS measured at different angles due to changing the contribution of the low energy component of the SCN spectra. The average energy of this is ~ 0.8 MeV. So the detector threshold should be rather small ~ 0.2 MeV.

The goal of this experiment is the ratio of "left-right" spectra as function of neutron energy. This ratio as function of FF masses and TKE is also interesting. The expected effect is rather small. So, ²⁵²Cf layer should be placed in the same chamber for verification of the stability of experimental equipment.

The "crucial problem" for understanding of mechanism of neutron emission is big difference between experimental value and NEAFA prediction for dTKE/dv. The third experiment may be named "*Investigation of neutron emission at high kinetic energy range*." The similar FF counter, the same neutrons detectors (only one neutron detector may be used) may be applied in this experiment also.

The goal of this experiment is detailed investigation of what neutron spectra are emitted at different kinetic energy and what is the neutron spectrum at TKE >190 MeV. The FF yield is rather small at high TKE. Therefore, rather intensive thermal neutron source should be used in this experiment. The ²⁵²Cf layer placed in the same fission detector is very important for this long time measurement.

References

- Capote R, Zolotarev K, Pronyaev V, Trkov A (2012) Validating the ENDF-B/VII ²³⁵U(n_{th},f) prompt fission neutron spectrum using updated dosimetery cross sections (IRDFF), PHYSOR 2012, USA, 15–20 April 2012
- Carjan N, Rizea M (2013) Current density and angular distribution of neutrons emitted during scission, report for ND2013 in press; M. Rizea, N.Carjan. Dynamical scission model. Nucl Phys A909:50
- 3. Carjan N (2013) Report for GAMMA-2 workshop, Sep. 2013, (private communication)
- Kornilov NV (2011) Prompt fission neutron spectra experimental mistakes or lack of understanding? Proceeding of ND2010. J Korean Phys Soc 59:1717
- 5. Kornilov NV (2012) Effect of angular-energy selection due to anisotropy of fission neutron emission in non-homogeneous environment. Int J Nucl Energy Sci Eng 2(4) pp 97–100
- 6. Kornilov N, Kagalenko A, Hambsch F-J (1999) Computing spactra of prompt fission neutron spectra on the basis of a new systematic of experimental data. Phys At Nucl 62(2):173
- Kornilov NV, Kagalenko AB, Poupko SV et al (2001) New evidence of an intense scission neutron sourcein the ²⁵²Cf spontaneous fission. Nucl Phys A686:187–203
- Kornilov N, Hambsch F-J, Fabry I et al (2007) New experimental and theoretical results for the ²³⁵U fission neutron spectrum. Int Conf Nucl Data Sci Technol:387 doi:10.1051/ndata:07735
- 9. Kornilov N, Hambsch F-J, Fabry I et al (2007) Left-right and angular asymmetry of fission neutron emission, JRC-IRMM, Scientific report
- Kornilov NV, Hambsch F-J, Vorobyev AS (2007) Neutron emission in fission. Nucl Phys A789:53
- 11. Kornilov N, Hambsch F-J, Fabry I et al (2010) The ²³⁵U(n,f) prompt fission neutron spectrum at 100K input neutron energy. NSE 165:117–127
- Kornilov N, Masse T, Graimes S, Voinov A (2011) New experimental proposal for ²³⁵U PFNS measurement to answer a fifty year old question. J ASTM Int 9(3). doi:110.1520/JAI104001, ISRD-14
- $13. \ \ Morettor\ LG\ (1972)\ Shell-correction\ calculations\ of\ fission\ decay\ widths\ and\ probabilities\ in\ superheavy\ nuclei.\ Nucl\ Phys\ A180:337$
- Zolotarev KI (2003) Evaluated cross section data from russian reactor dosimetry file. INDC(NDC) 448:25